NOTCH TIP STRESS STRAIN ANALYSIS IN BODIES SUBJECTED TO NON-PROPORTIONAL CYCLIC LOADS

by

Meera Nand Kaur Singh

A thesis
presented to the University of Waterloo
in fulfillment of the
thesis requirement for the degree of
Doctor of Philosophy
in
Mechanical Engineering

Waterloo, Ontario, Canada, 1998

© Meera Nand Kaur Singh 1998

National Library of Canada
Acquisitions and Bibliographic Services
395 Wellington Street
Ottawa ON K1A 0N4
Canada

Bibliothèque nationale du Canada
Acquisitions et services bibliographiques
395, rue Wellington
Ottawa ON K1A 0N4
Canada

Your file Votre référence

Our file Notre référence

The author has granted a non-exclusive licence allowing the National Library of Canada to reproduce, loan, distribute or sell copies of this thesis in microform, paper or electronic formats.

L'auteur a accordé une licence non exclusive permettant à la Bibliothèque nationale du Canada de reproduire, prêter, distribuer ou vendre des copies de cette thèse sous la forme de microfiche/film, de reproduction sur papier ou sur format électronique.

The author retains ownership of the copyright in this thesis. Neither the thesis nor substantial extracts from it may be printed or otherwise reproduced without the author's permission.

L'auteur conserve la propriété du droit d'auteur qui protège cette thèse. Ni la thèse ni des extraits substantiels de celle-ci ne doivent être imprimés ou autrement reproduits sans son autorisation.

0-612-30647-X

Canada

The University of Waterloo requires the signatures of all persons using or photocopying this thesis. Please sign below, and give the address and date.

ABSTRACT

Two methods for calculating notch tip stress and strain histories in elastic-plastic components subjected to non-proportional cyclic loads are presented. The key elements of the proposed methods are incremental relationships between elastic and elastic-plastic strain energy densities and material constitutive relations. The material is assumed to strain harden and a kinematic hardening model based on a multi-surface field of work hardening surfaces is employed.

Each method results in a set of seven independent algebraic equations. The equation sets can easily be solved for the notch tip elastic-plastic stress-strain histories with the knowledge of the materials uniaxial properties, the applied load, and the component geometry. Results of each method are compared with finite element and experimental data for monotonic and cyclic non-proportional loading sequences. The notch tip elastic-plastic strains found using each method predict the general trend in, and quantitatively agree well with the experimental and finite element data.

ACKNOWLEDGEMENTS

I would like to express my deepest gratitude to Dr. G. Glinka and Dr. R.N. Dubey for providing me with the opportunity to pursue this work. I would like to also thank them for their supervision, guidance and patience. I would further like to thank Dr. T. Topper and Dr. J Medley for providing encouragement and motivation at the University of Waterloo.

I would like to express my deepest appreciation to everyone at Zeus Engineering Ltd. in Calgary, Alberta, for giving me a practical insight into fatigue analysis, necessary technical support, and an affable work environment during my studies in Calgary.

There are too many dear friends that I thank for graciously being part of my support network during my studies. Special mention and lifelong appreciation are due to Wendy Cipera, Duane Cronin, Heather Faris, Janice Nicholls, Mary Romas, and Diana. Thammer, and Daniel Yaucoub. I would like to thank every member of my family: Mrs. Martha R. Singh, Dr. Mansa C. Singh, Indra A.K. Singh, Kiren K. Singh, Sheila K. Singh and Edmond J. Lefebvre, Carolyn J. Thom, Christopher G. Thom and Robert M. Thom, for providing me with the encouragement, love and support that made this work possible.

Finally, the financial support of the Government of Canada (NSERC) and the Government of Ontario (OGS) is gratefully acknowledged.

DEDICATION

To My Parents

Mrs. Martha R. Singh and Dr. Mansa C. Singh
- It's all His grace

TABLE OF CONTENTS

1. CHAPTER ONE: INTRODUCTION AND SCOPE 1

2. CHAPTER TWO: BACKGROUND AND LITERATURE REVIEW 5

2.1 Uniaxial Models 6
2.1.1 Body in Plane Stress 6
2.1.2 Body in Plane Strain 11

2.2 General Body Stress State 12
2.2.1 Proportional Models 13
2.2.2 Non-Proportional Models 16

2.3 Conclusions of the Literature Review 18

3. CHAPTER THREE: PROPOSED MULTIAXIAL MODEL 23

3.1 Incremental Equivalent Strain Energy Density (ESED) Relations 23

3.2 Incremental Neuber's Rule 27

3.3 Comparison of Proposed Methods With Finite Element Data 30
3.3.1 Energy Density Sensitivity to Load Path 31
3.3.1.1 Material Model 31
3.3.1.2 Method of Analysis and Results 32
3.3.2 Axial Stress - Strain Contribution to the Energy Densities 36
3.3.2.1 Material Model 36
3.3.2.2 Method of Results and Analyses 36
3.3.3 Summary of Numerical Assessment 38

4. CHAPTER FOUR: CONSTITUTIVE MODELLING 51

4.1 Elastic Constitutive Relations 51

4.2 Elastic-Plastic Constitutive Theory 52
4.2.1 The Yield Criterion 54
4.2.2 The Flow Rule 56
4.2.3 The Hardening Rule 57
4.2.3.1 Isotropic Hardening 57
4.2.3.2 Kinematic Hardening 59

4.3 Constitutive Behavior at the Notch Tip 66

5. CHAPTER FIVE: NOTCH TIP STRESS-STRAIN DETERMINATION 70

5.1 Notation 71

5.2 Initial Requirements 72
5.2.1 Material Properties / Yield Surface Definition 72
5.2.2 Elastic Stress-Strain History 75

5.3 Elastic Loading 76

5.4 Unloading Criterion 77

5.5 Elastic Unloading 78

5.6 Elastic-Plastic Loading 80
5.6.1 Local Versus Global Co-ordinate Systems 81
5.6.2 Dividing Input into Increments for Numerical Integration 83
5.6.3 Incremental Equivalent Strain Energy Density Solution Set 85
5.6.4 Incremental Neuber's Solution Set 93

5.7 Computer Implementation 99

6. CHAPTER SIX: COMPARISON OF SIMPLIFIED METHODOLIGIES TO EXPERIMENTAL AND FEM DATA 106

6.1 Proportional Monotonic Loading 106

6.2 Non-Proportional Monotonic Loading 109

6.3 Non-Proportional Cyclic Loading 112
6.3.1 Comparison of Results 114

7. CHAPTER SEVEN: CONCLUSIONS / RECOMMENDATIONS 142

REFERENCES 148

LIST OF FIGURES

Figure 1.1: Fatigue Crack at a Notch Root. 1

Figure 2.1: Elastic Stress Distribution in a Notched Bar Subjected to a Tensile Load. 20

Figure 2.2: State of Stress at the Notch Tip a) Plane Stress, b) Plane Strain, c) In General. 21

Figure 2.3: Geometry Used in Neuber's Analysis [5]. 22

Figure 2.4: Neuber's Rule. 22

Figure 2.5: Equivalent Strain Energy Density (ESED) Method. 22

Figure 3.1: Two Notched Bodies Made of a) Elastic and b) Elastic-Plastic Material. 39

Figure 3.2: a) Incremental Equivalent Strain Energy Density Method,b) Incremental Neuber's Rule. 40

Figure 3.3: Notched Cylindrical Bar Used in Numerical Assessment. 41

Figure 3.4: Finite Element Model of the Cylindrical Bar. 41

Figure 3.5: Material Model Used in Energy Assessment. 42

Figure 3.6: Load Paths Used in Energy Assessment a) Tension-Torsion, Proportional, b) Torsion-Tension, Proportional. 42

Figure 3.7: a) Strain Energy Density, b) Total Strain Energy Density ($\sigma^f_{n.s.} / \tau^f_{n.s.} = 0.32$). 43

Figure 3.8: a) Strain Energy Density, b) Total Strain Energy Density ($\sigma^f_{n.s.} / \tau^f_{n.s.} = 1.1$). 44

Figure 3.9: a) Strain Energy Density, b) Total Strain Energy Density ($\sigma^f_{n.s.} / \tau^f_{n.s.} = 3.2$). 45

Figure 3.10: a) Strain Energy Density, b) Total Strain Energy Density ($\sigma^f_{n.s.} = 277\text{MPa}, / \tau^f_{n.s.} = 251\text{MPa}$). 46

Figure 3.11: Material Model Used in Energy Assessment. 47

Figure 3.12: Load Paths Used in Axial Energy Assessment, a) Tension-Torsion, b) Torsion-Tension, c) Torsion-Combined Tension, Torsion. 47

Figure 3.13: Axial Energy Increments in Tension-Torsion Load Path, a) Strain Energy Density, b) Total Strain Energy Density. 48

Figure 3.14: Axial Energy Increments in Torsion-Tension Load Path, a) Strain Energy Density, b) Total Strain Energy Density. 49

Figure 3.15: Axial Energy Increments in Torsion-Combined Tension, Torsion Load Path, a) Strain Energy Density, b) Total Strain Energy Density. 50

Figure 4.1: von Mises Yield Criterion on the a) σ_1-σ_2 plane and b) π plane. 67

Figure 4.2: Isotropic Hardening. 68

Figure 4.3: Kinematic Hardening. 68

Figure 4.4: Piecewise Linearization of the Material σ–ε Curve and the Corresponding Hardening Surfaces. 69

Figure 4.5: The Mróz Translation Rule. 69

Figure 5.1: Unloading Criterion. 102

Figure 5.2: Elastic-Plastic Loading During Elastic Unloading Increment. 102

Figure 5.3: Comparison of Energy Densities in Body under Uniaxial Loading: a) Loading System, b) Fixed Coordinates, c) Local Coordinates. 103

Figure 5.4: Computer Flow Chart for Notch Tip Cyclic Elastic-Plastic Stress-Strain Analysis. 104

Figure 5.5: Computer Flow Chart for Plastic Straining. 105

Figure 6.1: Notched Bars in [55]:a) Mild Notch,b)Sharp Notch,c)Sharp-Deep Notch. 120

Figure 6.2: Proportional Loading Path in [55]. 120

Figure 6.3: Descretization of the Material Stress-Strain Curve in [55]. 121

Figure 6.4: Principal Surface Strain Components For Mild Notch. 121

Figure 6.5: Principal Surface Strain Components for Sharp Notch. 122

Figure 6.6: Principal Surface Strain Components for Sharp-Deep Notch. 122

Figure 6.7a: Axial Strain History for Tension-Torsion (Path 1). 123

Figure 6.7b: Shear Strain History for Tension-Torsion (Path 1). 123

Figure 6.7c: Normal Stress History for Tension-Torsion (Path 1). 124

Figure 6.7d: Shear Stress History for Tension-Torsion (Path 1). 124

Figure 6.7e: Transverse Stress History for Tension-Torsion (Path 1). 125

Figure 6.8a: Axial Strain History for Torsion-Tension (Path 2). 125

Figure 6.8b: Shear Strain History for Torsion-Tension (Path 2). 126

Figure 6.8c: Normal Stress History for Torsion-Tension (Path 2). 126

Figure 6.8d: Shear Stress History for Torsion-Tension (Path 2). 127

Figure 6.8e: Transverse Stress History for Torsion-Tension (Path 2). 127

Figure 6.9a: Axial Strain History for Tension-Combined Torsion-Tension (Path 3). 128

Figure 6.9b: Shear Strain History for Tension-Combined Torsion-Tension (Path 3). 128

Figure 6.9c: Normal Stress History for Tension-Combined Torsion-Tension (Path 3). 129

Figure 6.9d: Shear Stress History for Tension-Combined Torsion-Tension (Path 3). 129

Figure 6.9e: Transverse Stress History for Tension-Combined Torsion-Tension (Path 3). 130

Figure 6.10a: Load Path 4 - Torsion Combined Tension-Torsion
($\sigma^{f}_{n.s.} = 103$MPa, $\tau^{f}_{n.s.} = 90$MPa). 130

Figure 6.10b: Axial Strain History for Torsion Combined Tension-Torsion (Path 4). 131

Figure 6.10c: Shear Strain History for Torsion Combined Tension-Torsion (Path 4). 131

Figure 6.10d: Normal Stress History for Torsion Combined Tension-Torsion (Path 4). 132

Figure 6.10e: Shear Stress History for Torsion Combined Tension-Torsion (Path 4). 132

Figure 6.10f: Transverse Stress History for Torsion Combined Tension-Torsion (Path 4). 133

Figure 6.11: Descretization of the Stabilized Cyclic Stress-Strain Curve in [32]. 133

Figure 6.12a: Box Path A) Analyzed in [32] ($\sigma_{n.s.} = 258$ MPa $\tau_{n.s.} = 168$ MPa). 134

Figure 6.12b: Comparison of Simplified Models to Experimental Results for Box Path A). 134

Figure 6.12c: Comparison of Simplified Models to Finite Element Results for Box Path A). 135

Figure 6.13a: Box Path B) Analyzed in [32] ($\sigma_{n.s.} = 296$ MPa $\tau_{n.s.} = 193$ MPa). 135

Figure 6.13b: Comparison of Simplified Models to Experimental Results for Box Path A). 136

Figure 6.13c: Comparison of Simplified Models to Finite Element Results for Box Path A). 136

Figure 6.14a: Stress Path in [32] With 2:1 Ratio of Applied Tensile to Torsional Cycles. 137

Figure 6.14b: Comparison of Simplified Models to Experimental Results for 2:1 Ratio. 137

Figure 6.15a: Stress Path in [32] With 1:2 Ratio of Applied Tensile to Torsional Cycles. 138

Figure 6.15b: Comparison of Simplified Models to Experimental Results for 1:2 Ratio. 138

Figure 6.16a: Stress Path in [32] With 1:5 Ratio of Applied Tensile to Torsional Cycles. 139

Figure 6.16b: Comparison of Simplified Models to Experimental Results for 1:5 Ratio. 139

Figure 6.17a: Stress Path in [32] With Non-Zero Mean Stress. 140

Figure 6.17b: Incremental ESED Results for Non-Zero Mean Stress. 140

Figure 6.17c: Incremental Neuber's Results for Non-Zero Mean Stress. 141

Figure 6.17d: Finite Element Results for Non-Zero Mean Stress [32]. 141

LIST OF SYMBOLS [1]

(a)	actual values (elastic or elastic-plastic)
(e)	elastic values
(e-p)	elastic-plastic values
(f)	calculated at end of loading history
(E)	calculated using Equivalent Strain Energy Density (ESED) method
E	modulus of elasticity
E_s	secant modulus
$f(S_{ij})$, $F(S_{ij})$	yield surface functions
(FEM)	calculated using the finite element method
i,j,k,l	indices i,j,k,l = 1,2,3, summation is implied
k	factor to determine when stress point reaches yield surface if loading elastically
K_t	stress concentration factor
K_ε	strain concentration factor
K'	cyclic strength coefficient
(ℓ)	number of work hardening surfaces
LP	parameter in unloading criterion
(n)	denotes active hardening surface
n'	cyclic strain hardening exponent

$\hat{n}_{ij}$	components of the unit normal to the yield surface at the stress point
(N)	calculated using Neuber's method
N	number of constant strain energy density increments
(p)	plastic values
P	tensile axial load
$Q(\sigma_{ij})$	stress potential function
r	radius of yield surface in the π plane
R	gross radius of cylindrical bar
S	nominal stress
S_{eq}	equivalent nominal stress
S_{ij}	components of the deviatoric stress tensor
t	depth of notch
T	applied torque
W	strain energy density
$W_{\alpha\beta}$	axial strain energy densities
α,β	indices α,β = 1,2,3, no summation implied
α_{ij}	components of the back stress tensor
δ_{ij}	Kronecker delta
κ	parameter to determine the active yield surface
λ	varying factor of proportionality in flow rule
μ	indicates the magnitude of yield surface translation

ν	Poisson's ratio
Ω	total strain energy density
$\Omega_{\alpha\beta}$	axial components of total strain energy density
ρ	notch root radius
σ,ε	stress and strain associated with the material stress-strain curve
$\sigma_{eq},\varepsilon_{eq}$	equivalent stress and equivalent strain
$\sigma_{ij},\varepsilon_{ij}$	notch tip stress and strain components
$\sigma_{n.s.},\varepsilon_{n.s.}$	nominal tensile stress and strain in the net section
σ_o	yield stress in tension
$\tau_{n.s}$	nominal shear stress in the net section
ξ_{ij}	deviatoric components of the back stress tensor

[1] brackets denote quantities that appear in superscripts

1. CHAPTER ONE:

INTRODUCTION AND SCOPE

Engineering components frequently contain structural discontinuities such as fillets, holes, and keyways. These discontinuities disturb the stress field in a manner such that, locally, the stresses are higher than those in the net section. If the components are used in fatigue applications, these stress raisers act as perfect sites for crack initiation. Thus, if they are overlooked or their effect on the stress field is not minimized in all phases of design, the result is often premature component failure.



Figure 1.1: Fatigue Crack at a Notch Root

As a simple example, consider the oil field component shown in Figure 1.1. During manufacturing, the component was stamped to mark its size. The indentation in the component

caused by the stamp acted as a stress raiser in service. As can be seen, a fatigue crack started at the top of the stamped seven (7), propagated through the material, and resulted in failure of the component. Since this mark was not associated with the function of the component, and the depth of the stamp may have seemed insignificant relative to the diameter of the component, its effects on the structural integrity of the design was most likely overlooked. To the designer, such a detail mistakenly did not warrant the expenditure of a relatively complicated fatigue analysis.

In order to account for all stress raisers in design, but maintain a simple fatigue analysis, designers often make the assumption that the local stresses remain below the yield limit of the material. This, the stress-life method of fatigue analysis, is relatively simple and works well if the component is designed to withstand low stresses and the resulting lives are long. However, this method is limiting in low cycle applications, where the applied strains have a significant plastic component. In such cases, the assumption is made that although the nominal stresses in components should remain elastic, stresses in the vicinity of critical component locations may exceed the yield limit of the material. In other words, localized plasticity at stress raisers is often permitted in design. This philosophy is associated with the strain-life method of fatigue analysis, which provides a tool for estimating the number of cycles the component can withstand before a crack initiates at a notch root.

One of the preliminary steps in using the strain-life method of fatigue analysis is to determine the elastic-plastic strain history at a component's critical locations. The associated non-linear elastic-plastic analysis has traditionally been avoided since it necessitates either experimental investigations or numerical solution methods. These methods are time consuming and costly, particularly when the components modelled are subjected to lengthy histories of multiaxial loads. Thus, there has been a great effort in fatigue research to develop simplified analytical methods

for modeling the elastic-plastic stress-strain history at notches in bodies subjected to multiaxial loads. These methods generally use the results of an elastic notch tip analysis to predict the elastic-plastic notch tip strain field. Simplified methods have been developed for bodies subjected to uniaxial loads, and more recently have been generalized to address bodies subjected to multiaxial loads. The methods developed for multiaxial loading situations, however, have been only accepted in theory in cases where the principal stresses remain fixed in direction and ratio during a loading cycle. This assumption of proportional loading does not account for such common occurrences as the presence of a mean stress or rotating principal stresses and, as such, must often be relaxed in practice.

It is the intent of this work to develop and implement a simple and sufficiently accurate analytical method for modeling the notch tip elastic-plastic stress-strain history in components subjected to cyclic non-proportional loads. The research is divided into two parts:

(i) the development of an simplified incremental model for predicting elastic-plastic parameters at the notch tip in bodies subjected to multiaxial non-proportional loading sequences, and

(ii) the use of an appropriate material model in conjunction with the method developed in (i) to define the elastic-plastic notch tip stress-strain response.

In Chapter Two, a more thorough description of the notch problem is presented along with a comprehensive review of the simplified methods developed to date for estimating notch root strain histories. The review encompasses uniaxial models, and multiaxial proportional and non-proportional models. In Chapter Three, two simplified models are proposed that allow for the determination of the notch tip elastic-plastic strain and total strain energy densities from an elastic analysis. In Chapter Four, material constitutive behaviour is reviewed with specific reference to modelling cyclic material behaviour. In Chapter Five, the two methods developed in Chapter

Three are coupled with the cyclic plasticity model chosen in Chapter Four, and the methods are then applied to both loading and unloading. The computer program developed for the application of both simplified models and some details associated with the numerical solution procedure are also presented. The results obtained using the proposed methods are compared with finite element and experimental data in Chapter Six. Chapter Seven contains some concluding remarks and recommendations for future research.

2. CHAPTER TWO:

BACKGROUND AND LITERATURE REVIEW

The presence of a notch or any other geometrical discontinuity acts to locally disturb the stress field. Specifically, a non-uniform triaxial stress field arises in the plane of the notch, with the highest stress concentration near the discontinuity. This type of stress field exists even when a unidirectional tensile load is applied to an elastic body (Fig. 2.1). At the notch tip, there is a constraint imposed on the local deformation in the direction transverse to the applied load by the lower stressed bulk material away from the higher stressed material in the immediate region of the notch. In response to this constraint, transverse stresses are induced at the notch tip.

As in any typical boundary value problem, the notch tip stress and strain components can be found by locally satisfying the equations of equilibrium, the material constitutive relations, the compatibility equations and the boundary conditions. However, in the case of a notched body, closed form solutions to such an equation set are generally not available. Theoretically, numerical techniques such as the finite element or the boundary element methods can be used to simultaneously satisfy the field equations at the notch tip. These techniques often become complex and impractical when the structures modeled are subjected to histories of multiaxial loads. Researchers that have aimed at defining the notch tip stress-strain state have therefore focused primarily on defining an alternate, simplified set of equations that will approximate the real behavior of the material.

The simplified set of relations generally consist of two key elements: the material constitutive relations and the approximation formulas. The approximation formulas relate the local elastic-plastic notch tip stress and strain components to those predicted in an elastic analysis. Since the

accepted constitutive relations are similar or the same, the differences in the simplified models proposed in the literature generally lie in the approximation formulas.

The number and form of the approximation formulas required to form the complete set of relations that will determine the notch tip stress-strain field is dependent on the stress state at the notch tip. In general, the state of stress at the notch root (a traction free surface) is biaxial (Fig. 2.2c). Thus in the most general case, seven notch tip parameters need be defined: three stresses and four strains. In the early development of simplified models, researchers made assumptions about the state of stress in the body so as to reduce the corresponding number of required equations. Uniaxial models were first considered and were governed by the assumption that the notched body was either in a plane stress or a plane strain state. Developments have more recently been made to account for notch root multiaxiality in bodies subjected to either uniaxial or multiaxial nominal loads.

2.1 Uniaxial Models

2.1.1 Body in Plane Stress

Assume that the body dimensions and external loads in Figure 2.2 are such that the notched body is in a state of plane stress. Because of the free surface and assumption of plane stress, the stress state at the notch tip is uniaxial. Following the notation in Figure 2.2, the stress field at the notch tip can be represented by

$$\sigma_{ij} = \begin{bmatrix} 0 & 0 & 0 \\ 0 & \sigma_{22} & 0 \\ 0 & 0 & 0 \end{bmatrix}, \tag{2.1}$$

and the components of strain by

$$\varepsilon_{ij} = \begin{bmatrix} \varepsilon_{11} & 0 & 0 \\ 0 & \varepsilon_{22} & 0 \\ 0 & 0 & \varepsilon_{33} \end{bmatrix}. \tag{2.2}$$

Thus, in the case of a body in plane stress, there are generally four unknown notch tip parameters, and four independent relations are required to define the local stress-strain field. The material constitutive relations will provide three independent relations between the stresses and the strains, and thus only one additional relation is required.

Prior to 1948, research pertaining to the analysis of stress in the vicinity of geometrical discontinuities assumed elastic material behavior. The research focused primarily on determining theoretical elastic stress concentration factors (K_t) from either photoelastic analysis or classical elasticity theory. The stress concentration factor is a relation between the elastic stress at the point of highest stress concentration in the direction of the applied load, and the nominal stress. Following the notation in Figure 2.2, a uniaxial tensile load will result in the following stress concentration factor at the notch tip

$$K_t = \frac{\sigma_{22}^{e}}{\sigma_{n.s.}}. \tag{2.3}$$

Here, and throughout this thesis, the superscript "e" refers to the assumption of elastic material behavior, and the subscript "n.s". refers to the nominal net sectional stress, which references the applied load and the body's cross-sectional dimensions in the plane of the notch. The stress concentration factor is a geometry and mode of loading dependent parameter and is independent of the properties of the material, provided that the body remains elastic. One of the most comprehensive compilations of theoretical stress concentration factors is given by Peterson [1].

In 1948, Griffith [2] tested large aluminum panels with central circular holes with the aim of investigating the effect of plastic flow on the stress concentration factor. His results suggested that after the onset of plastic flow at the hole tip, the stress concentration factor does not remain constant, but decreases. Furthermore, he found that the strain concentration factor, defined as the ratio of local strain to the net sectional strain, or

$$K_\varepsilon = \frac{\varepsilon^a_{22}}{\varepsilon_{n.s.}}, \tag{2.4}$$

increases at the onset of local plastic flow. Here, the superscript "a" refers to actual notch tip strain, whether it be elastic or elastic-plastic. Griffith's experimental investigation prompted the development of analytical models that accounted for local plastic flow which, similar to the elastic stress concentration factor, related the boundary conditions on the far field to those at the notch tip.

Hardrath and Ohman [3] tested large aluminum panels with edge notches and fillets and compared their results to a generalization of Stowell's [4] model, which was originally proposed for one specific notch geometry. The resulting expression, given in [3] as

$$\sigma_{22} = \frac{\sigma^e_{22}}{K_t} + \left(\sigma^e_{22} - \frac{\sigma^e_{22}}{K_t}\right)\frac{E_s}{E}, \tag{2.5}$$

where σ_{22} is the actual notch tip stress and E_s is the secant modulus, showed close agreement with the experimental results.

The most frequently used approximation formula that relates notch tip elastic-plastic strain and stress to nominal or applied values was originally proposed by Neuber [5]. In his study, Neuber analyzed a semi-infinite prismatic non-linear body with an edge crack or sharp ended notch subjected to an anti-plane pure shear loading (Fig. 2.3). It should be noted that, in the case of

pure shear loading, there are only two unknown parameters at the notch tip: one shear stress, and one shear strain. Neuber observed that the shear stress distribution ahead of a notch is identical to that ahead of a crack provided that the root radii of the notch and crack are the same, and furthermore that the product of stress and strain at the notch tip is not dependent on the material's non-linear parameters. Neuber proposed that the product of the stress and strain at the notch tip in any arbitrary notched geometry in a prismatic body subjected to an anti-plane pure shear load can be related to the material's elastic parameters and the far field boundary conditions. The relation developed, known as Neuber's rule, has recently [6] been written in the form

$$\sigma_{22}^{e}\,\varepsilon_{22}^{e} \;=\; \sigma_{22}^{N}\,\varepsilon_{22}^{N}\,, \tag{2.6}$$

for any body in plane stress. Here, and throughout this thesis, the superscript "N" refers to the elastic-plastic notch tip values as estimated by Neuber's rule. Equation (2.6) states that the actual total strain energy density (the sum of the strain energy density and the complementary strain energy density) at the notch tip is equal to that which would be obtained if the material were to remain elastic as the loads are applied. This additional energy relation can be used in conjunction with a uniaxial constitutive relation to define both the local elastic-plastic strain and the local stress components. A graphical representation of Neuber's rule is shown in Figure 2.4.

Papirno [7] compared the Hardrath-Ohman relation (eqn. 2.5) to Neuber's rule (eqn. 2.6) by comparing results obtained using both theories to those obtained in an experimental investigation of thin notched steel plates. In [7], Papirno concluded that Neuber's rule was more accurate.

Topper et al. [8] extended Neuber's rule to address several notched geometries in members subjected to cyclically applied uniaxial loads. Neuber's rule in its cyclic form was found to be in good agreement with experimental results for notched aluminum alloy sheets where plane stress conditions prevailed at the notch tip. Their results further suggested that smooth specimen

fatigue data could be used to estimate the fatigue life of notched aluminum components.

Lies et al. [9], Conle and Nowack [10], and Guillot and Sharpe [11] experimentally examined the applicability of Neuber's rule in quantifying notch tip inelastic strains and stress in thin aluminum and mild steel sheets for several loading sequences. Their results suggested that Neuber's rule tends to overestimate the notch tip stresses and strains.

Motivated by a crack tip stress analysis performed by Hutchinson [12], Molski and Glinka [13] postulated that, for a body in plane stress, the actual strain energy density at a notch tip is exactly the same as that if the body were to remain elastic. This method, known as the equivalent strain energy density (ESED) method, can be written in terms of stresses and strains as

$$\frac{1}{2}\sigma_{22}^{\epsilon}\,\varepsilon_{22}^{\epsilon} \;=\; \int_{0}^{\varepsilon_{22}^{E}} \sigma_{22}^{E}\, d\,\varepsilon_{22}^{E}\,. \tag{2.7}$$

Here, and throughout this thesis, the superscript "E" refers to the elastic-plastic notch tip stresses and strains as estimated by the ESED method. Equation (2.7) can be used in conjunction with the uniaxial stress-strain relations to determine the notch tip stress-strain field. It was shown [14] that the ESED method made it possible to calculate inelastic notch tip strains in several notched bodies subjected to monotonic loads under plane stress conditions. Glinka [15] later extended the ESED method to address bodies subjected to cyclically applied uniaxial loads and, furthermore, improved the original model by the addition of a factor that accounted for the stress redistribution due to local plastic yielding. It became apparent in [15] that the ESED method tends to underestimate the inelastic notch tip strains and stresses. A graphical representation of the ESED method is shown in Figure 2.5.

2.1.2 Body in Plane Strain

Assume that the body dimensions and external loads shown in Figure 2.2 are such that the body is in a state of plane strain. Because of the free surface, and the constraint imposed on the transverse strain components by assuming the body to be in plane strain, the state of stress at the notch tip is biaxial. Following the notation in Figure 2.2, the stress field at the notch tip can be represented by

$$\sigma_{ij} = \begin{bmatrix} 0 & 0 & 0 \\ 0 & \sigma_{22} & 0 \\ 0 & 0 & \sigma_{33} \end{bmatrix}, \tag{2.8}$$

and the components of strain by

$$\varepsilon_{ij} = \begin{bmatrix} \varepsilon_{11} & 0 & 0 \\ 0 & \varepsilon_{22} & 0 \\ 0 & 0 & 0 \end{bmatrix}. \tag{2.9}$$

As in the case of plane stress, there are four unknown notch tip components, and thus four equations are required to define the local stress-strain state. Since the material constitutive relations will provide three, only one additional relation is required. Therefore, the case of plane strain is considered to be a uniaxial model. However, the plane strain simplified models must differ from the plane stress models since, in the case of plane strain, the existing transverse component of stress is affected by the aforementioned notch tip constraint and must be considered in the development.

In order to account for this constraint, Walker [16], Dowling et al. [17] and Gemma [18] assumed that Neuber's rule could be used in its original form provided that the notch root constraint was considered in the material constitutive relations.

Fuchs and Stephens [19] revised Neuber's rule itself with a factor that accounted for the notch root constraint. However, in an experimental investigation of the method, Sharpe and Wang [20] found little improvement over the original Neuber's rule when the notch tip strains became plastic.

Following the approach proposed by Dowling et al. [17]. Glinka et al. [21] showed that the ESED relation (2.7) could be used in conjunction with the modified uniaxial stress-strain curve defined in [17] to solve for the stress and strain components in the direction of the applied load for any material model.

Currently, either Neuber's rule or the ESED method are being used in notch tip stress-strain analysis. Sharpe et al. [22] compared Neuber's rule and the ESED method with experimental results on various notched geometries. The results of their study indicate that Neuber's relation should be used when a body is in a plane stress state, and the ESED plane strain model when there is a large constraint at the notch tip. Tipton [23] presented a review article on the development and use of Neuber's rule for fatigue analysis.

2.2 General Body Stress State

In general, the state of stress near the notch tip is triaxial at the notch tip, biaxial due to the free surface. With the reference axes chosen as in Figure 2.2, the biaxial stress field at the notch tip can be represented by

$$\sigma_{ij} = \begin{bmatrix} 0 & 0 & 0 \\ 0 & \sigma_{22} & \sigma_{23} \\ 0 & \sigma_{32} & \sigma_{33} \end{bmatrix}, \tag{2.10}$$

and the components of strain by

$$\varepsilon_{ij} = \begin{bmatrix} \varepsilon_{11} & 0 & 0 \\ 0 & \varepsilon_{22} & \varepsilon_{23} \\ 0 & \varepsilon_{32} & \varepsilon_{33} \end{bmatrix}. \tag{2.11}$$

Since equilibrium of the element at the notch tip is assumed, $\sigma_{23} = \sigma_{32}$, and $\varepsilon_{23} = \varepsilon_{32}$. Thus, there are seven unknowns at the notch tip: three stresses and four strains. Therefore, a set of seven independent equations are required to completely define the stress-strain state at the notch tip. The material constitutive relations will provide four equations, so that three additional relations are required.

The type of simplified equation set required to define the notch tip stress-strain state is dependent on how the deviatoric stress tensor at the notch tip increases with the applied load. If it increases proportionally, deformation plasticity can be used in the formulation and if not, the final notch tip stress state is dependent on the loading path and the relations must be developed in an incremental form.

2.2.1 Proportional Models

If either a uniaxial or multiaxial proportional loading system is applied to a notched body, it is generally assumed that the deviatoric stresses at the notch tip remain in nearly fixed proportion throughout the loading history.

A generalization of Neuber's rule proposed by Hoffmann and Seeger [24,25] addresses multiaxial proportional loading sequences. In their study, Hoffmann and Seeger extend Neuber's rule by replacing the uniaxial stress and strain with equivalent stress and strain, as

$$\sigma^a_{eq}\,\varepsilon^a_{eq} \;=\; \sigma^e_{eq}\,\varepsilon^e_{eq}\,, \tag{2.12}$$

where $\varepsilon_{eq}{}^a$ and $\sigma_{eq}{}^a$ are the notch tip elastic-plastic equivalent strain and stress respectively, and $\varepsilon_{eq}{}^e$ and $\sigma_{eq}{}^e$ are those which would be obtained in an elastic analysis. They define two additional relations based on the assumptions that (i) the actual principal directions are identical to those that would be obtained in an elastic analysis, and (ii) that the ratio of the minimum principal strain components at the notch tip remain constant during loading. It should be noted that this generalization neglects the hydrostatic component of stress and cannot be reduced to any of the aforementioned plane strain models.

In a recent study, Moftakhar [6] analyzed the behavior of two identical notched geometries subjected to the same traction boundary conditions. One body was made of an elastic-plastic material while the other was made of an elastic material, having the same elastic constants as the elastic-plastic body. In his analysis, he showed that if the notch tip deviatoric stress tensor remains in fixed proportion throughout the loading history, and if the plasticity at the notch tip in the elastic-plastic body is localized, then the total strain energy density (Ω^e) at the notch tip in the elastic body is always greater than that in the actual elastic-plastic body (Ω^a), or,

$$\Omega^e \;\geq \Omega^a\,, \tag{2.13}$$

where (Ω^e) and (Ω^a) are defined as

$$\Omega^e \;=\; \sigma^e_{ij}\,\varepsilon^e_{ij} \;\text{ and }\; \Omega^a \;=\; \sigma^a_{ij}\,\varepsilon^a_{ij}\,, \tag{2.14}$$

and i,j = 1,2,3 and summation is implied. Inequality (2.13) suggests that the total strain energy

density at the notch tip in an elastic-plastic body is less than the total strain energy density at the notch tip if the body were to remain elastic.

In [6], it was concluded that inequality (2.13) is a generalized form of Neuber's rule for a notched body subjected to a multiaxial proportional loading sequence. This conclusion was based on three factors. Firstly, as in the uniaxial case, inequality (2.13) represents an elastic approximation to the actual total strain energy density at the notch tip. Secondly, inequality (2.13) reduces to Neuber's rule in its uniaxial form (eqn.2.6) when a plane stress or plane strain state is assumed. Finally, inequality (2.13) suggests that the elastic approximation will yield an upper limit on the total strain energy density at the notch tip. This is consistent with the aforementioned numerical and experimental results for notched bodies subjected to uniaxial loads, which conclude that Neuber's rule tends to overestimate the notch tip elastic-plastic strains and stresses. The generalization of Neuber's rule in the form of eqn.(2.13) is also suggested by Lemaitre and Chaboche [26].

Similarly, in [6], it was proven that for the case of proportional loading, the equivalent strain energy density at the notch tip in the elastic body, $W^e(\varepsilon)$, is always less than that at the notch tip in the actual elastic-plastic body, $W^a(\varepsilon)$, or

$$W^e(\varepsilon) \leq W^a(\varepsilon), \tag{2.15}$$

where $W^e(\varepsilon)$ and $W^a(\varepsilon)$ are defined as

$$W^e(\varepsilon) = \frac{1}{2}\sigma_{ij}^e \varepsilon_{ij}^e \quad , \quad W^a(\varepsilon) = \int_0^{\varepsilon_{ij}^a} \sigma_{ij}^a \, d\,\varepsilon_{ij}^a . \tag{2.16}$$

Inequality (2.15) suggests that the strain energy density at the notch tip in an elastic-plastic body is greater than the strain energy density at the notch tip if the body were to remain elastic.

In [6] it is concluded that inequality (2.15) represents the generalized form of the ESED method for a notched body subjected to a multiaxial proportional loading system. The justification for this conclusion was similar to that given for the generalized form of Neuber's rule. That is, inequality (2.15) represents an elastic approximation to the actual strain energy density at the notch tip, it reduces to its uniaxial form (eqn. 2.7) when plane stress or plane strain is assumed, and the inequality in (2.15) agrees with uniaxial numerical and experimental studies that conclude that the ESED method tends to underestimate notch tip inelastic strains and stresses.

In [6], the two additional equations required to define all notch tip stress and strain components were based on the assumption that the contribution of each stress-strain component to the total strain energy density at the notch tip is the same in the elastic case as is in the elastic-plastic case. They used the resulting two equations in conjunction with either energy model and Henky's total deformation flow rule to define the complete elastic-plastic notch tip stress-strain state.

Numerical and experimental studies were conducted (Moftakhar and Glinka [27], Moftakhar et al. [28], Sørbø and Härkegård [29]) and the results showed that generalized Neuber's rule (eqn.2.13) will predict an upper bound, and the generalized ESED (eqn.2.15) a lower bound approximation to the actual notch tip stresses and strains.

2.2.2 Non-Proportional Models

When an external loading system is applied to a notched body in a non-proportional manner, the resulting notch tip stresses and strains do not behave proportionally, and simplified models must be developed in an incremental form.

Hoffmann et al. [30] presented a simplified model to estimate notch root elastic-plastic stresses and strains in bodies subjected to non-proportional loading systems. In their model, the notch root strain history is calculated for each mode of loading by following the same solution procedure as in [24] and [25] for proportional loading. A compatibility iteration is subsequently used to account for the interaction between the strain components that arises in non-proportional loading. Their calculations compared well with finite element results.

More recently, Barkey et al. [31,32] presented a method for estimating elastic-plastic notch tip strains in notched bars subjected to cyclic proportional and non-proportional loading sequences. In their method, they incorporate the effect of the notch directly into the constitutive relations. This is done by defining an anisotropic structural yield surface in nominal stress space. The hardening parameter is found by using the uniaxial form of the ESED method to construct a uniaxial nominal load-notch plastic strain curve. Their results compared well with experimental non-proportional tension-torsion tests on a notched steel bar. However, the method does not account for elastic coupling at the notch root between any two nominal stresses (for example, in the case of combined bending and axial loading of a notched round bar).

Following the same approach as in [31] and [32], Köttgen et al. [33] incorporated the notch effect into the constitutive relations. They did this by first obtaining a "pseudo" stress history by assuming elastic material behavior. The yield criterion and multi-surface type flow rule were written in terms of the elastic history, with the hardening parameter obtained using a pseudo stress versus local plastic strain curve obtained using a uniaxial simplified rule. The resulting elastic-plastic strain increments were subsequently fed back into the flow rule (written in terms of true stresses) to obtain the notch tip stress history. They also proposed a similar method starting

with a "pseudo" strain history, defined similar to the "pseudo" stress history.

Lee et al. [34] and Gu and Lee [35] proposed a similar approach as above for non-proportional loading. The main difference between each approach is in the plasticity model used. Specifically, in [34], a two surface kinematic and in [35], an endochronic plasticity model is utilized.

In [36] and [37], Singh et al. proposed a method for estimating notch root strains in bodies subjected to non-proportional monotonic loading sequences. The approach is an incremental generalization of the ESED method and Neuber's rule. The resulting set of algebraic equations are relatively simple to solve, and the results compared well with those obtained in a finite element analysis.

2.3 Conclusions of the Literature Review

The underlying premise of virtually all simplified models for predicting notch root stress-strain behavior is that a relationship exists between the stress state at the notch tip predicted by elastic-plastic theory and that predicted by linear elastic theory. This approach can be justified assuming that the notch tip plastic zone is localized and highly controlled by the relatively large surrounding elastic field. This localized plasticity assumption is consistent with the philosophy of the strain-life method of fatigue analysis.

For the case when the notched body is in a state of either plane stress or plane strain, it is generally accepted that either Neuber's rule or the ESED method can be used in conjunction with the material flow rule to approximate the complete notch tip elastic-plastic stress-strain behavior.

Multiaxial notch tip stress states have only recently been addressed. For proportional loading sequences, the generalizations of Neuber's rule and the ESED method recently proposed in [6] are superior to others since they predict a band between which the actual notch tip stresses and strains will always fall. Specifically, it predicts that this band is bounded on the lower end by the notch tip stress-strain state predicted by the generalized ESED method, and on the upper end by that predicted by the generalized Neuber's rule.

Simplified models for multiaxial non-proportional loading sequences have only recently appeared in the literature. Since no one model has been generally accepted, there continues to be a rigorous effort by researchers to develop theory in this area.

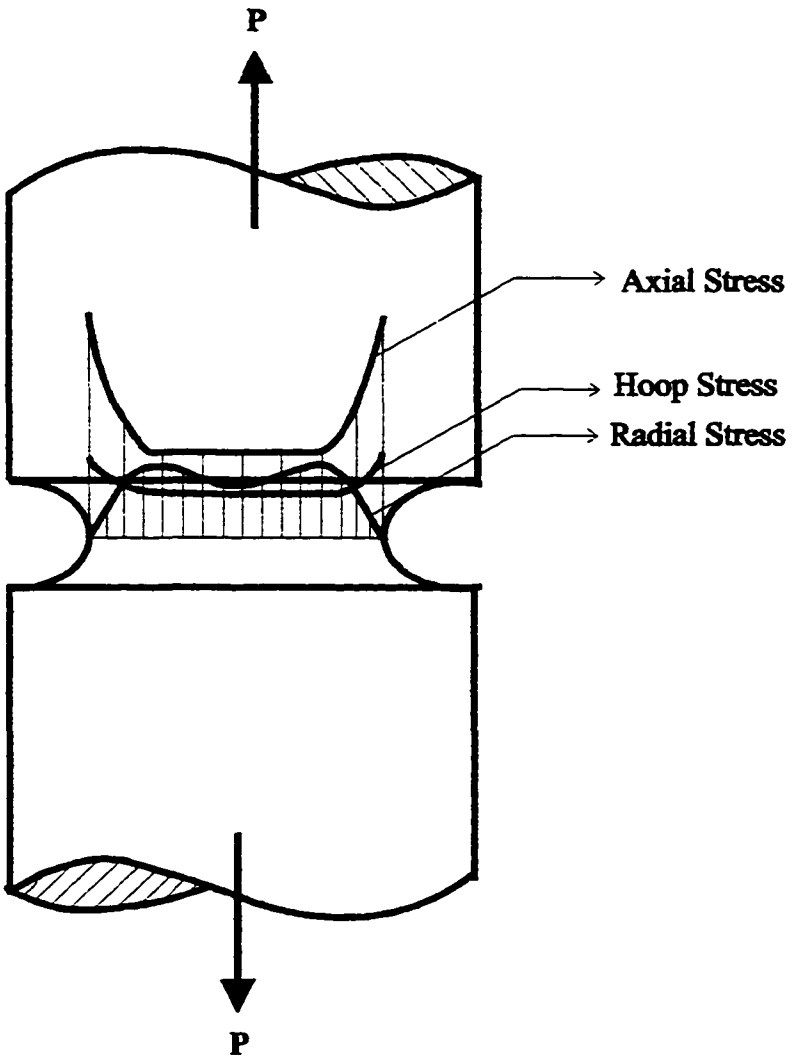
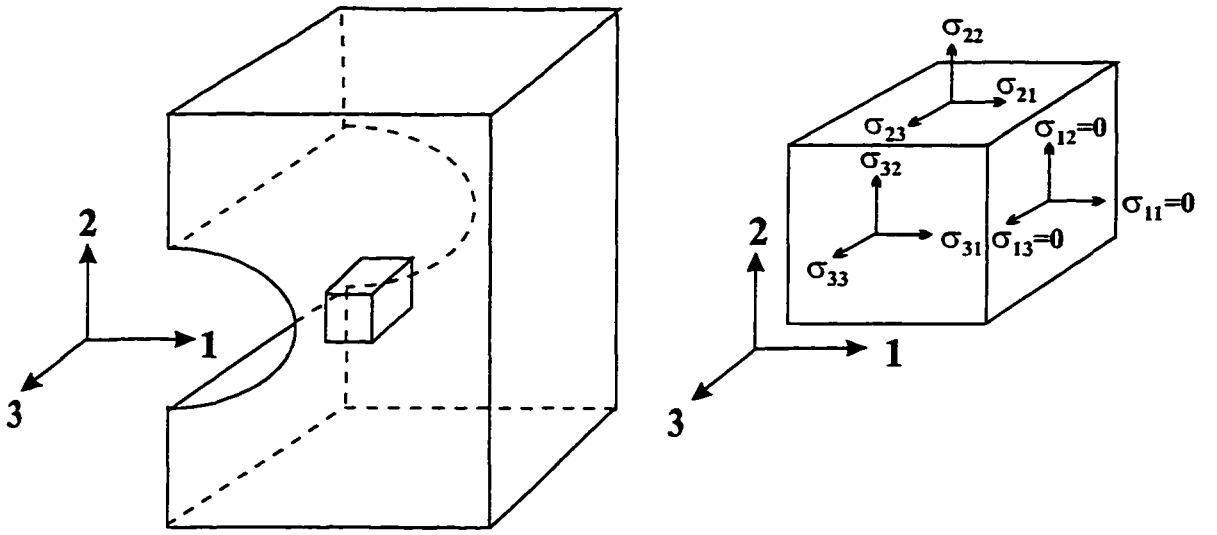


Figure 2.1: Elastic Stress Distribution in a Notched Bar Subjected to a Tensile Load



$$\sigma_{ij} = \begin{vmatrix} 0 & 0 & 0 \\ 0 & \sigma_{22} & 0 \\ 0 & 0 & 0 \end{vmatrix} \qquad \sigma_{ij} = \begin{vmatrix} 0 & 0 & 0 \\ 0 & \sigma_{22} & 0 \\ 0 & 0 & \sigma_{33} \end{vmatrix} \qquad \sigma_{ij} = \begin{vmatrix} 0 & 0 & 0 \\ 0 & \sigma_{22} & \sigma_{23} \\ 0 & \sigma_{32} & \sigma_{33} \end{vmatrix}$$

$$\varepsilon_{ij} = \begin{vmatrix} \varepsilon_{11} & 0 & 0 \\ 0 & \varepsilon_{22} & 0 \\ 0 & 0 & \varepsilon_{33} \end{vmatrix} \qquad \varepsilon_{ij} = \begin{vmatrix} \varepsilon_{11} & 0 & 0 \\ 0 & \varepsilon_{22} & 0 \\ 0 & 0 & 0 \end{vmatrix} \qquad \varepsilon_{ij} = \begin{vmatrix} \varepsilon_{11} & 0 & 0 \\ 0 & \varepsilon_{22} & \varepsilon_{23} \\ 0 & \varepsilon_{32} & \varepsilon_{33} \end{vmatrix}$$

a) b) c)

Figure 2.2: State of Stress at the Notch Tip a) Plane Stress, b) Plane Strain, c) In General

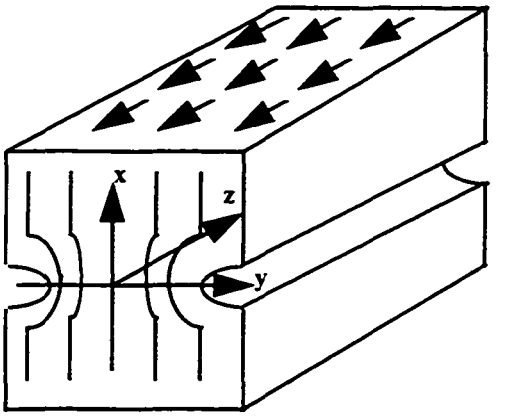


Figure 2.3: Geometry Used in Neuber's Analysis [5]

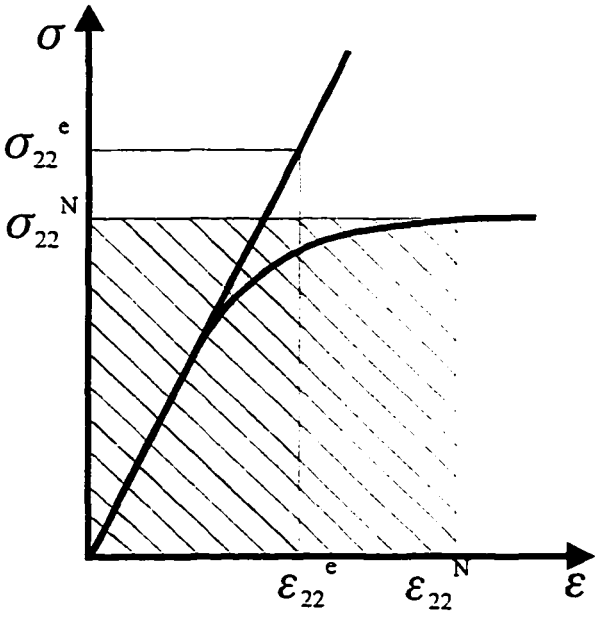


Figure 2.4: Neuber's Rule

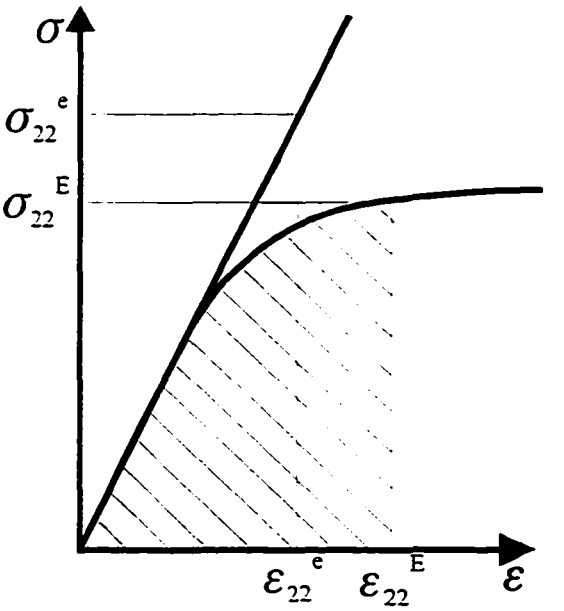


Figure 2.5: Equivalent Strain Energy Density (ESED) Method

3. CHAPTER THREE:

PROPOSED MULTIAXIAL MODEL

The objective of the proposed research is to develop and implement a simple yet sufficiently accurate method for determining the elastic-plastic strains and stresses at the notch tip of bodies subjected to non-proportional cyclic loading sequences. In Chapter Two, it was shown that in order to completely describe notch tip elastic-plastic behavior, a set of seven independent equations is required. In this Chapter, the three equations based on the strain energy density principles published in [36] and [37] are presented. The remaining four of these equations can be found by applying an appropriate constitutive model, as will be detailed in Chapter Four.

All simplified models proposed to date have used an elastic notch tip stress-strain analysis to predict actual elastic-plastic notch tip behavior. However, due to the differences between elastic and elastic-plastic material behavior, it is impossible to derive exact relationships between stress-strain fields obtained from a linear elastic analysis and those obtained from an elastic-plastic analysis. Thus, two models are presented here to address notched bodies subjected to non-proportional monotonic loading sequences. These models have their roots in the equivalent strain energy density (ESED) method and Neuber's rule and will be categorized accordingly in the following sections.

3.1 Incremental Equivalent Strain Energy Density (ESED) Relations

Consider two geometrically identical notched bodies subjected to the same traction boundary conditions as shown in Figure 3.1. Let one body be made of an elastic-plastic material, and the

other of an elastic material, both having the same elastic constants. In [13] it was shown that the strain energy density at the notch tip in an elastic-plastic body can be approximated by that obtained at the notch tip in the elastic body if the external loads in the two bodies remain the same throughout a uniaxial loading history.

In a body subjected to a non-proportional loading system, the strain state is dependent on the applied loading path. Thus, equations that describe the behavior of the strain energy density at a notch tip in an elastic-plastic body must be calculated at each instant of loading. In this section, the ESED method will be developed in an incremental form such that the path dependent nature of the material subjected to a non-proportional loading path is respected.

Assume that a notched body, such as either shown in Figure 3.1, has been loaded from zero to a known reference state. If an increment of load is applied to the body, there will be a corresponding increase in strain energy in the body. This increment in energy per unit volume on any element of the body during straining can be written as

$$dW^a = \sigma_{ij}^a \, d\varepsilon_{ij}^a, \tag{3.1}$$

where W denotes the strain energy density in the element, and the superscript "a" refers to the actual elemental values, whether they be elastic or elastic-plastic.

Consider now an element at the notch tip in the elastic-plastic body in Figure 3.1b. Assume that (i) the nominal stresses are elastic and (ii) if the notch tip strains are plastic, the notch tip behavior is largely controlled by that of the surrounding elastic field. Under these assumptions, it is proposed that for a given increment in external load, the corresponding increment in the strain

energy density at the notch tip in the elastic-plastic body can be approximated by that obtained if the body were to remain elastic throughout the loading history (Fig. 3.1a). This proposal can be expressed as

$$\begin{aligned} dW^e &= dW^E \\ &\text{or} \\ \sigma_{ij}^e \, d\varepsilon_{ij}^e &= \sigma_{ij}^E \, d\varepsilon_{ij}^E \end{aligned} \qquad (3.2)$$

In equation (3.2), the superscript "e" refers to hypothetical elastic behavior and the superscript "E" refers to elastic or elastic-plastic values as approximated by the proposed energy method.

Equation (3.2) can be called a generalized incremental form of the equivalent strain energy density method since it reduces to the original form of the ESED method (eqn.2.7) for uniaxial notch tip stress states. Furthermore, it represents a statement of equality between the notch tip strain energy density obtained from a linear elastic solution and that obtained from an elastic-plastic analysis.

It should be noted that eqn.(3.2) implies that, at the end of a load path, the sum of the increments in the actual strain energy density is approximated by the sum of the increments in the load path independent elastic strain energy density. As such, if eqn.(3.2) holds true for non-proportional loading, then the assumption must be made that the strain energy density is insensitive to the applied loading path. This can be primarily justified by the assumption of localized plasticity. Furthermore, it has been shown numerically in [6] that, for a given proportional loading sequence, the strain energy density is somewhat insensitive to the slight non-proportionality in the notch tip deviatoric stresses.

If the strain energy density is, in fact, truly insensitive to the applied load path, it should follow that the inequality developed in [6] (eqn.2.15) for notched bodies subjected to proportionally applied loads should also hold at the end of a non-proportional loading path. That is, the sum of the increments in the strain energy density over the loading path calculated using the ESED method should form a lower bound elastic approximation to the actual strain energy density at the end of the loading path.

The constitutive relations used in conjunction with the generalized ESED method will be sufficient to describe only five of the seven unknown notch tip stress-strain increments. Therefore, two more independent equations are required to completely define the notch tip stress-strain state for a given increment in the applied load. For this purpose, it is proposed that the contribution of each elastic-plastic stress-strain component to the increment in strain energy density at the notch tip is the same as the contribution of each stress-strain component to the increment in strain energy density at the notch tip given that the body were to remain elastic during the loading history. This proposal can be expressed as

$$\frac{\sigma^{e}_{\alpha\beta} d\varepsilon^{e}_{\alpha\beta}}{\sigma^{e}_{ij} d\varepsilon^{e}_{ij}} = \frac{\sigma^{E}_{\alpha\beta} d\varepsilon^{E}_{\alpha\beta}}{\sigma^{E}_{ij} d\varepsilon^{E}_{ij}} . \tag{3.3}$$

In eqn.(3.3), i,j,α,β = 1, 2, 3, and summation over i and j is implied, but not over α and β. It should be noted that, although eqn.(3.3) implies three relations at the notch tip, only two are independent. Equation (3.3) is also supported by Chu and Conle [38], who presented preliminary results comparing some proportional results of a similar "work path" equation to two other hypothesized additional equations.

If eqn.(3.3) is used in conjunction with eqn.(3.2), then eqns.(3.3) become

$$\sigma^{e}_{\alpha\beta}\, d\varepsilon^{e}_{\alpha\beta} = \sigma^{E}_{\alpha\beta} d\varepsilon^{E}_{\alpha\beta} \quad . \tag{3.4}$$

A graphical representation of the three relations implied by eqn.(3.4) is shown in Figure 3.2a.

3.2 Incremental Neuber's Rule

Consider again the two notched bodies shown in Figure 3.1. Neuber's rule (eqn.2.6) is a statement of equality between the total strain energy density at the notch tip in the elastic-plastic body and at the notch tip in the elastic body, when the loads applied to both geometrically identical bodies remain the same and uniaxial. Neuber's rule was later generalized [6] to address notched bodies subjected to multiaxial proportional loading sequences. In order to account for the path dependent nature of the notch tip strains when the external loads are applied in a non-proportional manner, Neuber's rule will be developed here in an incremental form.

If an increment in load is applied to a body, there will be a corresponding increment in the total strain energy in the body. The total strain energy refers to the sum of the strain energy density (as described above) and the complementary strain energy density. This increase in total strain energy per unit volume on any element of the body during straining can be written as

$$d\Omega^{a} = \sigma^{a}_{ij} d\varepsilon^{a}_{ij} + \varepsilon^{a}_{ij} d\sigma^{a}_{ij}\,, \tag{3.5}$$

where Ω denotes the total strain energy density in the element, and again, the superscript "a" refers to the actual elemental values, whether they be elastic or elastic-plastic.

Consider again an element at the notch tip in Figure 3.1b. Assume that the nominal stresses are elastic and that if the notch tip strains are plastic, the notch tip behavior is largely controlled by that of the surrounding elastic field. Under these assumptions, it is proposed that for a given increment in external load, the corresponding increment in the total strain energy density at the notch tip in the elastic-plastic body (Fig 3.1b) can be approximated by that obtained if the body were to remain elastic throughout the loading history (Fig 3.1a). Mathematically, this proposal can be written as

$$d\Omega^e = d\Omega^N$$

$$\text{or} \qquad (3.6)$$

$$\sigma_{ij}^e \, d\varepsilon_{ij}^e + \varepsilon_{ij}^e \, d\sigma_{ij}^e = \sigma_{ij}^N \, d\varepsilon_{ij}^N + \varepsilon_{ij}^N \, d\sigma_{ij}^N$$

In eqn.(3.6), the superscript "e" refers to hypothetical elastic behavior and the superscript "N" refers to elastic or elastic-plastic values as approximated by the proposed energy method.

Equation (3.6) can be called a generalized form of Neuber's rule since it reduces to Neuber's rule in its original form (eqn.2.6) for uniaxial notch tip stress states. Furthermore, it represents a statement of equality between the notch tip total strain energy density obtained from a linear elastic solution and that obtained from an elastic-plastic analysis.

It should be noted that eqn.(3.6) implies that at the end of a load path, the sum of the increments in the actual total strain energy density is approximated by the sum of the increments in the load path independent elastic total strain energy density. As such, if eqn.(3.6) holds true for non-proportional loading, then the assumption must be made that the total strain energy density is insensitive to the applied loading path. Again, this assumption can be justified by the localized

plasticity assumption and further that it has been shown numerically in [6] that for a given proportional loading sequence, the total strain energy density is somewhat insensitive to the non-proportionality in the notch tip deviatoric stresses.

If the total strain energy density is actually insensitive to the loading path, it should follow that the inequality developed in [6] (eqn.2.13) should also hold at the end of a non-proportional loading path. That is, the sum of the increments of the total strain energy density over the loading path calculated using the incremental Neuber's method, should form an upper bound elastic approximation to the actual total strain energy density at the end of the loading path.

The constitutive relations used in conjunction with the generalized Neuber's rule will only be sufficient to describe five of the seven unknown notch tip stress-strain increments. Therefore, two more independent equations are required to completely define the notch tip stress-strain state for a given increment in the applied load. For this purpose, it is proposed that the contribution of each elastic-plastic stress-strain component to the total strain energy density at the notch tip is the same as the contribution of each stress-strain component to the total strain energy density at the notch tip given that the body were to remain elastic during the loading history. This proposal can be expressed as

$$\frac{\sigma^{e}_{\alpha\beta}\, d\varepsilon^{e}_{\alpha\beta} + \varepsilon^{e}_{\alpha\beta}\, d\sigma^{e}_{\alpha\beta}}{\sigma^{e}_{ij}\, d\varepsilon^{e}_{ij} + \varepsilon^{e}_{ij}\, d\sigma^{e}_{ij}} = \frac{\sigma^{N}_{\alpha\beta}\, d\varepsilon^{N}_{\alpha\beta} + \varepsilon^{N}_{\alpha\beta}\, d\sigma^{N}_{\alpha\beta}}{\sigma^{N}_{ij}\, d\varepsilon^{N}_{ij} + \varepsilon^{N}_{ij}\, d\sigma^{N}_{ij}} \quad . \tag{3.7}$$

As in eqn.(3.3), in eqn.(3.7) i,j,α,β = 1, 2, 3, summation is implied over i and j but not over α and β. If eqn.(3.7) is used in conjunction with the generalized Neuber's rule, then combining eqns.(3.6) and (3.7) yields the following

$$\sigma^{e}_{\alpha\beta}\, d\varepsilon^{e}_{\alpha\beta} + \varepsilon^{e}_{\alpha\beta}\, d\sigma^{e}_{\alpha\beta} = \sigma^{N}_{\alpha\beta} d\varepsilon^{N}_{\alpha\beta} + \varepsilon^{N}_{\alpha\beta} d\sigma^{N}_{\alpha\beta} \quad . \tag{3.8}$$

The three relations implied by eqn.(3.8) are illustrated in Figure 3.2b.

3.3 Comparison of Proposed Methods with Finite Element Data

In this section, the accuracy of the proposed generalized ESED method and Neuber's rule are assessed by comparing various notch tip parameters obtained using the models to those obtained using the finite element method (FEM). The FEM elastic-plastic results were obtained using the ABAQUS [39] finite element package.

The geometry of the chosen model is that of the circumferentially notched bar shown in Figure 3.3. Loads applied to the bar were chosen to be tension and torsion, applied along various non-proportional monotonic loading paths. Because of symmetry, only half of the bar was modeled (Fig. 3.4). The torsional load was applied in terms of displacement boundary conditions on the end nodes, and the tensile load in terms of pressure on the faces of the end elements. The nominal torsional, $\tau_{n.s.}$, and tensile, $\sigma_{n.s.}$, stresses are defined as

$$\sigma_{n.s.} = \frac{P}{\pi (R - t)^2} \; ; \; \tau_{n.s.} = \frac{2\,T}{\pi (R - t)^3} \; , \tag{3.9}$$

where P and T are the applied tensile and torsional loads respectively, R is the radius of the bar, and t is the depth of the notch (Fig. 3.3). The elastic stress concentration factors of the notched bar were determined by carrying out two elastic FEM analyses. In the first, an arbitrary tensile load was applied to the bar and the axial and transverse stress concentrations were found to be

$\sigma_{22}^e/\sigma_{n.s.}$ =3.31 and $\sigma_{33}^e/\sigma_{n.s.}$ =0.94, respectively. In the second analysis, an arbitrary torsional load was applied to the bar and the shear concentration was found to be $\sigma_{23}^e/\tau_{n.s.}$ =1.94. The directions denoted are those shown in Figure 2.2.

Two analyses were carried out on the notched bar. The first analysis was designed to test the hypothesis on which both the incremental ESED (eqn. 3.2) and Neuber's (eqn. 3.6) equations are based: the energy densities are somewhat insensitive to the applied loading path. It was further designed to test the corollary of this hypothesis. That is, for non-proportional loading, the ESED method represents a lower bound elastic approximation to the actual notch tip energy density and Neuber's rule represents an upper bound elastic approximation to the actual notch tip total strain energy density. The second analysis was designed to assess the hypothesis that the contributions of each of the axial stress-strain components to the energy densities at the notch tip is the same in the elastic and elastic-plastic bodies (ie. eqns.3.3 and 3.7).

3.3.1 Energy Density Sensitivity to Load Path

3.3.1.1 Material Model

The material of the bar was chosen to have a tri-linear stress-strain curve (Fig. 3.5), defined as

$$\varepsilon = \frac{\sigma}{E} \quad \text{for } \sigma \leq \sigma_o$$

$$\varepsilon = \frac{\sigma_o}{E} + \frac{\sigma - \sigma_o}{H} \quad \text{for } \sigma_o \leq \sigma \leq \sigma_1 \qquad (3.10)$$

$$\sigma = \sigma_1 \quad \text{elsewhere}$$

$$\frac{H}{E} = .009 : \frac{\sigma_o}{E} = .0058 ; \ \sigma_o = 550 \text{ MPa} ; \ \sigma_1 = 600 \text{ MPa}$$

It should be noted that the slope of the plastic portion of the uniaxial curve is very small. This was chosen to highlight the numerical error in the proposed methods, since in this case, a small increment in applied load will result in a large increment in the strains.

3.3.1.2 Method of Analysis and Results

The elastic-plastic FEM model was analyzed for the tension-torsion (Fig. 3.6a), torsion-tension (Fig. 3.6b), and for comparison, the proportional (Fig. 3.6a,b) loading paths. In each case, the strain energy density, W^{FEM}, and the total strain energy density Ω^{FEM}, at the end of loading paths 1 through 12 were noted. The ESED (W^E) and Neuber's (Ω^N) elastic approximations to the energy densities were calculated based on eqns. (3.2) and (3.6) respectively, and knowing the elastic stress concentration factors and the applied loads. Between subsequent load paths, the ratio of the final applied nominal tensile to torsional stresses was kept constant, but the final magnitudes of each stress was increased. This procedure was repeated until the applied loads were sufficient to cause general yielding in the net section at the end of the loading paths (path 12). Since tensile and torsional stresses have different contributions to plasticity (and hence

energy densities), three different ratios of tensile to torsional net section stress at the end of the loading path were analyzed: $\sigma_{n.s.}{}^{f}/\tau_{n.s.}{}^{f} = 0.32$, 1.1, and 3.2.

The strain energy density (W^{FEM}) and the total strain energy density (Ω^{FEM}) determined from the elastic-plastic FEM analyses, and the predictions of the ESED method (W^{E}) and Neuber's rule (Ω^{N}) are plotted at the end of the loading paths. These are plotted against the normalized nominal equivalent net sectional stress S_{eq}/σ_o defined as

$$\frac{S_{eq}}{\sigma_o} = \frac{\sqrt{\sigma_{n.s.}^2 + 3\tau_{n.s}^2}}{\sigma_o} \quad . \tag{3.11}$$

Plots of the energy densities against S_{eq}/σ_o are shown in Figs. 3.7, 3.8 and 3.9 for the ratios of $\sigma_{n.s.}{}^{f}/\tau_{n.s.}{}^{f} = 0.32$, 1.1, and 3.2 respectively. Since all figures have the same general trend, the results pertaining to the sensitivity of the energy densities to loading path will first be discussed followed by those pertaining to the applicability of the upper and lower bound energy elastic approximations to the analyzed non-proportional loading sequences.

Sensitivity to Loading Path

In general, up until the point of yielding at the notch tip, the strain energy densities are the same for both loading sequences. This is expected since the final stress-strain state is load-path independent in the elastic range. Just after the final net sectional stresses sufficient to insure notch tip plasticity, the energy densities for each loading path begin to diverge. The divergence becomes more pronounced as the final equivalent net section stress ratio (S_{eq}/σ_o) increases.

It is noted that the divergence of the energy plots between each loading sequence becomes more

pronounced as the ratio of $\sigma_{n.s.}^{f}/\tau_{n.s.}^{f}$ increases. Furthermore, it is observed that the total strain energy density seems to be less sensitive to loading path than is the strain energy density. For $\sigma_{n.s.}^{f}/\tau_{n.s.}^{f} = 0.32$, the differences in the energies between the loading paths is negligible up until almost general yielding of the net section, but the difference is higher for the ratios of 1.1 and 3.2, and is most pronounced in the strain energy density plots (Figs 3.8b, 3.9b). However, it should be noted that for $\sigma_{n.s.}^{f}/\tau_{n.s.}^{f} = 3.2$, the difference in the strain energy density (Fig. 3.9b) between each loading sequence for $S_{eq}/\sigma_o \sim 1$ (indicating general yielding of the net section) is only 10%. This 10% divergence will result in a very small difference in notch tip stress and strain components. Moreover, in reality, general yielding conditions in the net section need not be analyzed using simplified models since the governing assumption of localized plasticity is violated.

Figures 3.10 show the plots of the energy densities as the loads are increased from zero following the tension-torsion and torsion-tension load paths 11 with a final ratio of $\sigma_{n.s.}^{f} / \tau_{n.s.}^{f} = 1.1$. In both Figures 3.10a and 3.10b, the energy densities for both loading sequences are different throughout the loading history. These converge at the end of the loading paths, when the final magnitudes of both tension and torsional net sectional stress are the same. These plots further highlight the relative insensitivity of the final energy densities to loading sequence.

Applicability of Energy Band

In all figures, it is observed that up until the point of yielding, both generalized elastic solutions are identical to the finite element results for both loading sequences. This is expected since the stress and strain components are independent of loading path in the elastic range. After the onset of plasticity at the notch tip, the actual results diverge from the approximate solutions.

Comparing the energy densities as the ratio $\sigma_{n.s.}{}^{f}/\tau_{n.s.}{}^{f}$ increases (as the amount of tension increases relative to the torsion), it is observed that the equivalent normalized net section stress ratio necessary to violate the generalized Neuber's elastic solution increases. This is expected since a torsional stress will induce plasticity sooner than a tensile stress and this would occur even if loads were being applied in a proportional manner.

For the ratio $\sigma_{n.s.}{}^{f}/\tau_{n.s.}{}^{f} = 1.1$, the model was also analyzed for a proportionally applied load. In Figure 3.8a, it can be seen that for the most part, the proportional results are virtually the same as the non-proportional results. However, the non-proportionally applied loading sequence results in the violation of the Neuber's solution at a lower S_{eq}/σ_o ratio than for the proportional results. The strain energy densities (Fig. 3.8b) in the case of the proportional load are lower, and thus better predicted by the ESED solution, than they are in the case of a non-proportionally applied load. However, again the difference in the results between all loading paths is small until almost general yielding of the net section.

In all plots, it is noted that the generalized Neuber's rule forms the upper limit on the total strain energy density, until virtually general yielding of the net section. Furthermore, it is observed that the ESED method always predicts the lower limit of the actual strain energy densities at the notch tip.

3.3.2 Axial Stress - Strain Contribution to the Energy Densities

3.3.2.1 Material Model

The material of the bar was chosen to have a cyclic stress-strain curve given by the Ramberg-Osgood relationship,

$$\varepsilon = \frac{\sigma}{E} + \left(\frac{\sigma}{K'}\right)^{1/n'}, \tag{3.12}$$

with parameters, E = 202 GPa, ν = 0.3, σ_o = 202 MPa, n' = 0.208, and K' = 1258 MPa. The material stress-strain curve was approximated by several linear segments in both the FEM and simplified analyses (Fig. 3.11).

3.3.2.2 Method of Results and Analyses

The elastic-plastic FEM model was analyzed for the tension-torsion (Fig. 3.12a), torsion-tension (Fig. 3.12b), and a torsion-combined tension, torsion (Fig. 3.12c) loading path. The applied load levels were chosen for each loading path to be 50% higher than would be required to cause yielding at the notch tip if each was applied alone. Specifically, in all cases, $\sigma_{n.s.}^{\ f}$ = 103 MPa, and $\tau_{n.s.}^{\ f}$ = 90 MPa. The final ratio of the net sectional stresses was then $\sigma_{n.s.}^{\ f}/\tau_{n.s.}^{\ f}$ = 1.133. The normalized nominal equivalent net sectional stress ratio at the end of the loading history was then: S_{eq}/σ_o = 0.92, indicating almost general yielding conditions in the net section. After set increments in the external load were applied to the body, the elastic-plastic notch tip stress and strain components were recorded. From the recorded data, the contributions of each axial stress-

strain component to the increments in energy densities at the notch tip were calculated based on equations (3.3) and (3.7). The elastic contributions to the energy densities were calculated similarly knowing the load increments, the stress concentration factors and the material's elastic properties.

Figures 3.13, 3.14, 3.15 show plots of the equivalent net sectional stress ratio (eqn. 3.11) verses the energy ratios defined by equations (3.3) and (3.7) for the tension-torsion, torsion-tension, and torsion-combined torsion-tension load paths respectively. In the figures, the superscript "e-p" denotes elastic-plastic, and superscript "e" denotes elastic finite element data.

Assessment of Energy Ratio Equations

In all plots, it is noted that all ratios remain the same until the onset of plasticity and that the divergence from unity increases when the mode of loading changes. The divergence from unity appears to be most prevalent in the direction where the stresses are the lowest. That is, in the direction transverse to the axis of the bar. In this direction, the strains are relatively low and thus the numerical error is the highest. In the plots of the energy ratio equations for the tension-torsion loading paths (Figs. 3.13a and b), the average of the largest divergence from unity (averaged in the three directions) in the strain energy density (eqn.3.3) and total strain energy density (eqn.3.7) equations are approximately 16% and 5%, respectively. In the plots for the torsion-tension loading path (Figs, 3.14a and b), the average divergence from unity in the three directions is approximately 12% and 18% for the strain energy density and total strain energy density equations, respectively. In the case of the torsion-combined torsion - tension loading path (Figs.3.15a and b), the largest average divergence is 7% and 13% for the strain energy density ratio and the total strain energy density ratio equations, respectively. It should be noted that the

divergence from unity was generally calculated at the end of the loading path, where the assumption of localized plasticity is violated. It should also be noted that, since energy is a multiple of stress and strain, the divergence in the energy ratio equations will result in a smaller error in the actual stress and strain values at the notch tip.

3.3.3 Summary of Numerical Assessment

In the first numerical analysis, the hypothesis that the energy densities are somewhat insensitive to the load path was tested and the results imply that a generalization of the ESED method in the form of eqn.(3.2), and a generalization of the Neuber's rule in eqn.(3.6), is justified. It was further shown that for a non-proportional loading system, the generalized Neuber's rule predicts an upper bound on the FEM results for the total strain energy density at the notch tip. The generalized ESED method resulted in a lower bound on the FEM results for the strain energy density at the notch tip. Additional numerical analysis and experimental investigation should be carried out to examine this conclusion. However, the material model chosen was intended to highlight the error in the numerical solutions and, furthermore, the loading paths chosen were highly non-proportional. Therefore, it is fully expected that any further studies will support this conclusion. It should be noted, however, that this conclusion cannot be made in the case of cyclic loading.

The second analysis was designed to assess the additional equations used in the incremental ESED formulation (eqns.3.3) and in the incremental Neuber's formulation (eqns.3.7). The analysis showed that the equations work well almost up until general yielding of the net section.

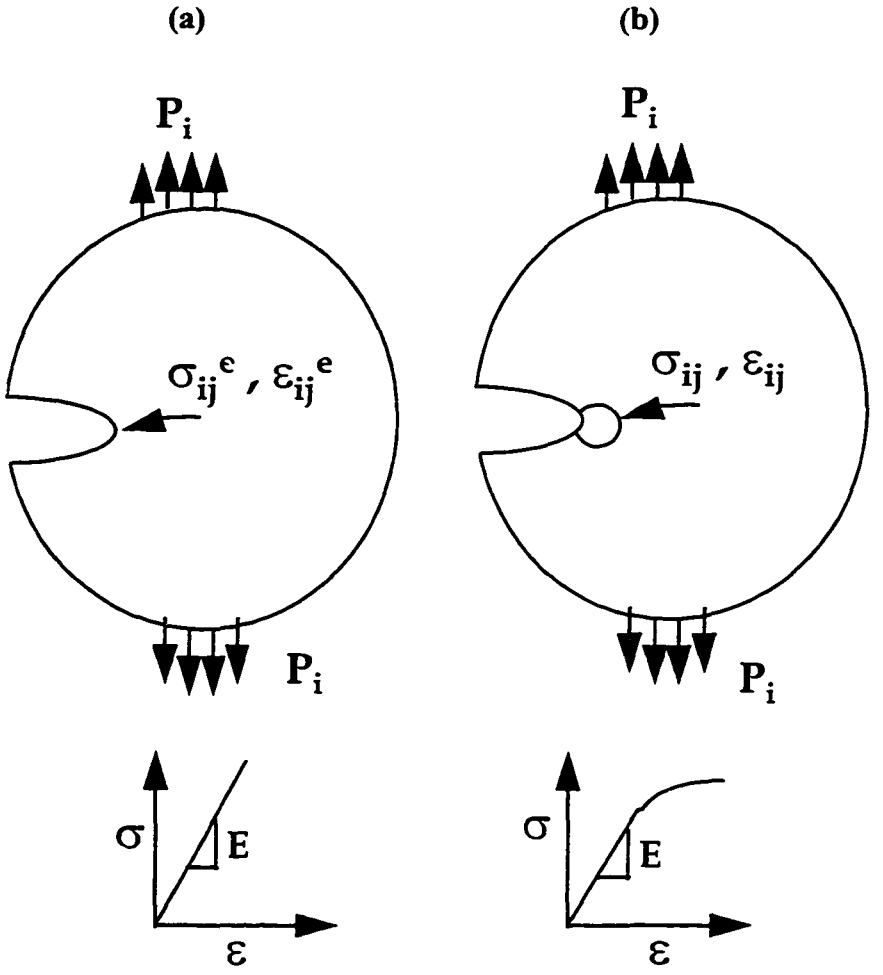


Figure 3.1: Two Notched Bodies Made of a) Elastic and b) Elastic-Plastic Material

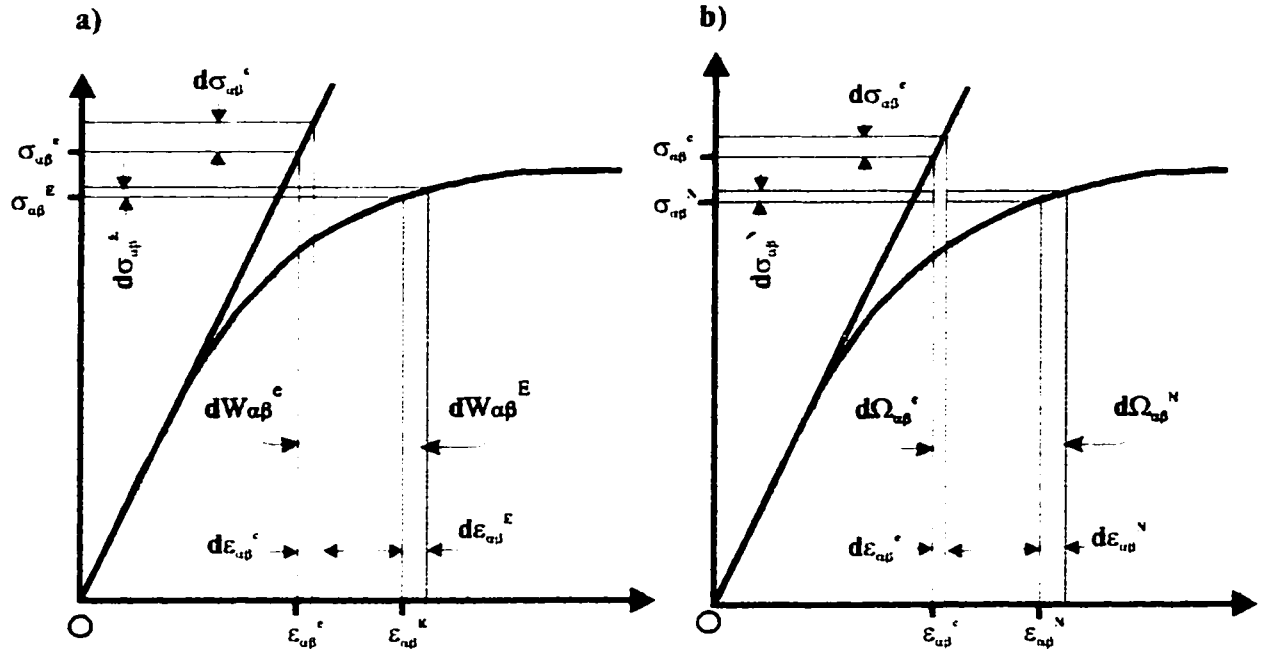


Figure 3.2: a) Incremental Equivalent Strain Energy Density Method, b) Incremental Neuber's Rule

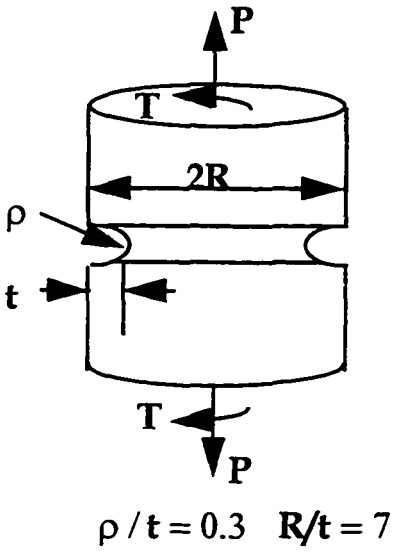


Figure 3.3: Notched Cylindrical Bar Used in Numerical Assessment

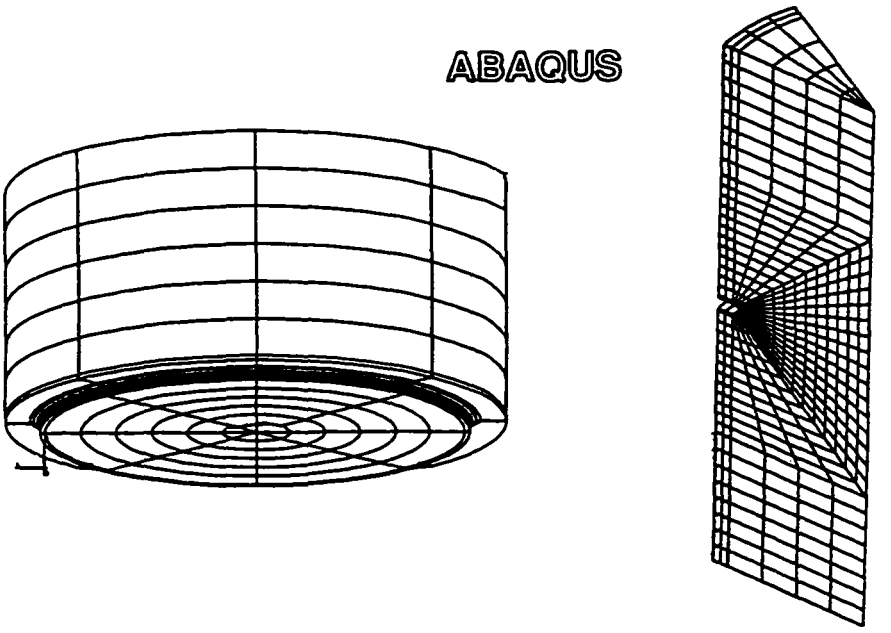


Figure 3.4: Finite Element Model of the Cylindrical Bar

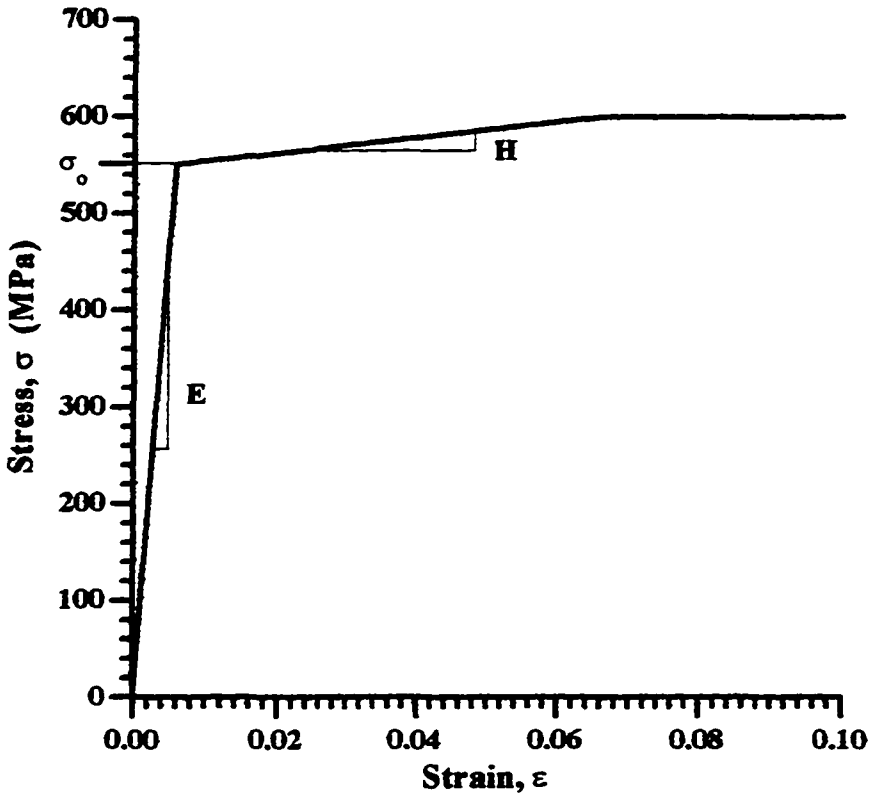


Figure 3.5: Material Model Used in Energy Assessment.

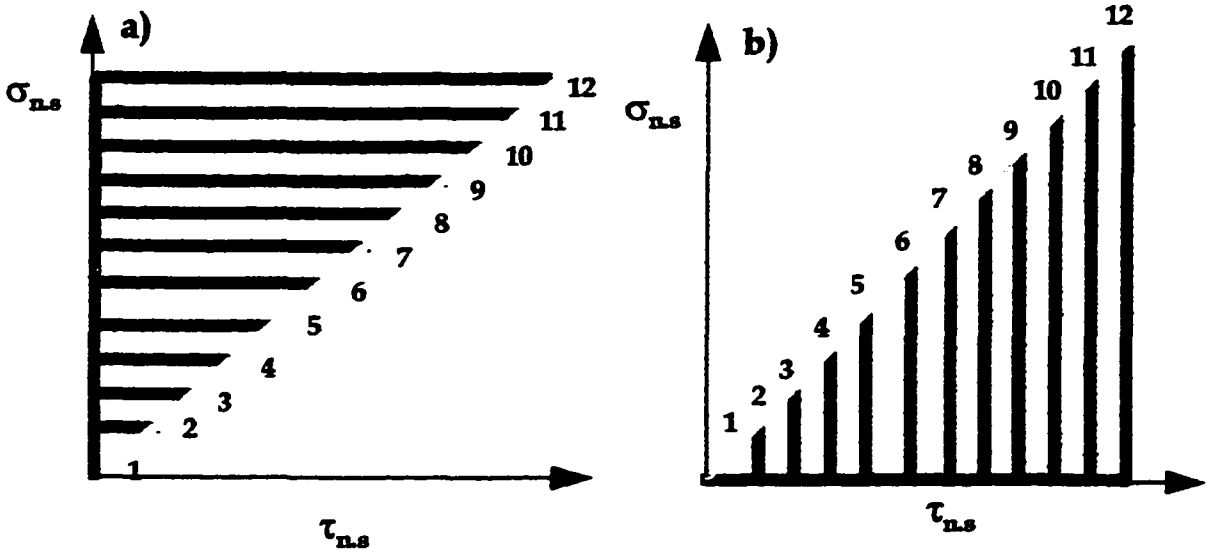


Figure 3.6: Load Paths Used in Energy Assessment a) Tension-Torsion, Proportional, b) Torsion-Tension, Proportional.

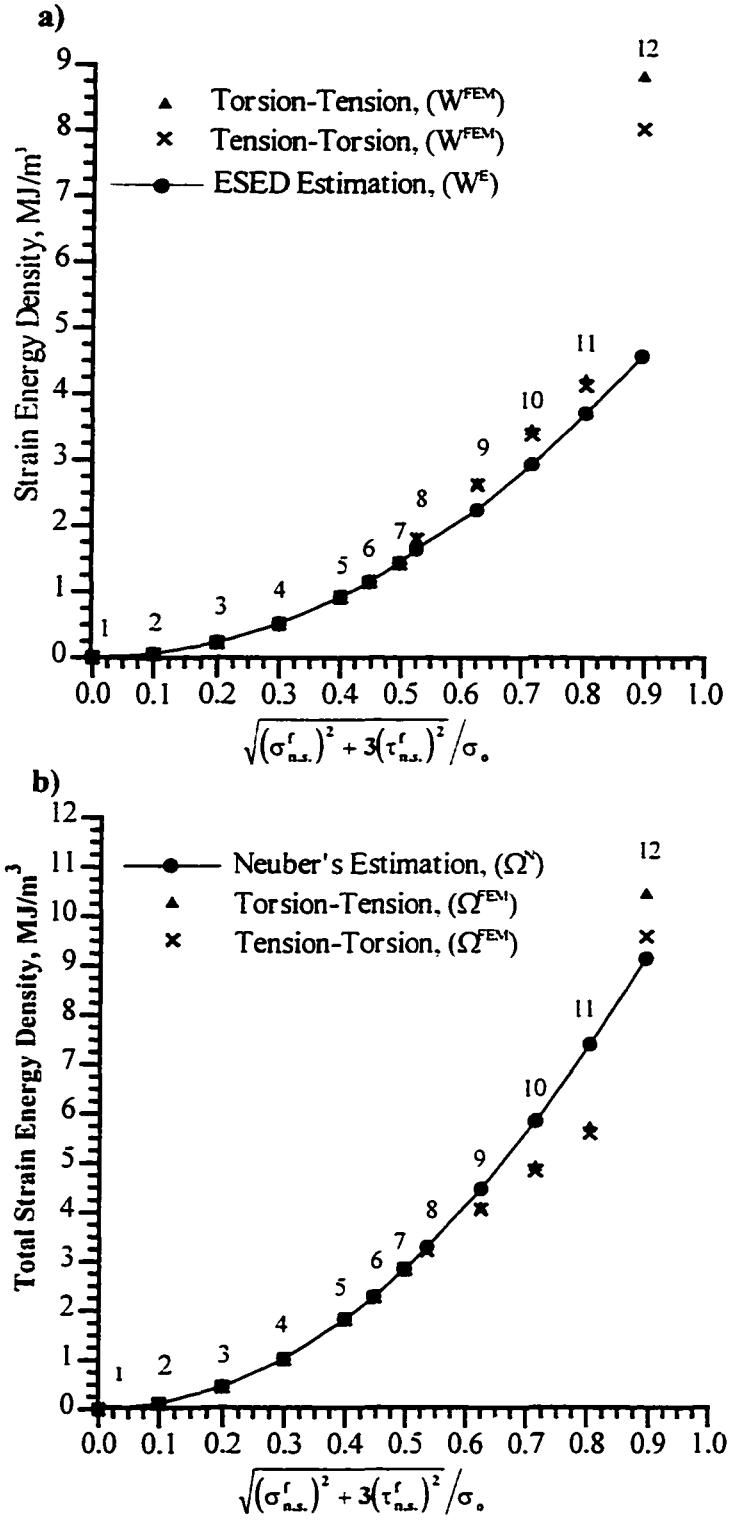


Figure 3.7: a) Strain Energy Density, b) Total Strain Energy Density ($\sigma^{f}_{n.s.} / \tau^{f}_{n.s.} = 0.32$).

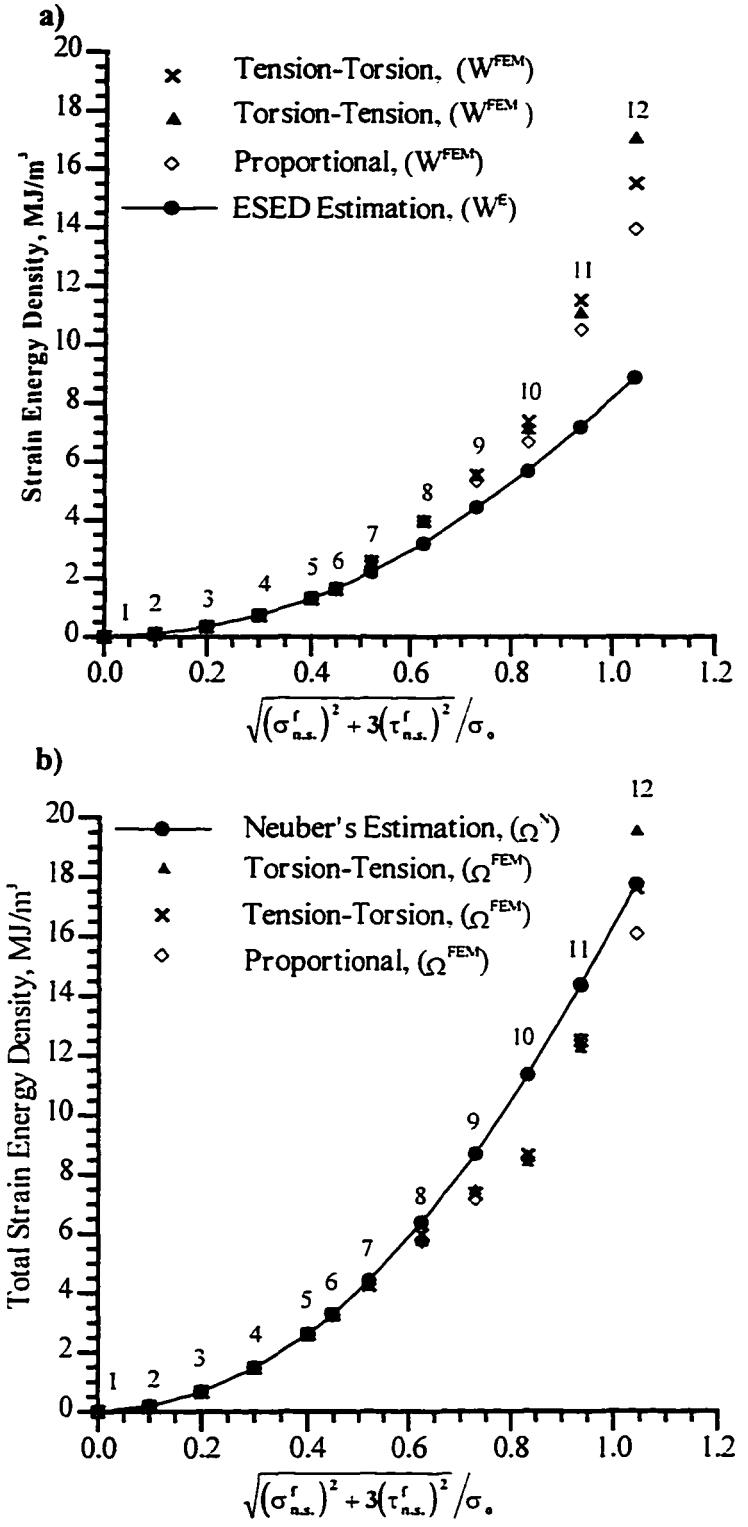


Figure 3.8: a) Strain Energy Density, b) Total Strain Energy Density ($\sigma^{f}_{n.s.} / \tau^{f}_{n.s.} = 1.1$).

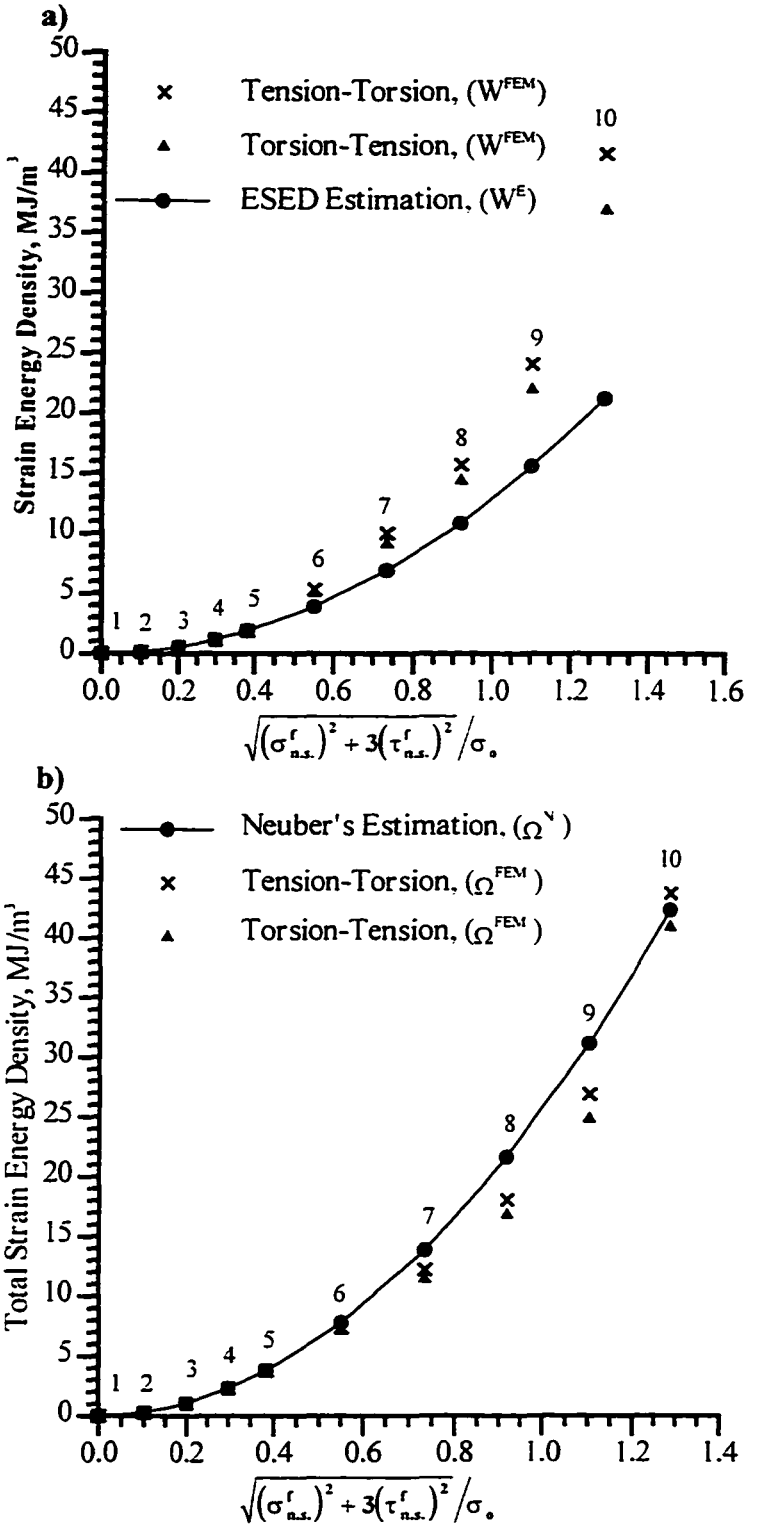
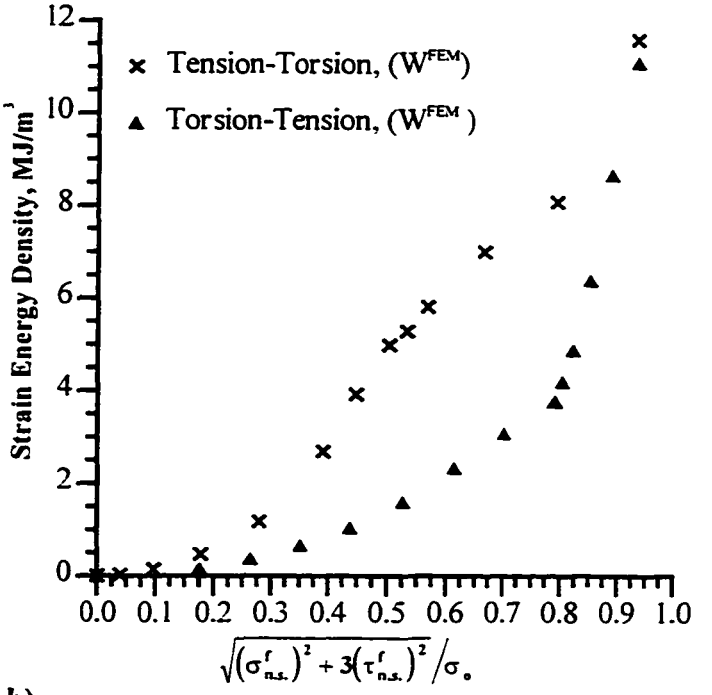


Figure 3.9: a) Strain Energy Density, b) Total Strain Energy Density ($\sigma^f_{n.s.} / \tau^f_{n.s.} = 3.2$).

a)



b)

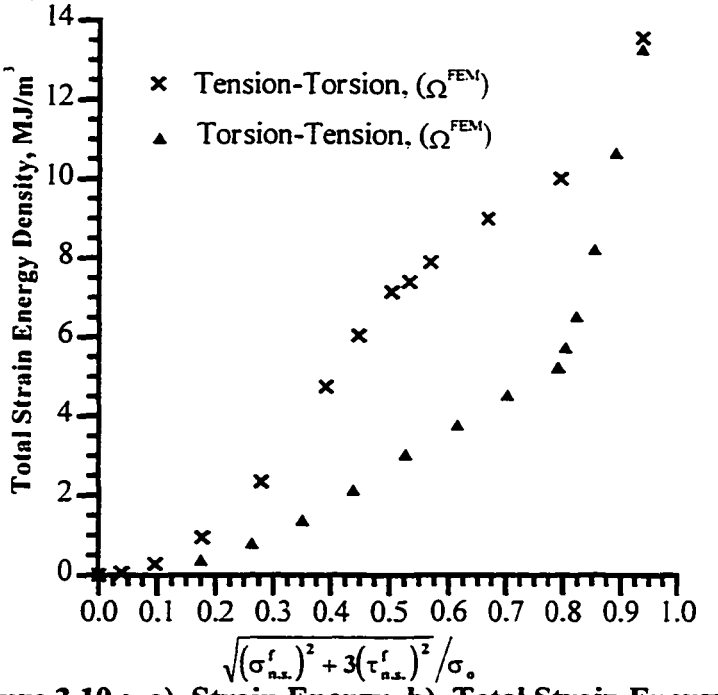


Figure 3.10 : a) Strain Energy, b) Total Strain Energy Density
$(\sigma^{f}_{n.s} = 277\text{MPa}, \tau^{f}_{n.s} = 251\text{MPa})$

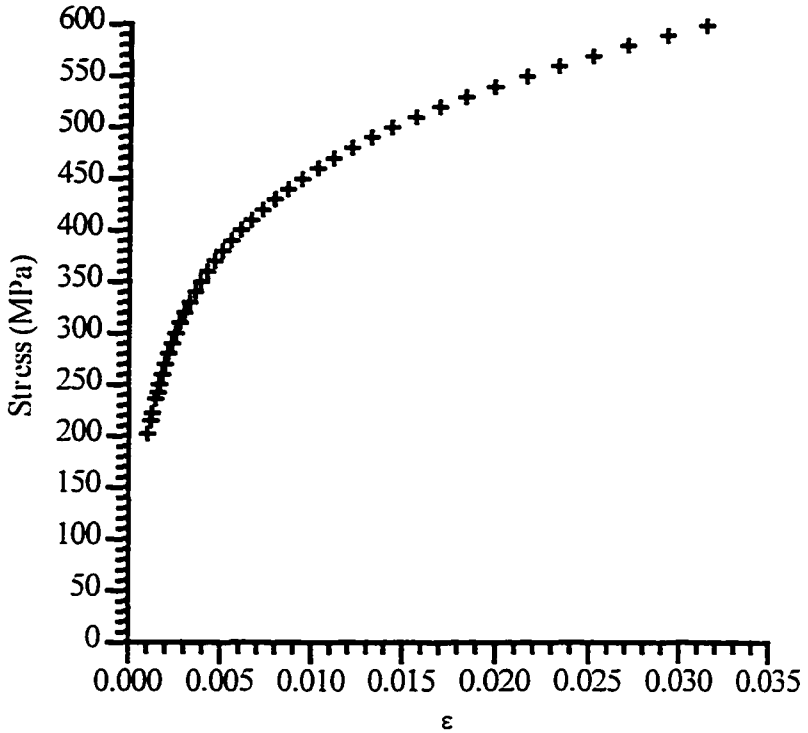


Figure 3.11: Material Model Used in Axial Energy Assessment.

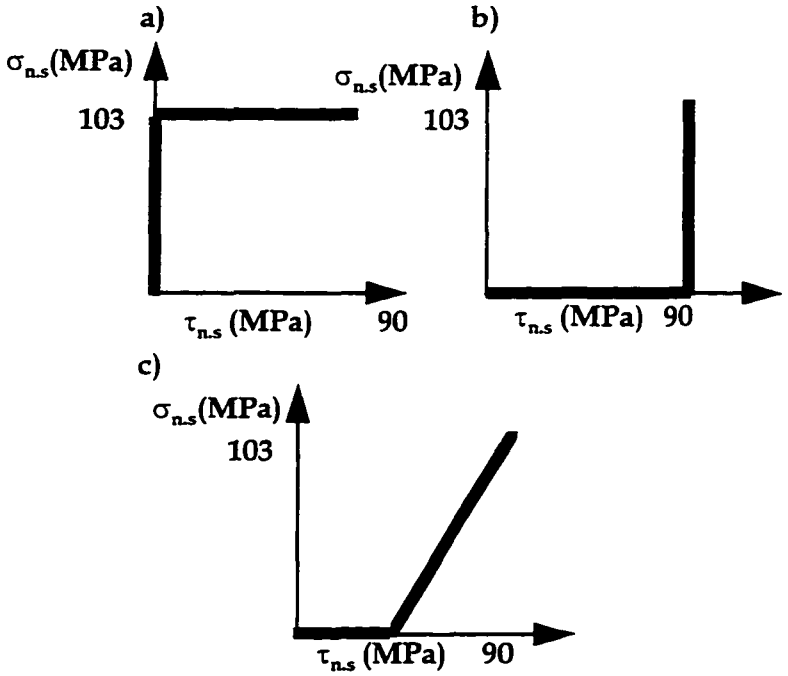


Figure 3.12: Load Paths Used in Axial Energy Assessment, a) Tension - Torsion, b) Torsion-Tension, c) Torsion-Combined Tension, Torsion

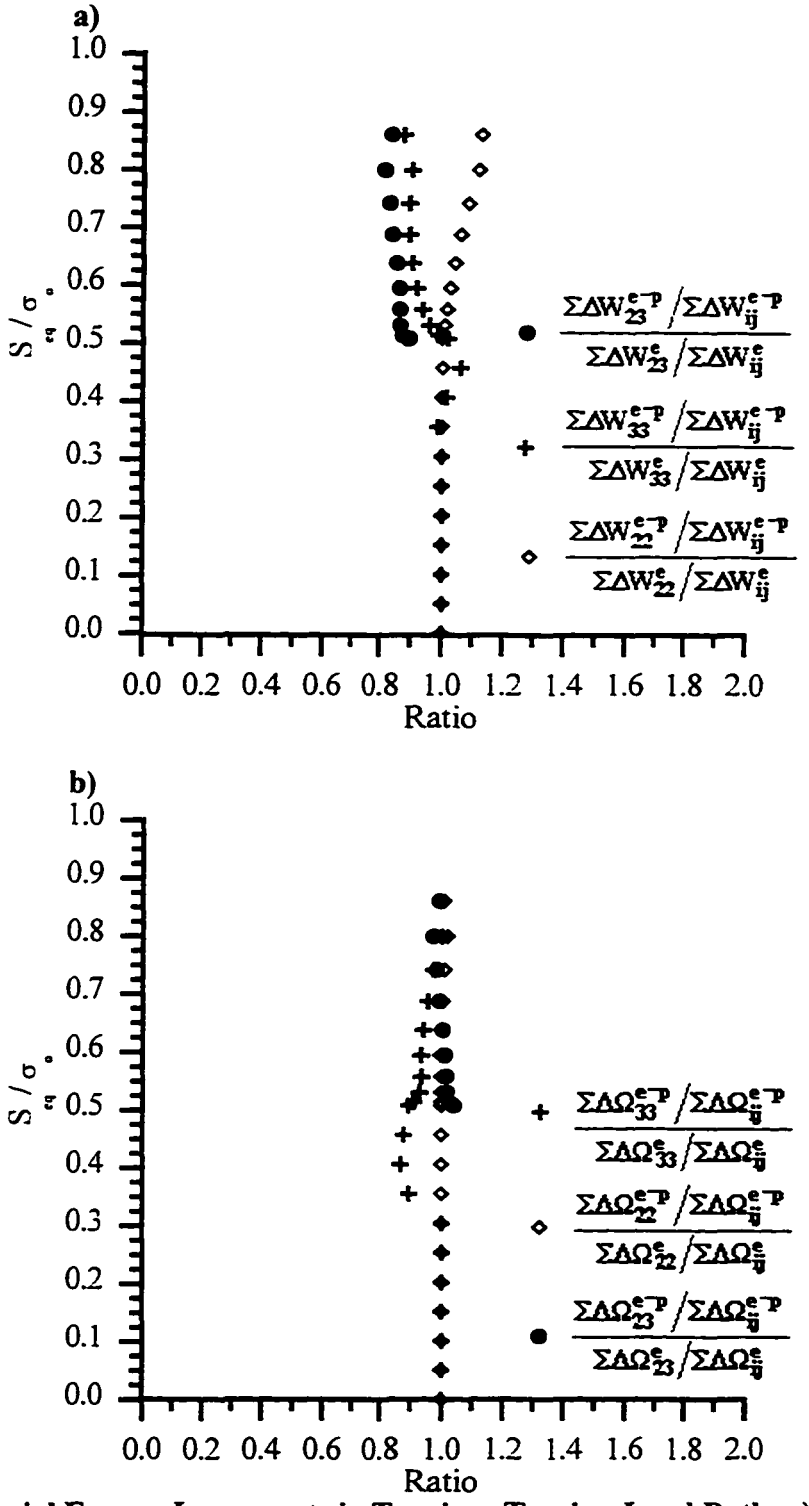


Figure 3.13: Axial Energy Increments in Tension- Torsion Load Path, a) Strain Energy Density, b) Total Strain Energy Density.

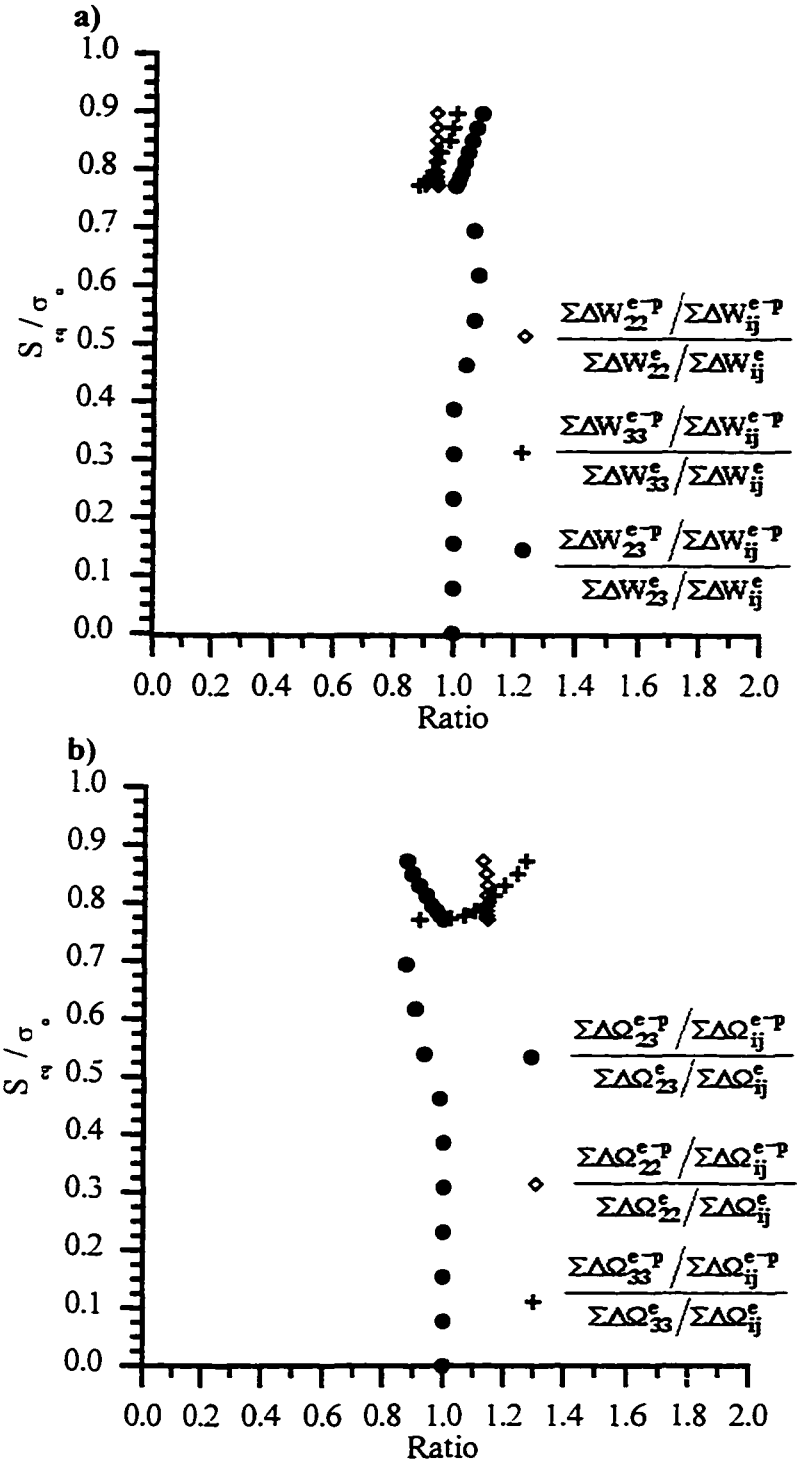


Figure 3.14: Axial Energy Increments in Torsion-Tension Load Path, a) Strain Energy Density, b) Total Strain Energy Density

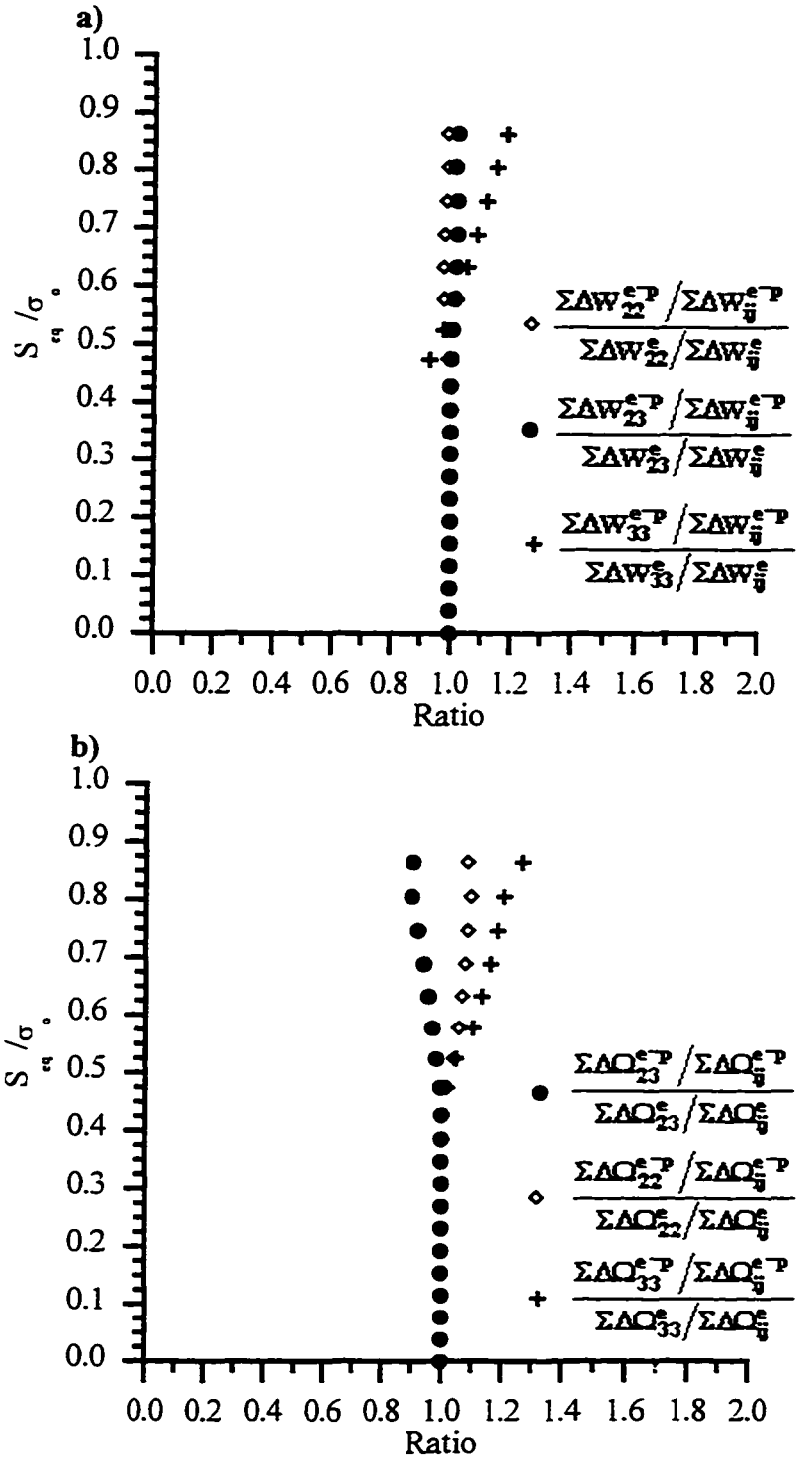


Figure 3.15: Axial Energy Increments in Torsion-Combined Tension, Torsion Load Path, a) Strain Energy Density, b) Total Strain Energy Density

4. CHAPTER FOUR:

CONSTITUTIVE MODELLING

In Chapter Two, it was shown that a set of seven independent equations is required to fully describe the notch tip stress and strain field in a body subjected to a non-proportional loading sequence. In Chapter Three, two simplified methods, the incremental ESED and incremental the Neuber's methods, were presented. Each method provides three independent relations for estimating notch tip elastic-plastic parameters. To complete each set of seven equations, four additional equations are required and can be described by the constitutive behavior of the material. Although constitutive theory is well known and can be found in references such as [26], [40]-[42], its fundamental relations, expressed in notation used in the thesis, are presented in this chapter. This enables a clear formulation of the complete set of relations necessary to solve for the seven unknown increments at the notch tip when the body is subjected to a cyclic load.

4.1 Elastic Constitutive Relations

When a body is said to be loaded elastically, it is assumed that the deformation process is reversible. That is, when the load is removed from the body, the body returns to its original state and the loading process has no effects on the behavior of the material upon subsequent

loading. Elastic material behavior further implies a direct or one-to-one relationship between stress and strain. For a linear elastic isotropic body, the relationship between stress and strain at any point in the body can be represented by Hooke's Law in the form

$$\varepsilon_{ij}^{e} = \frac{1+\nu}{E}\sigma_{ij} - \frac{\nu}{E}\sigma_{kk}\delta_{ij}, \tag{4.1}$$

where δ_{ij} is the Kroneker delta. When loaded, most materials exhibit a range of deformation that is reversible before the load is large enough to exceed the material's yield limit and permanent or plastic deformations occur.

4.2 Elastic-Plastic Constitutive Theory

When plastic deformation occurs in a body, the loading process becomes irreversible. That is, permanent deformation remains in the body after the load is removed. Fundamental plasticity theory states that the final stress-strain state is dependent on the applied loading path, unless the loads are increased in a manner such that the deviatoric stresses increase in a constant ratio throughout the loading history. In such a case, the final plastic strains are independent of the loading path, and this is generally assured if the loads are applied in a proportional manner. Thus, as in the elastic case, there is a one-to-one correspondence between stress and strain when the loads are applied in a proportional manner.

However, in the case of a notched body subject to a proportionally applied loading system, because of the effect of the stress concentration, it can not necessarily be assumed that the deviatoric stresses at the notch tip also behave proportionally. Certainly if the notched body is subjected to a non-proportional loading system, the final notch tip stress-strain state will depend on the applied loading path.

As such, relations that define the local stress-strain state in any notched body subjected to a non-proportionally applied loading system must be developed in an incremental form. That is, they must, for a given increment in the applied load, enable the stress and strain increments to be determined. The stress-strain state after the load increment has been applied can then be found by the addition of the previous stress-strain components and the stress-strain increments.

In order to model the incremental constitutive behavior of the material properly, three relations are required. The first relation is the yield criterion, which is a statement of the state of stress in the material at yield. The second relation is the flow rule, which relates the stress tensor to the strain tensor in the plastic range. The third relation is the hardening rule, which dictates how the yielding criterion changes during the course of the loading.

4.2.1 The Yield Criterion

In a simple tensile test, a uniaxial tensile load is applied to a body to determine the stress-strain behavior of the material. When the load is first applied, the process is generally reversible or elastic, and Hooke's Law is applicable. This region of reversibility continues until the elastic limit, or yield point is reached. Beyond the yield point, the stress is no longer proportionally related to the strain. Thus, if a body is subjected to a uniaxial load, the point at which the material starts to deform plastically can be determined from a simple tensile test. However, if there are several stress components acting at a point in different directions, as is the case at the notch tip, a criterion is required that will dictate the combination of the acting stresses at yield.

In the most general case, the yield criterion will depend on the complete state of stress at a point in the body and, respecting the symmetry of the stress tensor, will be a function of six independent components of stress. Since it is generally assumed that hydrostatic tension or compression does not influence yielding, the yield function can be written in terms of deviatoric components, S_{ij}, as

$$f(S_{ij}) = K, \tag{4.2}$$

where K is a known function, or,

$$F(S_{ij}) = 0, \tag{4.3}$$

and

$$S_{ij} = \sigma_{ij} - \frac{1}{3}\sigma_{kk}\delta_{ij}. \tag{4.4}$$

The function F in (4.3) is called a yield function and the surface in stress space that it describes is called a yield surface. The yield surface represents a boundary between the region of elastic and elastic-plastic stress states. Stress states that lie within the yield surface are a result of elastic deformation, and those exterior to the yield surface can only be reached by plastic deformation. Since plastic deformations must be consistent with the changes in the yield surface, any stress state that resulted from a plastic deformation must lie on the yield surface.

Numerous criteria have been proposed for the yielding of materials of which the von Mises criterion is used most commonly in cyclic applications. The von Mises yield criterion assumes that yielding occurs when the distortion energy density at a point in a loaded body equals the distortion energy density in a rod of the same material as the body at yield (σ_o) in tension. The von Mises yield criterion can be written on the basis of eqn.(4.3) as

$$F(S_{ij}) = f(S_{ij}) - \sigma_o^2 = \frac{3}{2}S_{ij}S_{ij} - \sigma_o^2 = 0. \tag{4.5}$$

The von Mises criterion described by eqn.(4.5) has an advantageous geometric representation in stress space. Specifically, it can be represented as an ellipse in a two-dimensional principal stress space (σ_1-σ_2) as shown in Figure 4.1a. In three-dimensional principal stress space it can be represented on its deviatoric stress plane, or the π plane, as a circle of radius $\sqrt{(2/3)}\,\sigma_o$ as shown in Figure 4.1b. For ductile materials, the von Mises yield criterion is generally considered to fit experimental data better than other theories.

4.2.2 The Flow Rule

The relationship between stress and strain in incremental plasticity is governed by the flow rule. Plasticity theory assumes that the plastic strain increments, $d\varepsilon_{ij}^{p}$, are directly proportional to the partial derivatives of a stress potential function, $Q(\sigma_{ij})$. That is,

$$d\varepsilon_{ij}^{p} = \lambda \frac{\partial Q}{\partial \sigma_{ij}}, \tag{4.6}$$

where λ is a positive scalar that indicates the magnitude of, and the potential function $Q(\sigma_{ij})$ indicates the direction of plastic flow. When the potential function is the same as the yield function, $F(\sigma_{ij})$ (eqn.4.3), the resulting flow rule,

$$d\varepsilon_{ij}^{p} = \lambda \frac{\partial F}{\partial \sigma_{ij}} = \lambda \frac{\partial f}{\partial \sigma_{ij}}, \tag{4.7}$$

is called the associated flow rule. Equation (4.7) states that the plastic strain increment is normal to the yield surface. The flow rule can be written in a more general form as

$$d\varepsilon_{ij}^{p} = \frac{1}{K_p} \hat{n}_{ij} (\hat{n}_{kl} d\sigma_{kl}), \tag{4.8}$$

where $\hat{n}_{ij}$ are the components of the unit normal to the yield surface and are defined as

$$\hat{n}_{ij} = \frac{\dfrac{\partial F}{\partial S_{ij}}}{\left(\dfrac{\partial F}{\partial S_{kl}} \dfrac{\partial F}{\partial S_{kl}} \right)^{(1/2)}}, \tag{4.9}$$

and K_p is the hardening modulus that can be obtained from a uniaxial tensile test. Equation (4.8) can be applied to bodies that are loaded proportionally as well as non-proportionally and is written independent of the hardening behavior of the body.

The total increment in strain at any point in a body can be found by adding the elastic and plastic components as

$$d\varepsilon_{ij} = d\varepsilon_{ij}^{e} + d\varepsilon_{ij}^{p}. \tag{4.10}$$

4.2.3 The Hardening Rule

Consider the case where a body is subjected to a uniaxial tensile load that results in a stress σ that is greater than the initial yield limit σ_o of the material. If the body is then unloaded elastically, and then reloaded, the material will not yield at the initial yield limit, but at the higher stress level σ. This yielding behavior is inherent in work hardening materials. It indicates that the yield surface must transform under subsequent loading.

4.2.3.1 Isotropic Hardening

Isotropic hardening is based on the assumption that an isotropic body remains isotropic under plastic loading. Isotropic hardening was first proposed by Hill [40] and is shown in Figure 4.2

for uniaxial loading. In Figure 4.2, the initial yield surface is shown to expand uniformly as the material hardens from point **a** to point **b**, with its center remaining at the origin. If the load is removed and reapplied in compression, the material will yield in compression at the stress $\sigma_c = -\sigma_b$. Isotropic hardening dictates a uniform increase in strength of the material in all directions.

If the von Mises yield criterion is used in the isotropic hardening model, the yield criterion can be stated as

$$F(S_{ij}) = \frac{3}{2} S_{ij} S_{ij} - \bar{\sigma}_{eq}^{2} = 0, \tag{4.11}$$

where $\bar{\sigma}_{eq}$ is the largest value of the equivalent stress attained during loading (σ_b in Fig. 4.2). Substituting eqns. (4.1),(4.8), (4.9) and (4.11), into eqn. (4.10) yields

$$d\varepsilon_{ij} = \frac{1+\nu}{E} d\sigma_{ij} - \frac{\nu}{E} d\sigma_{kk} \delta_{ij} + \frac{3}{2} \frac{S_{ij} S_{kl} d\sigma_{kl}}{K_p \bar{\sigma}_{eq}^{2}}. \tag{4.12}$$

Note that in eqn.(4.12), δ_{ij} is the Kronecker delta

Isotropic hardening does not account for the anisotropy inherent in plastic deformations. In other words, the Bauschinger effect is neglected in the isotropic hardening model.

4.2.3.2 Kinematic Hardening

To account for the Baushinger effect, Prager [43] postulated that the initial yield surface translates at the onset of plastic flow. The concept of kinematic hardening is illustrated for uniaxial loading in Figure 4.3. In Figure 4.3, the initial yield surface moves with the stress point as the material hardens from point **a** to **b**. Upon unloading and reloading in compression, the material yields at **c**, where $\sigma_c < -\sigma_b$. In kinematic hardening, as indicated in Figure 4.3, the yield surface retains its original shape during plastic deformation, as governed by the initial yield stress σ_o, but translates by the amount $d\xi_{ij}$ for a given increment in the deviatoric stress tensor. The tensor $[\xi]$ represents the coordinates of the center of the yield surface. If the von Mises yield criterion is used, then the equation that defines the yield surface is

$$F(S_{ij},\xi_{ij}) = \frac{3}{2}(S_{ij}-\xi_{ij})(S_{ij}-\xi_{ij}) - \sigma_o^{\,2} = 0, \tag{4.13}$$

where ξ_{ij} are the deviatoric components of the back stress tensor $[\alpha]$, or

$$\xi_{ij} = \alpha_{ij} - \frac{1}{3}\delta_{ij}\alpha_{kk}. \tag{4.14}$$

The associated flow rule can be obtained by substituting eqns.(4.13), (4.8), (4.9), and (4.1) into eqn. (4.10) and is written as

$$d\varepsilon_{ij} = \frac{1+\nu}{E}d\sigma_{ij} - \frac{\nu}{E}d\sigma_{kk}\delta_{ij} + \frac{3}{2}\frac{(S_{ij}-\xi_{ij})(S_{kl}-\xi_{kl})d\sigma_{kl}}{K_p\sigma_o^2}. \tag{4.15}$$

Most cyclic plasticity models are based on the concept of a translating yield surface. The differences in the cyclic plasticity models presented in the literature generally lie in the translation rule which governs the movement of the yield surface and thus the value of $d\xi_{ij}$ in Figure 4.3. Prager's [43] translation rule assumes that the yield surface translates in the direction of the exterior normal at the stress point, or,

$$d\xi_{ij} = \mu d\varepsilon_{ij}^{p}. \tag{4.16}$$

An alternate translation rule was proposed by Ziegler [44] as

$$d\xi_{ij} = d\mu(S_{ij} - \xi_{ij}) \ , \tag{4.17}$$

which states that the yield surface translates in the direction of the vector that connects the center of the yield surface to the stress point. Although both the Prager and Ziegler rules do account for the Bauschinger effect, they have been found to poorly predict the hardening behavior of bodies subjected to non-proportional loads [45],[46].

To better model the load path dependent properties of materials, Mróz [47] generalized the kinematic hardening model by introducing the concept of a field of ℓ initially concentric work hardening surfaces and prescribing a translation rule for the surfaces moving with respect to one another.

In the Mróz model, each surface is defined by its center coordinates, $\xi_{ij}^{(\ell)}$, a yield stress, $\sigma_{\circ}^{(\ell)}$, and a plastic tangent modulus, $E_{p}^{\prime(\ell)}$. The model assumes that each surface can be described

by the same relationship as the yield criterion. If the von Mises criterion is used, then each surface is defined as

$$F^{(\prime)}(S_{ij},\xi_{ij}) = \frac{3}{2}(S_{ij}-\xi_{ij}^{(\prime)})(S_{ij}-\xi_{ij}^{(\prime)}) - \sigma_o^{(\prime)2} = 0. \tag{4.18}$$

The initial surface in stress space is the initial yield surface, and the outer surfaces become "active" at higher equivalent stress levels. The equivalent stress and the plastic tangent modulus associated with each surface can be found by descretizing the uniaxial stress-strain curve. This concept of a field of work hardening surfaces is illustrated in Figure 4.4.

The total strain increment can be obtained by substituting eqns. (4.18), (4.8) ,(4.9), and (4.1), into eqn. (4.10) and can be written as

$$d\varepsilon_{ij} = \frac{1+\nu}{E}d\sigma_{ij} - \frac{\nu}{E}d\sigma_{kk}\delta_{ij} + \frac{3}{2}\frac{(S_{ij}-\xi_{ij}^{(n)})(S_{kl}-\xi_{kl}^{(n)})d\sigma_{kl}}{K_p^{(n)}\sigma_o^{(n)2}}, \tag{4.19}$$

where the superscript "n" is used to denote the "active" yield surface and the hardening modulus $K_p^{(n)}$ is now associated with the "active" (nth) surface and can be determined from the uniaxial tensile test.

The determination of the active surface is governed by prescribing a translation rule for surfaces moving with respect to each other over distances given by the stress increments. Mróz bases this translation rule on the concept of mutual tangency. Specifically, Mróz assumes that, upon elastic-plastic loading, the surfaces move within each other and they do not intersect. If, however, they come into contact with one another, or become mutually tangent, they move

together as one rigid body. The active surface is then determined by the largest hardening surface tangent to the yield surface. Thus, if loading only in tension (see Fig. 4.4), the stress point moves from zero until it hits the first yield surface $F^{(1)}$ at **a**. The yield surface $F^{(1)}$ is then the active surface and it translates along the σ_1 axis with the stress point until it hits $F^{(2)}$ at **b**. Upon subsequent loading, both surfaces $F^{(1)}$ and $F^{(2)}$ move with the stress point ($F^{(2)}$ now being the active surface) until $F^{(3)}$ is reached at point **c**. Upon unloading, the stress point moves inside the first yield surface, $F^{(1)}$, until it reaches the boundary, where plastic loading again begins with $F^{(1)}$ being the active surface.

Figure 4.5 illustrates the rule developed by Mróz, based on the concept of mutual tangency, that defines the translation $d\xi_{ij}^{(n)}$ of one surface $F^{(n)}$ with respect to the next $F^{(n-1)}$. Assume that the state of stress lies on the active surface $F^{(n)}$ at point P. Mróz proposed that the active surface will translate along PR as

$$d\xi_{ij}^{(n)} = d\mu(S_{ij}^{(n-1)} - S_{ij}^{(n)}). \tag{4.20}$$

where $d\mu$ is the magnitude of the translation, and $(S_{ij}^{(n-1)} - S_{ij}^{(n)})$ governs the direction of translation. Mróz defines the point R as the conjugate of point P on the immediate outer surface $F^{(n-1)}$, or the point on $F^{(n-1)}$ that has the same direction normal as $F^{(n)}$ has at P, or

$$\hat{n}_{ij}^{R} = \hat{n}_{ij}^{P}, \tag{4.21}$$

where $\hat{n}_{ij}$ is given by eqn.(4.9). If two surfaces $F^{(n)}$ and $F^{(n-1)}$ are defined using the von Mises yield criterion, then substituting eqn.(4.18) into eqn.(4.21) defines the point R as

$$S_{ij}^{(n+1)} = \xi_{ij}^{(n+1)} + \frac{\sigma_o^{(n+1)}}{\sigma_o^{(n)}}(S_{ij}^{(n)} - \xi_{ij}^{(n)}) . \tag{4.22}$$

Substituting eqn.(4.22) into eqn.(4.20) gives

$$d\xi_{ij}^{(n)} = \frac{d\mu}{\sigma_o^{(n)}}\left[S_{ij}^{(n)}(\sigma_o^{(n+1)} - \sigma_o^{(n)}) - (\xi_{ij}^{(n)}\sigma_o^{(n+1)} - \xi_{ij}^{(n-1)}\sigma_o^{(n)})\right]. \tag{4.23}$$

The magnitude of the translation $d\mu$ is found by imposing the condition that the stress point must lie on the yield surface during plastic deformation (the consistency condition). That is, after infinitesimal changes in $d\sigma_{ij}$ and $d\varepsilon_{ij}$ have occurred, the material must still satisfy eqn. (4.18), or

$$dF^{(n)}(S_{ij}, \xi_{ij}^{(n)}) = 0 . \tag{4.24}$$

Expanding eqn.(4.24) using Taylors series yields

$$\frac{\partial F^{(n)}}{\partial S_{ij}} dS_{ij} + \frac{\partial F^{(n)}}{\partial \xi_{ij}^{(n)}} d\xi_{ij}^{(n)} + \frac{1}{2}\left[\frac{\partial F^{(n)2}}{\partial S_{ij}\partial S_{kl}} dS_{ij}dS_{kl} + 2\frac{\partial F^{(n)2}}{\partial S_{ij}\partial \xi_{kl}^{(n)}} dS_{ij}d\xi_{kl}^{(n)} + \frac{\partial F^{(n)2}}{\partial \xi_{ij}\partial \xi_{kl}} d\xi_{ij}d\xi_{kl}\right] + ... = 0$$

.(4.25)

Note here that the second order terms are included in this expansion since it has been found that the first order approximation is not sufficiently accurate when descretized. Substituting eqns. (4.18) and (4.20) into eqn. (4.25) yields the following quadratic in $d\mu$

$$d\mu^2\left[\left(S_{ij}^{(n+1)} - S_{ij}^{(n)}\right)\left(S_{ij}^{(n+1)} - S_{ij}^{(n)}\right)\right] - 2d\mu\left[\left(S_{ij}^{(n+1)} - S_{ij}^{(n)}\right)\left(\left(S_{ij}^{(n)} - \xi_{ij}^{(n)}\right) + dS_{ij}\right)\right]$$

$$+\left[2\left(S_{ij}^{(n)} - \xi_{ij}^{(n)}\right)dS_{ij} + dS_{ij}dS_{ij}\right] = 0 . \tag{4.26}$$

Note that the correct root of the equation will restrict $d\mu$ to: $0 < d\mu < 1$. If the second order terms in eqn.(4.26) are neglected, it reduces to the more common form of the consistency condition of

$$d\mu = \frac{\left(S_{ij}^{(n)} - \xi_{ij}^{(n)}\right) dS_{ij}^{(n)}}{\left(S_{kl}^{(n)} - \xi_{kl}^{(n)}\right)\left(S_{kl}^{(n+1)} - S_{kl}^{(n)}\right)}. \tag{4.27}$$

It should be noted that for each translation of the active surface, the surfaces interior to, and thus tangent to, that active surface must also be translated such that they move together as a rigid body with the stress point. Thus, the centers of each hardening surface interior to that active must lie on a straight line connecting the coordinates of the center of the active yield surface $\xi_{ij}^{(n)}$ to the stress point S_{ij}. The center, $\xi_{ij}^{(n-1)}$ of $F^{(n-1)}$ for example can thus be described by its position relative to $F^{(n)}$ as

$$S_{ij} - \xi_{ij}^{(n)} = \frac{\sigma_o^{(n)}}{\sigma_o^{(n-1)}}\left(S_{ij} - \xi_{ij}^{(n-1)}\right), \tag{4.28}$$

where S_{ij} denotes the stress state after the body has gone through the plastic strain increment $d\varepsilon_{ij}$.

Thus in utilizing the multiple surface hardening rule proposed by Mróz, the plastic strain increment on the active surface can be found using equation (4.19). The translation of the active surface can then be found using eqns. (4.22)-(4.26), and the translation of surfaces interior to the active surface using (4.28).

Several modifications of the Mróz model have been proposed in the literature. Garud [48], for example, proposed an alternate translation rule that avoids the intersection of the ellipses that could occur in some cases in the original Mróz model. Jiang and Sehitoglu [49] have presented a good comparison between the Mróz and the Garud models.

Chu [50] proposed a modification to the Mróz model that circumvents the often cited problem with the Mróz model. That is, the large computer storage requirement associated with the necessity to store the location of each surface. Chu's model retains the idea of a field of work-hardening surfaces and utilizes an infinite number of surfaces and tracts only the movement of the active surface, defined as the largest surface that passes through the yield surface.

An alternative model was also proposed by Kurath and Jiang [51]. The strength of this model lies in its ability to model ratchetting effects.

The problem of excessive storage requirements in the Mróz model is also overcome by the use of two surface plasticity models, originally proposed by Dafalias and Popov [52]. Two surface models use the yield surface to differentiate between elastic and elastic-plastic behavior, and a limit surface, which defines the point where the material becomes linear at large strains. In order to properly define a two surface plasticity model, an appropriate translation rule must be selected or defined, and a proper methodology must be adopted for calculating the plastic modulus.

4.3 Constitutive Behavior at the Notch Tip

In fatigue analysis of notched bodies subjected to uniaxial or multiaxial proportional loads, the material constitutive behavior is generally described by the Masing [53] hypothesis. Masing's hypothesis is a kinematic hardening rule that states that the cyclic stress-strain material response can be obtained by doubling the uniaxial cyclic stress-strain curve. In the case of notched bodies subjected to non-proportional loads, a plasticity model must be adopted that accounts for path dependent material constitutive behavior.

Although any constitutive model that incorporates path dependent material behavior can be used in conjunction with the ESED or Neuber's simplified equations, the Mróz model is used in this work. This is primarily justified by the ease of use and understanding of the model and furthermore, the rapid advancements in computing technology has trivialized the argument of its necessity of excessive storage space.

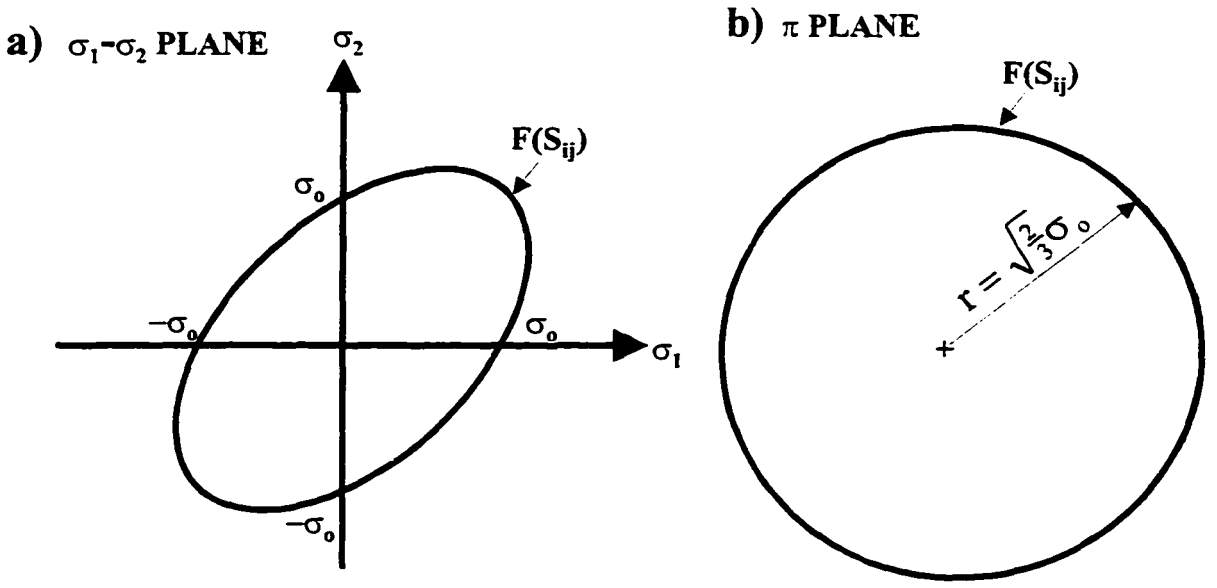


Figure 4.1: von Mises Yield Criterion on the a) σ_1-σ_2 plane and b) π plane

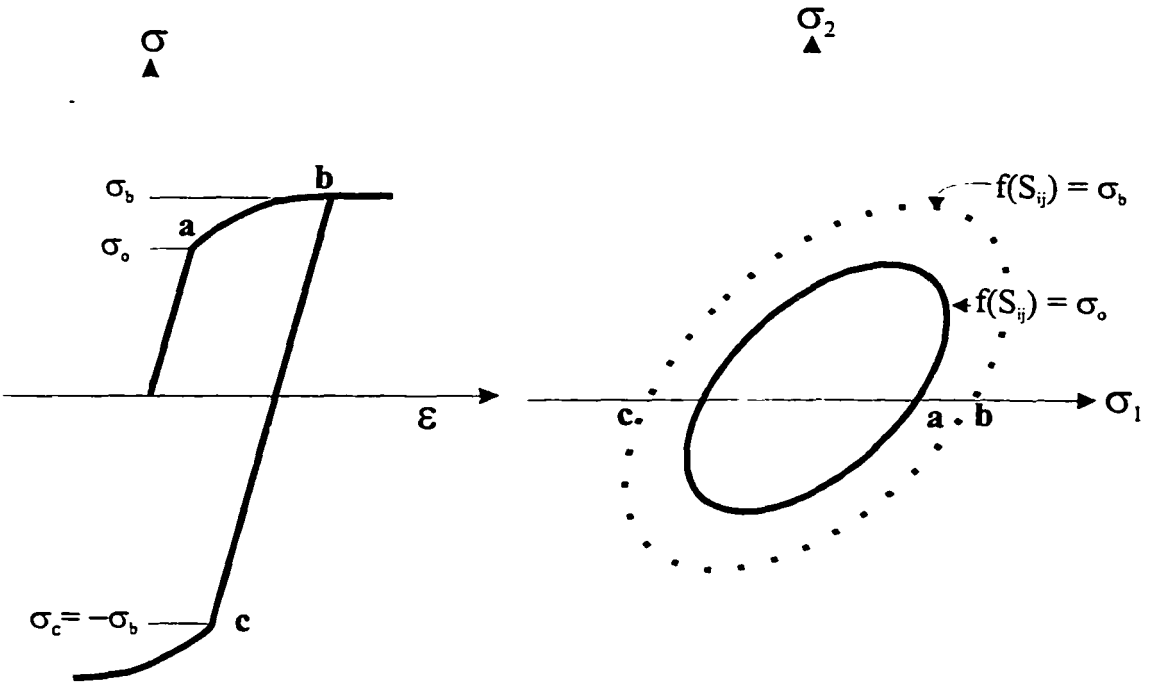


Figure 4.2: Isotropic Hardening

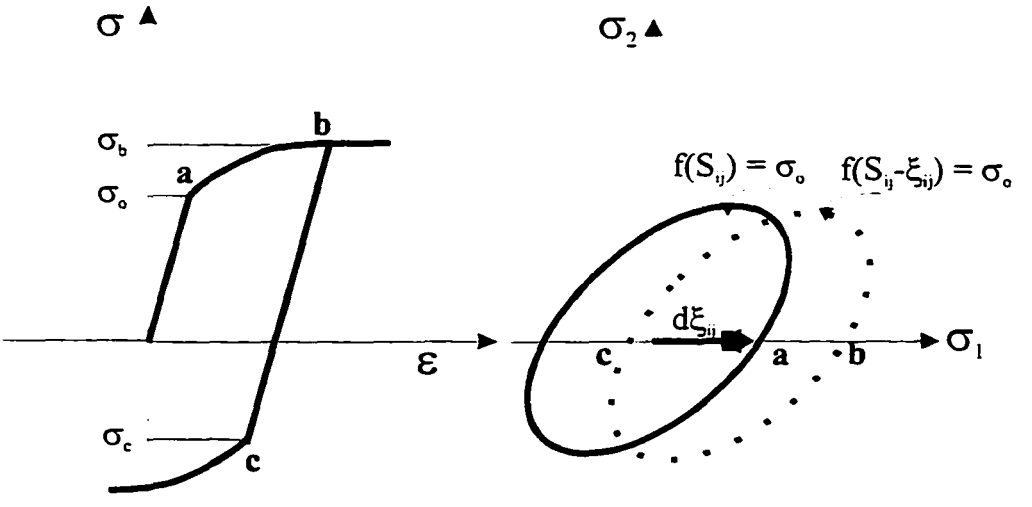


Figure 4.3: Kinematic Hardening

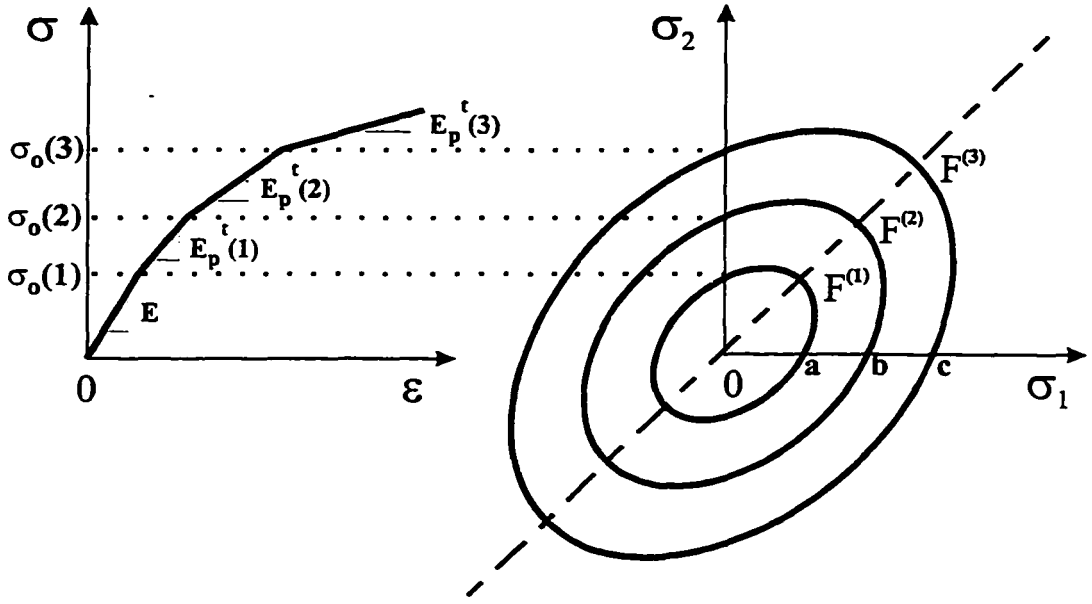


Figure 4.4: Piecewise Linearization of the Material σ–ε Curve and the Corresponding Hardening Surfaces

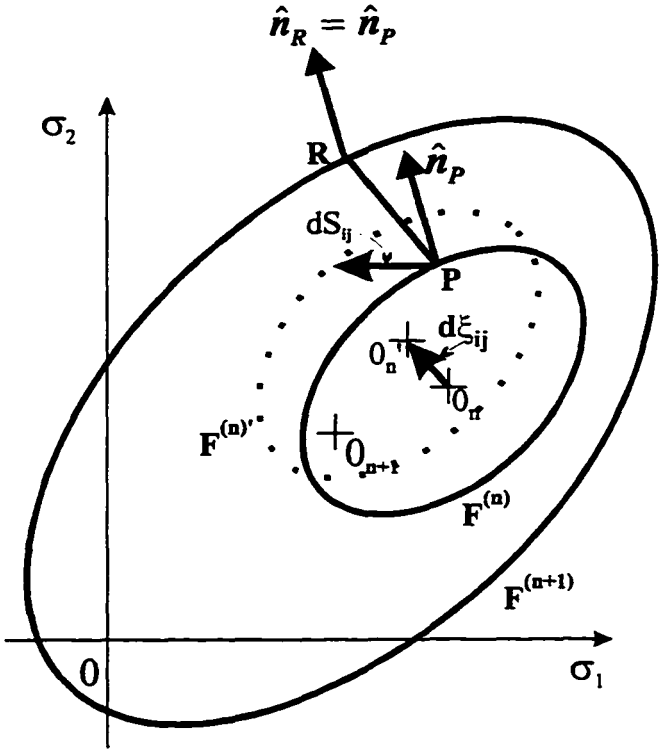


Figure 4.5: The Mróz Translation Rule

5. CHAPTER FIVE:

NOTCH TIP STRESS-STRAIN DETERMINATION

The relationships presented in Chapters Three and Four can be used to solve for the material stress-strain response while a body is undergoing plastic deformation. When a body is subjected to cyclic load, at any point during the cycle the straining may be a result of elastic loading, elastic unloading, or elastic-plastic loading. To fully model the elastic-plastic stress-strain response to an applied loading cycle, equations that delineate each region, and for each region of straining, must be developed. Traditionally, cyclic plasticity methods for determining the response of a material when a cyclic load is applied are used to determine a stress history knowing an elastic-plastic strain history or vise versa. However, in the simplified analyses presented in Chapter Three, it is proposed that the only required knowledge is a notch tip elastic stress history and the properties of the material. Therefore, the method of calculating the notch tip behavior using the simplified equation sets does not follow the conventional plasticity methodology. Specifically, the unloading criterion, the plasticity equations, and the elastic unloading methodology must be written to respect the available input into the simplified analyses.

In this chapter, the complete methodology for solving for the notch tip stress-strain components at any point during a loading cycle using the simplified methods proposed in Chapter Three is detailed. Specifically, the required initial data and calculations are presented

followed by the procedure for describing the unloading criterion and elastic unloading. The method used for describing elastic-plastic loading using either of the proposed incremental equation sets in conjunction with the Mróz multi-surface plasticity model is then presented. Finally, the computer algorithms for implementing the models are described. When required for clarity, the equations presented in Chapters Three and Four in index notation will be expressed in component form following the conventions shown in Figure 2.2.

5.1 Notation

The two independent methods, the incremental Neuber's and ESED methods, are each capable of solving for the notch stress-strain history. To differentiate between methods, all elastic-plastic quantities that refer to the incremental Neuber's method of calculation will have a superscript N, and those referring to the ESED method, a superscript E. Thus, in the most general case, the notch tip elastic-plastic strain and stress tensors expanded on the element are expressible as

$$\sigma_{ij}^{E} = \begin{bmatrix} 0 & 0 & 0 \\ 0 & \sigma_{22}^{E} & \sigma_{23}^{E} \\ 0 & \sigma_{32}^{E} & \sigma_{33}^{E} \end{bmatrix}, \text{ and } \varepsilon_{ij}^{E} = \begin{bmatrix} \varepsilon_{11}^{E} & 0 & 0 \\ 0 & \varepsilon_{22}^{E} & \varepsilon_{23}^{E} \\ 0 & \varepsilon_{32}^{E} & \varepsilon_{33}^{E} \end{bmatrix}, \qquad (5.1a,b)$$

when using the incremental ESED method, and

$$\sigma_{ij}^{N} = \begin{bmatrix} 0 & 0 & 0 \\ 0 & \sigma_{22}^{N} & \sigma_{23}^{N} \\ 0 & \sigma_{32}^{N} & \sigma_{33}^{N} \end{bmatrix}, \text{ and } \varepsilon_{ij}^{E} = \begin{bmatrix} \varepsilon_{11}^{N} & 0 & 0 \\ 0 & \varepsilon_{22}^{N} & \varepsilon_{23}^{N} \\ 0 & \varepsilon_{32}^{N} & \varepsilon_{33}^{N} \end{bmatrix}, \quad (5.2a,b)$$

when using the incremental Neuber's method.

5.2 Initial Requirements

In order to use either the incremental Neuber's or ESED methodology, two sets of input data are required. The first set describes the material properties, and the second, the elastic notch tip stress history.

5.2.1 Material Properties/ Yield Surface Definition

It is assumed that the material is elastic-plastic and that the stabilized cyclic stress-strain curve is defined. The use of the cyclic stress-strain curve assumes a cyclically stable response from the initial loading. However, modeling the cyclic hardening or softening characteristics makes the analyses unnecessarily complex since no significant effect has been found on life predictions when this transient behavior is ignored.

To implement the Mróz multiple surface plasticity model, the uniaxial stress-strain curve must be descretized into segments. Each segment is described by a plastic tangent modulus and an

equivalent stress. Any uniaxial stress-strain curve can be descretized in such a manner and the resulting strain at any point Q can be related to the stress as

$$\varepsilon(Q) = \frac{\sigma_o^{(1)}}{E} + \sum_{i=1}^{n-1} \frac{\sigma_o^{(i+1)} - \sigma_o^{(i)}}{E_p^{t(i)}} + \frac{\sigma(Q) - \sigma_o^{(n)}}{E_p^{t(n)}}. \tag{5.3}$$

In the above equation, n denotes the current or "active" part of the uniaxial curve.

With the knowledge of the uniaxial stress-strain diagram, the hardening modulus $K_p^{(n)}$ defined in eqn (4.19) can be determined for each active surface. That is, if we specialize the flow rule for uniaxial loading, we obtain

$$d\varepsilon^p = \frac{3}{2} \frac{(S_{11} - \xi_{11}^{(n)})^2 d\sigma}{K_p^{(n)} \sigma_o^{(n)2}}, \tag{5.4}$$

where from eqn.(4.18)

$$\sigma_o^{(n)2} = \frac{3}{2}\left[(S_{11} - \xi_{11}^{(n)})^2 + (S_{22} - \xi_{22}^{(n)})^2 + (S_{33} - \xi_{33}^{(n)})^2\right], \tag{5.5}$$

and for uniaxial loading,

$$S_{ij} = \begin{bmatrix} \frac{2}{3}\sigma & 0 & 0 \\ 0 & -\frac{1}{3}\sigma & 0 \\ 0 & 0 & -\frac{1}{3}\sigma \end{bmatrix}, \tag{5.6}$$

$$\xi_{ij} = \begin{bmatrix} \frac{2}{3}\alpha & 0 & 0 \\ 0 & -\frac{1}{3}\alpha & 0 \\ 0 & 0 & -\frac{1}{3}\alpha \end{bmatrix}. \tag{5.7}$$

Substituting (5.6) and (5.7) into (5.5) and rearranging yields

$$\sigma_o^{(n)2} = \frac{9}{4}(S_{11} - \xi_{11}^{(n)})^2 . \tag{5.8}$$

Substituting (5.8) into (5.4) yields

$$K_p^{(n)} = \frac{2}{3}\frac{d\sigma}{d\varepsilon^p} . \tag{5.9}$$

If we differentiate the plastic part of eqn.(5.3) and substitute it into (5.9), then the plasticity constant of the active surface can be defined as

$$K_p^{(n)} = \frac{2}{3}\frac{d\sigma}{d\varepsilon^p} = \frac{2}{3}\left[\frac{1}{\frac{1}{E_p^{t(n)}} - \frac{1}{E}}\right] . \tag{5.10}$$

It should be noted that the method of descretizing the uniaxial stress strain curve in the form of eqn.(5.3) is not obvious. In general, stabilized cyclic stress strain curves are available for materials in the form of the Ramberg-Osgood equation (3.12). The equation indicates that plastic strains are present at the start of loading and thus it does not exhibit a clearly defined yield limit. In the Mróz model, however, the initial yield surface separates elastic from elastic-plastic material behavior and therefore must be of a finite size. Thus, a yield limit must be chosen for the Ramberg-Osgood curve. A poor choice of the yield limit leads to significant errors in the stress-strain results. Methods for choosing an appropriate yield limit are given in [32] and [54].

Another consideration in descretizing the uniaxial curve is the proper choice of the number of yield surfaces. Too few surfaces leads to errors in the results. If too many surfaces are used, an excessive amount of storage space is required to store the back stress tensors of each surface, and furthermore, the stress increments in the plastic region must be very small so that a single increment does not result in skipping surfaces. Generally, it is advantageous to descretize the stress-strain curve so as to result in more plasticity surfaces where the change in the slope of the uniaxial stress-strain curve is the greatest.

5.2.2 Elastic Stress-Strain History

In order to utilize either of the simplified equation methodologies, the elastic stress history at the notch tip is required. That is, the stress-strain history at the notch tip must be known assuming the body under consideration behaves elastically throughout the loading cycle. The elastic stress tensor defined on the notch tip element shown in Figure 2.2 is

$$\sigma_{ij}^{e} = \begin{bmatrix} 0 & 0 & 0 \\ 0 & \sigma_{22}^{e} & \sigma_{23}^{e} \\ 0 & \sigma_{32}^{e} & \sigma_{33}^{e} \end{bmatrix}, \tag{5.11}$$

and can be determined from an elastic finite element analysis of the body or from stress concentration factors available in closed form for certain geometries. The elastic strain tensor,

$$\varepsilon_{ij}^{e} = \begin{bmatrix} \varepsilon_{11}^{e} & 0 & 0 \\ 0 & \varepsilon_{22}^{e} & \varepsilon_{23}^{e} \\ 0 & \varepsilon_{32}^{e} & \varepsilon_{33}^{e} \end{bmatrix}, \tag{5.12}$$

can be found by applying Hooke's Law.

5.3 Elastic Loading

At the beginning of an initial loading cycle, it is assumed that all strains are elastic. Thus initially the notch tip stress-strain response is identical to the available elastic solution, or

$$\sigma_{ij}^{N} = \sigma_{ij}^{E} = \sigma_{ij}^{e}, \tag{5.13}$$

and

$$\varepsilon_{ij}^{N} = \varepsilon_{ij}^{E} = \varepsilon_{ij}^{e}. \tag{5.14}$$

The initial elastic region continues until the initial yield surface is reached. That is, (using eqn.4.18) until

$$F^{(1)}(S_{ij}, \xi_{ij}) = \frac{3}{2} S_{ij}^{e} S_{ij}^{e} - \sigma_{o}^{2} = 0, \tag{5.15}$$

since initially $\xi_{ij}^{(1)} = 0$, and $\sigma_{o}^{(1)} = \sigma_{o}$. Expanding this equation on the notch tip element gives

$$\sigma_{22}^{e\,2} + \sigma_{33}^{e\,2} - \sigma_{22}^{e}\sigma_{33}^{e} + 3\sigma_{23}^{e\,2} - \sigma_{o}^{2} = 0. \tag{5.16}$$

5.4 Unloading Criterion

When the stress state lies on the yield surface, subsequent straining may be the result of elastic unloading or elastic-plastic loading. Which mode of loading is taking place is governed by the unloading criterion.

Plasticity theory dictates that elastic-plastic loading takes place when the stress increment is moving out from the yield surface. If we consider a yield surface function $F(S_{ij})$ (Fig.5.1), then the loading condition requires that the projection of the stress increment onto the normal of the yield surface must be greater than zero for elastic-plastic loading to take place, or

$$\frac{\partial F}{\partial S_{ij}} \cdot dS_{ij} > 0 \quad \text{for elastic-plastic loading.} \tag{5.17}$$

Thus, unloading takes place when the stress increment moves inward from the yield surface or

$$\frac{\partial F}{\partial S_{ij}} \cdot dS_{ij} \leq 0 \quad \text{for elastic unloading.} \tag{5.18}$$

It should be noted that if the inequality in relation (5.18) is equal, then neutral loading is said to occur. That is, the stress increment is tangential to the yield surface. Since computer implementation of this unloading criterion makes it virtually impossible to identify neutral loading, it is presented above as an unloading condition.

In traditional plasticity algorithms, the above loading/unloading conditions are evaluated with the knowledge of the current stress state S_{ij}. If the strain history is known, then the stress increments dS_{ij} are calculated from the strains using elastic stress-strain relations. Using the simplified equation methodology, the increments in the stress and strains are known for the case of an elastic body, that is dS_{ij} can be defined by the elastic increment dS_{ij}^{e}. Substituting the yield surface equation (4.18) for kinematic hardening into the unloading criterion, and changing differentials to finite increments for numerical implementation gives

$$LP = \left(S_{22}^{E} - \xi_{22}^{E}\right)\Delta\sigma_{22}^{e} + \left(S_{33}^{E} - \xi_{33}^{E}\right)\Delta\sigma_{33}^{e} + 2\left(S_{23}^{E} - \xi_{23}^{E}\right)\Delta\sigma_{23}^{e}, \tag{5.19}$$

for the ESED methodology and,

$$LP = \left(S_{22}^{N} - \xi_{22}^{N}\right)\Delta\sigma_{22}^{e} + \left(S_{33}^{N} - \xi_{33}^{N}\right)\Delta\sigma_{33}^{e} + 2\left(S_{23}^{N} - \xi_{23}^{N}\right)\Delta\sigma_{23}^{e}, \tag{5.20}$$

if the incremental Neuber's method is being used. In both cases, LP is the loading parameter that dictates if elastic-plastic loading or if unloading takes place, as

$$LP \begin{cases} > 0 & \text{Elastic} - \text{Plastic Loading} \\ \\ \leq 0 & \text{Elastic Unloading} \end{cases}. \tag{5.21}$$

5.5 Elastic Unloading

If it has been determined that the external load will cause the body to unload elastically, it is necessary to determine whether or not the body will begin to deform in an elastic-plastic

manner during that load increment. For example, consider the case as shown in Figure 5.2 where the initial stress state as calculated by the incremental ESED method (S_{ij}^{E}) or Neuber's (S_{ij}^{N}) method lies on the inner most yield surface. If unloading is to occur during the step, the stress path must follow that of the elastic solution. That is, during elastic unloading

$$\Delta S_{ij}^{E} = \Delta S_{ij}^{e}, \tag{5.22}$$

and

$$\Delta S_{ij}^{N} = \Delta S_{ij}^{e}. \tag{5.23}$$

If the stress increment ΔS_{ij}^{e} intersects the yield surface at $S_{ij}^{N'}$ or $S_{ij}^{E'}$ then this new stress state is found for the incremental Neuber's and ESED equation sets respectively as

$$S_{ij}^{N'} = S_{ij}^{N} + k\Delta S_{ij}^{e}, \tag{5.24}$$

$$S_{ij}^{E'} = S_{ij}^{E} + k\Delta S_{ij}^{e}. \tag{5.25}$$

where k is a parameter greater than zero that denotes where and if the loading path intersects the yield surface. That is:

$$k \begin{cases} < 1 & \text{elastic – plastic loading will occur} \\ = 1 & \text{new stress state lies on the yield surface} \\ > 1 & \text{new stress state is elastic} \end{cases}. \tag{5.26}$$

The parameter k is determined by the condition that the new stress state $S_{ij}^{E'}$ or $S_{ij}^{N'}$ must lie on the innermost yield surface. That is, for the incremental ESED solution set

$$\left[\left(S_{ij}^{E}+k\Delta S_{ij}^{e}\right)-\xi_{ij}^{(1)E}\right]\cdot\left[\left(S_{ij}^{E}+k\Delta S_{ij}^{e}\right)-\xi_{ij}^{(1)E}\right]=\frac{2}{3}\sigma_{o}^{(1)2}, \tag{5.27}$$

or in the case of the incremental Neuber's solution set

$$\left[\left(S_{ij}^{N}+k\Delta S_{ij}^{e}\right)-\xi_{ij}^{(1)N}\right]\cdot\left[\left(S_{ij}^{N}+k\Delta S_{ij}^{e}\right)-\xi_{ij}^{(1)N}\right]=\frac{2}{3}\sigma_{o}^{(1)2}. \tag{5.28}$$

The above two equations result in the following quadratic equations in terms of k:

$$\left[\left(\Delta S_{ij}^{e}\cdot\Delta S_{ij}^{e}\right)\right]k^{2}+\left[2\Delta S_{ij}^{e}\cdot\left(S_{ij}^{E}-\xi_{ij}^{(1)E}\right)\right]k+\left[\left(S_{ij}^{E}-\xi_{ij}^{(1)E}\right)\cdot\left(S_{ij}^{E}-\xi_{ij}^{(1)E}\right)-\frac{2}{3}\sigma_{o}^{(1)2}\right]=0, \tag{5.29}$$

$$\left[\left(\Delta S_{ij}^{e}\cdot\Delta S_{ij}^{e}\right)\right]k^{2}+\left[2\Delta S_{ij}^{e}\cdot\left(S_{ij}^{N}-\xi_{ij}^{(1)N}\right)\right]k+\left[\left(S_{ij}^{N}-\xi_{ij}^{(1)N}\right)\cdot\left(S_{ij}^{N}-\xi_{ij}^{(1)N}\right)-\frac{2}{3}\sigma_{o}^{(1)2}\right]=0, \tag{5.30}$$

for the ESED and Neuber's solution sets, respectively. Each of the quadratics defined by eqns.(5.29) and (5.30) will result in two values for k. The correct root will be the largest value of k greater than zero. If the value of k is less than one, elastic-plastic loading will commence at the stress state defined by eqns. (5.24) or (5.25).

5.6 Elastic-Plastic Loading

When an increment in external load results in plastic deformation at the notch tip, then either the incremental Neuber's or ESED equations can be used in conjunction with the constitutive equations to solve for the notch tip stress and strain increments. In this section, both of the proposed solution sets are presented.

5.6.1 Local Versus Global Co-ordinate Systems

As previously discussed, in the analysis of smooth specimens under uniaxial cyclic loads, Masing's hypothesis is generally used to determine the relationship between stress and strain at any point in the load cycle. In using Masing's hypothesis, each cycle is reduced to a series of monotonic loading steps with boundaries at the point of each load reversal. At the end of each step, the coordinate system for the next step on the stress-strain diagram is changed with its origin being translated to the current stress and strain state. The relationship between stress and strain in subsequent steps is obtained by doubling the stabilized cyclic stress-strain curve and writing the resulting relation in terms of the local coordinate system. Thus, the Masing hypothesis is a method for determining the cyclic stress-strain response and, although mathematically more cumbersome, can be written on the fixed coordinate axis for each reversal in the applied load.

In the case of notched specimens subjected to uniaxial loads, both the uniaxial Neuber's and ESED relations were extended to address unloading by comparing elastic and elastic-plastic energies on the local coordinate frame. One of the more obvious reasons for doing so is the mathematical simplicity in using the equations in conjunction with Masing's hypothesis if written in the local coordinate frame. One of the more subtle reasons, from the point of view of the energy equations, is that it is necessary to work in the local frame to insure compatibility

of the signs of the energy increments. To illustrate this point, consider a notched body subjected to a uniaxial load and assume that a plane stress state exists at the notch tip. Suppose the body has been loaded from zero to some nominal stress S_1 in tension as shown in Figure 5.3a. The stress and strain in the notch tip in the case of an elastic body are known as σ_1^e and ε_1^e, respectively. Using, for example, the uniaxial ESED equations (2.7), the corresponding elastic-plastic strain and stress are found to be ε_1^E and σ_1^E (Fig. 5.3b). Now assume that the nominal is reduced to S_p, where S_p will result in yielding at the notch in the elastic-plastic body. Before the elastic-plastic body yields at point p, the stress and strain increments are the same in both bodies, but the stress in the elastic-plastic body is less after each increment than in the elastic body (since $\sigma_1^E < \sigma_1^e$). Thus in the elastic-plastic body, yielding may occur at a point p, where $\sigma_p^E<0$. If the elastic-plastic response is required at point p', then one would be forced to compare a positive increment in energy in the elastic-plastic case, to a negative value in the elastic case (Fig. 5.3b). If however, local coordinates are used, as shown in Fig. 5.3c, then the signs of both elastic and elastic-plastic energy increments would be positive and a valid comparison would be made.

In the case of non-proportional loading, the multi-surface model used in this work does not require a coordinate transformation. However, to insure compatibility in the signs of elastic and elastic-plastic energy densities, it is proposed that the equations be solved in a local coordinate frame. The direction and origin of the local coordinate frame is dependent on the direction of the equivalent stress in the elastic solution.

It is proposed that the elastic equivalent stress be initially calculated at the end of the first and at the beginning of the second loading step. If the direction of the equivalent stress changes, the origin of the coordinate system to be used for energy density calculations in the second step lies at the stress/strain state at the end of the first step. That is, at $O_2(\sigma_{ij}^{eo}, \varepsilon_{ij}^{eo})$ in the elastic solution and $O_2(\sigma_{ij}^{Eo},\varepsilon_{ij}^{Eo})$ or $O_2(\sigma_{ij}^{No}, \varepsilon_{ij}^{No})$ in the elastic-plastic solution. If the direction of the elastic equivalent stress does not change, then the origin for the second step remains at the origin of the fixed or global frame. For subsequent steps, the elastic equivalent stresses are calculated and compared in the new local coordinate frames.

5.6.2 Dividing Input into Increments for Numerical Integration

In the plastic range, the strain response is load path dependent. As such, the energy equations must be evaluated at each instant of the applied load. For numerical purposes, the differentials in the strains and stresses in the equation sets are changed to small increments and the elastic-plastic incremental response to a small increment in the elastic history (which dictates the loading path) is sought from the equations. In other words, knowing the current stress-strain state ($\sigma_{ij}^{E}/\sigma_{ij}^{N},\varepsilon_{ij}^{E}/\varepsilon_{ij}^{N}$), the equations are used to find the elastic-plastic strain $\Delta\varepsilon_{ij}^{E}/\Delta\varepsilon_{ij}^{N}$ and stress $\Delta\sigma_{ij}^{E}/\Delta\sigma_{ij}^{N}$ increments in response to a small increment in the elastic history $\Delta\sigma_{ij}^{e}, \Delta\varepsilon_{ij}^{e}$. The stress-strain state after the increment in load has been applied is then obtained by summation.

Since we are integrating strain (ESED) and total strain (Neuber's) energy densities along the loading path, it is proposed that a given step in the elastic history be divided into small increments in the energy densities for numerical implementation. Since the equations are to be solved in local coordinates, the increments in the elastic energy densities are taken with reference to the local frame.

Assume that at step (i) in the elastic history, the stress/strain state is given by $\sigma_{ij}^{e(i)}$ and $\varepsilon_{ij}^{e(i)}$, and at step (i+1) by $\sigma_{ij}^{e(i+1)}$ and $\varepsilon_{ij}^{e(i+1)}$. Assume further that it has been determined that the origin of the local coordinate frame for the step is given by $O_i(\sigma_{ij}^{eo},\varepsilon_{ij}^{eo})$. Then the local increments in elastic strain energy density (if using the ESED relations) can be found as

$$\Delta W^e = \left(\sigma_{ij}^{e(i)} - \sigma_{ij}^{eo}\right)\left(\varepsilon_{ij}^{e(i+1)} - \varepsilon_{ij}^{e(i)}\right) + \tfrac{1}{2}\left(\sigma_{ij}^{e(i+1)} - \sigma_{ij}^{e(i)}\right)\left(\varepsilon_{ij}^{e(i+1)} - \varepsilon_{ij}^{e(i)}\right)\Big/N\,, \qquad (5.31)$$

and in the total strain energy density (if using Neubers relations) as

$$\Delta\Omega^e = 2\Delta W^e\,. \qquad (5.32)$$

In the above equations, N denotes the desired number of increments. The above two equations hold regardless of the orientation of the local coordinate axis.

5.6.3 Incremental Equivalent Strain Energy Density Solution Set

In order to model the elastic-plastic stress-strain response to an increment in the elastic stress history using the ESED method, two calculations are required. The first calculation A) consists of solving the equation set defined by the incremental constitutive relations (4.19) and the incremental ESED equations (3.4) simultaneously for the increments in elastic-plastic notch tip strains and stresses. The second calculation B) consists of updating the yield surface configuration in accordance with the translation rule, and the stress and strain tensor for subsequent elastic-plastic straining calculations.

A) Calculation of Elastic-Plastic Strain and Stress Increments

Constitutive Relations:

The constitutive relations utilized are given by eqn.(4.19) in Chapter 4. Expanded on the notch tip element, with the differentials changed to small increments for numerical implementation, the four relations between stress and strain increments are given as:

$$\Delta\varepsilon_{11}^{E} = \left[-\frac{\nu}{E}+\frac{9\gamma^{(n)}}{4\sigma_o^{(n)2}}\,(S_{11}^{E}-\xi_{11}^{(n)E})(S_{22}^{E}-\xi_{22}^{(n)E})\right]\Delta\sigma_{22}^{E}$$

$$+\left[-\frac{\nu}{E}+\frac{9\gamma^{(n)}}{4\sigma_o^{(n)2}}\,(S_{11}^{E}-\xi_{11}^{(n)E})(S_{33}^{E}-\xi_{33}^{(n)E})\right]\Delta\sigma_{33}^{E}+\left[\frac{9\gamma^{(n)}}{2\sigma_o^{(n)2}}\left(S_{11}^{E}-\xi_{11}^{(n)E}\right)\left(S_{23}^{E}-\xi_{23}^{(n)E}\right)\right]\Delta\sigma_{23}^{E},$$

(5.33)

$$\Delta\varepsilon_{22}^{E} = \left[\frac{1}{E}+\frac{9\gamma^{(n)}}{4\sigma_o^{(n)2}}\,(S_{22}^{E}-\xi_{22}^{(n)E})^2\right]\Delta\sigma_{22}^{E} + \left[-\frac{\nu}{E}+\frac{9\gamma^{(n)}}{4\sigma_o^{(n)2}}\,(S_{22}^{E}-\xi_{22}^{(n)E})(S_{33}^{E}-\xi_{33}^{(n)E})\right]\Delta\sigma_{33}^{E}$$

$$+\left[\frac{9\gamma^{(n)}}{2\sigma_o^{(n)2}}\,(S_{22}^{E}-\xi_{22}^{(n)E})(S_{23}^{E}-\xi_{23}^{(n)E})\right]\Delta\sigma_{23}^{E}, \qquad (5.34)$$

$$\Delta\varepsilon_{33}^{E} = \left[\frac{1}{E}+\frac{9\gamma^{(n)}}{4\sigma_o^{(n)2}}\,(S_{33}^{E}-\xi_{33}^{(n)E})(S_{22}^{E}-\xi_{22}^{(n)E})\right]\Delta\sigma_{22}^{E} + \left[-\frac{\nu}{E}+\frac{9\gamma^{(n)}}{4\sigma_o^{(n)2}}\,(S_{33}^{E}-\xi_{33}^{(n)E})^2\right]\Delta\sigma_{33}^{E}$$

$$+\left[\frac{9\gamma^{(n)}}{2\sigma_o^{(n)2}}\,(S_{33}^{E}-\xi_{33}^{(n)E})(S_{23}^{E}-\xi_{23}^{(n)E})\right]\Delta\sigma_{23}^{E}, \qquad (5.35)$$

and

$$\Delta\varepsilon_{23}^{E} = \left[\frac{9\gamma^{(n)}}{4\sigma_o^{(n)2}}\,(S_{23}^{E}-\xi_{23}^{(n)E})(S_{22}^{E}-\xi_{22}^{(n)E})\right]\Delta\sigma_{22}^{E} + \left[\frac{9\gamma^{(n)}}{4\sigma_o^{(n)2}}(S_{23}^{E}-\xi_{23}^{(n)E})(S_{33}^{E}-\xi_{33}^{(n)E})\right]\Delta\sigma_{33}^{E}$$

$$+\left[\frac{1+\nu}{E}+\frac{9\gamma^{(n)}}{2\sigma_o^{(n)2}}\,(S_{23}^{E}-\xi_{23}^{(n)E})^2\right]\Delta\sigma_{23}^{E}, \qquad (5.36)$$

where $\gamma^{(n)} = \dfrac{2}{3K_p^{(n)}}$. Note that in the above equations S_{ij}^{E}, $\xi_{ij}^{(n)E}$, $\gamma^{(n)}$, and $\sigma_o^{(n)}$ are known from the stress state prior to the load increment and the unknowns in the above equations are $\Delta\sigma_{ij}^{E}$ and $\Delta\varepsilon_{ij}^{E}$.

Incremental ESED Relations:

The incremental ESED equations are given by eqns.(3.4) in Chapter Three. Expanded on the notch tip element, and changing differentials to increments, they are expressed as

$$\left(\sigma_{22}^{e}-\sigma_{22}^{eo}\right)\Delta\varepsilon_{22}^{e}+\frac{1}{2}\Delta\sigma_{22}^{e}\Delta\varepsilon_{22}^{e} \;=\; \left(\sigma_{22}^{E}-\sigma_{22}^{Eo}\right)\Delta\varepsilon_{22}^{E}+\frac{1}{2}\Delta\sigma_{22}^{E}\Delta\varepsilon_{22}^{E}, \qquad (5.37)$$

$$\left(\sigma_{33}^{e}-\sigma_{33}^{eo}\right)\Delta\varepsilon_{33}^{e}+\frac{1}{2}\Delta\sigma_{33}^{e}\Delta\varepsilon_{33}^{e} \;=\; \left(\sigma_{33}^{E}-\sigma_{33}^{Eo}\right)\Delta\varepsilon_{33}^{E}+\frac{1}{2}\Delta\sigma_{33}^{E}\Delta\varepsilon_{33}^{E}, \qquad (5.38)$$

$$\left(\sigma_{23}^{e}-\sigma_{23}^{eo}\right)\Delta\varepsilon_{23}^{e}+\frac{1}{2}\Delta\sigma_{23}^{e}\Delta\varepsilon_{23}^{e} \;=\; \left(\sigma_{23}^{E}-\sigma_{23}^{Eo}\right)\Delta\varepsilon_{23}^{E}+\frac{1}{2}\Delta\sigma_{23}^{E}\Delta\varepsilon_{23}^{E}, \qquad (5.39)$$

where higher order terms have been added here for increased accuracy. The above equations represent energy increments on the local coordinate frame with the origin for the step (i) being at $O_i^e(\sigma_{ij}^{oe}\,\varepsilon_{ij}^{oe})$ in the elastic body and $O_i^E(\sigma_{ij}^{oE}\,\varepsilon_{ij}^{oE})$ in the elastic-plastic body. All values in stress and strain in the above equations, however, are written to reference the global or fixed coordinate frame.

The set of seven algebraic equations given by eqns.(5.33 - 5.39) is sufficient to solve for the seven unknown increments of stress and strain at the notch tip. Since the equation set is non-linear, the solution to the equations requires an iterative approach. In the current analyses, the equation sets are first solved ignoring the non-linear terms in the ESED equations. That is, assuming that $\frac{1}{2}\Delta\sigma_{\alpha\beta}\Delta\varepsilon_{\alpha\beta}=0$ in eqns.(5.37-5.39). By doing so, the equation set reduces to a set of seven linear algebraic equations for which a closed form solution is easily attainable. For increased accuracy, the set of seven non-linear equations is solved using the Newton-Raphson method. The initial guesses for the stress-strain increments used in the Newton-Raphson routine are those found from the linear solution.

B) Translating the Yield Surface

After solving for the increments in the notch tip stresses, it is necessary to update the yield surface configuration by employing the multi-surface hardening rule proposed by Mróz. The first step in employing the hardening rule is to determine which surface is active after the notch tip stresses have increased by an amount $\Delta\sigma_{ij}^{E}$. Specifically, if $F^{(n)}$ is the active plasticity surface before the stress increment, it is necessary to determine whether the new stress state remains on $F^{(n)}$, or if it lies on $F^{(n-1)}$. The active surface can be found by determining what fraction, κ, of the stress increment, $\Delta\sigma_{ij}^{E}$, results in a stress state that lies on the outer hardening surface, $F^{(n-1)}$. In other words, find the value of κ such that the new stress state $\sigma_{ij}^{E} + \kappa\Delta\sigma_{ij}^{E}$ lies on the outer yield surface given by

$$\left[\left(S_{ij}^{E} + \kappa\Delta S_{ij}^{E}\right) - \xi_{ij}^{(n-1)\,E}\right]\cdot\left[\left(S_{ij}^{E} + \kappa\Delta S_{ij}^{E}\right) - \xi_{ij}^{(n-1)\,E}\right] = \frac{2}{3}\sigma_{o}^{(n-1)\,2}. \tag{5.40}$$

Equation (5.40) results in the following quadratic in κ

$$\left[\left(\Delta S_{ij}^{E}\cdot\Delta S_{ij}^{E}\right)\right]\kappa^{2} + \left[2\Delta S_{ij}^{E}\cdot\left(S_{ij}^{E} - \xi_{ij}^{(n-1)\,E}\right)\right]\kappa + \left[\left(S_{ij}^{E} - \xi_{ij}^{(n-1)\,E}\right)\cdot\left(S_{ij}^{E} - \xi_{ij}^{(n-1)\,E}\right) - \frac{2}{3}\sigma_{o}^{(n-1)\,2}\right] = 0. \tag{5.41}$$

The correct root of eqn. (5.41) will yield a value of κ greater than zero. The value of κ determines the active yield surface as

$$\kappa \begin{cases} \leq 1 \text{ the new active surface is } F^{(n+1)} \\ > 1 \; F^{(n)} \text{ remains the active surface} \end{cases} . \tag{5.42}$$

If the value of κ is less than one, then the updated stress state $\sigma_{ij}^{E}+\kappa\Delta\sigma_{ij}^{E}$ lies on the yield surface $F^{(n+1)}$. The increment in the strain energy density in the elastic body that brought the stress state to the new yield surface must be divided into two increments. The first increment, to bring the new elastic-plastic stress state to the new yield surface, and the second for subsequent straining on the new yield surface $F^{(n+1)}$.

To determine the portion of the elastic increment that brought the elastic-plastic strain and stress increment to the new surface, the energy equation given by eqn.(3.2) is used, or

$$\Delta W^{E} = \Delta W^{e} . \tag{5.43}$$

where the absence of subscripts implies the equation of energy density, rather than energy density axial contributions. In this part of the increment, the elastic-plastic quantities are known. That is, the stress increments are given by $\kappa\Delta\sigma_{ij}^{E}$ and the strain increments can be calculated from eqns.(5.33 - 5.36) on the active surface $F^{(n)}$. Thus, on the notch tip element

$$\begin{aligned} \Delta W^{E} = &\left(\sigma_{22}^{E} - \sigma_{22}^{Eo}\right)\Delta\varepsilon_{22}^{E} + \left(\sigma_{33}^{E} - \sigma_{33}^{Eo}\right)\Delta\varepsilon_{33}^{E} + 2\left(\sigma_{23}^{E} - \sigma_{23}^{Eo}\right)\Delta\varepsilon_{23}^{E} \\ &+ \tfrac{1}{2}\Delta\sigma_{22}^{E}\Delta\varepsilon_{22}^{E} + \tfrac{1}{2}\Delta\sigma_{33}^{E}\Delta\varepsilon_{33}^{E} + \Delta\sigma_{23}^{E}\Delta\varepsilon_{23}^{E}, \end{aligned} \tag{5.44}$$

can be calculated from known quantities. The corresponding elastic energy increment, ΔW^{e} can be determined by finding the elastic fraction κ^{e} of the total elastic stress increment $\Delta\sigma_{ij}^{e}$

that satisfies eqn.(5.43). Thus, for the elastic increment, the energy density can be written using Hooke's law and the value of κ^e can be determined from

$$A\kappa^{e\,2} + B\kappa^e + C = 0. \qquad (5.45a,b,c,d)$$

where

$$A = \left(\Delta\sigma_{22}^{e\,2} + \Delta\sigma_{33}^{e\,2} - 2\nu\Delta\sigma_{22}^{e}\Delta\sigma_{33}^{e} + 2\Delta\sigma_{23}^{e\,2}(1+\nu)\right),$$

$$B = 2\left[\left(\sigma_{22}^{e} - \sigma_{22}^{e0}\right)\left(\Delta\sigma_{22}^{e} - \nu\Delta\sigma_{33}^{e}\right) + \left(\sigma_{33}^{e} - \sigma_{33}^{e0}\right)\left(\Delta\sigma_{33}^{e} - \nu\Delta\sigma_{33}^{e}\right) + 2\left(\sigma_{23}^{e} - \sigma_{23}^{e0}\right)(1+\nu)\Delta\sigma_{23}^{e}\right],$$

and,

$$C = -2E\Delta W^{E}.$$

The correct root of the quadratic will yield a value of κ^e between zero and one. Thus, the portion of the elastic increment $\kappa^e\Delta\sigma_{ij}^e$ results in the elastic-plastic strain state just on the new active surface $F^{(n-1)}$. The remainder of the increment $(1-\kappa^e)\Delta\sigma_{ij}^e$ results in an elastic-plastic state that moves with $F^{(n-1)}$. The equation set (5.33-5.39) must be recalculated for the remainder of the increment, with the surface $F^{(n-1)}$ being active.

Whether or not the active yield surface changes, the yield surface configuration must be updated at the end of each increment. According to the translation rule proposed by Mróz, the back stress tensor α_{ij} translates in accordance with eqn.(4.20) for a given increment in the notch tip stresses. Changing the differentials in eqn.(4.20) to finite increments, and writing the

equations in stress space, rather than in deviatoric space, gives the following equations for the translation of the active yield surface $F^{(n)}$:

$$\Delta\alpha_{22}^{E(n)} = \Delta\mu\,(\sigma_{22}^{E(n+1)} - \sigma_{22}^{E}),$$

$$\Delta\alpha_{33}^{E(n)} = \Delta\mu\,(\sigma_{33}^{E(n+1)} - \sigma_{33}^{E}). \qquad (5.46a,b,c)$$

$$\Delta\alpha_{23}^{E(n)} = \Delta\mu\,(\sigma_{23}^{E(n+1)} - \sigma_{23}^{E}),$$

where,

$$\sigma_{22}^{E(n+1)} = \alpha_{22}^{(n+1)} + \frac{\sigma_o^{(n+1)}}{\sigma_o^{(n)}}(\sigma_{22}^{E} - \alpha_{22}^{(n)}),$$

$$\sigma_{33}^{E(n+1)} = \alpha_{33}^{(n+1)} + \frac{\sigma_o^{(n+1)}}{\sigma_o^{(n)}}(\sigma_{33}^{E} - \alpha_{33}^{(n)}). \qquad (5.47a,b,c)$$

$$\sigma_{23}^{E(n+1)} = \alpha_{23}^{(n+1)} + \frac{\sigma_o^{(n+1)}}{\sigma_o^{(n)}}(\sigma_{23}^{E} - \alpha_{23}^{(n)}).$$

The parameter $\Delta\mu$ can be found by expanding the consistency condition (eqn.4.26) on the notch tip element, or

$$A\Delta\mu^2 + B\Delta\mu + C = 0. \qquad (5.48a,b,c,d)$$

where

$$A = \left(\sigma_{22}^{E(n+1)} - \sigma_{22}^{E}\right)^2 + \left(\sigma_{33}^{E(n+1)} - \sigma_{33}^{E}\right)^2 - \left(\sigma_{22}^{E(n+1)} - \sigma_{22}^{E}\right)\left(\sigma_{33}^{E(n+1)} - \sigma_{33}^{E}\right) + 3\left(\sigma_{23}^{E(n+1)} - \sigma_{23}^{E}\right)^2,$$

$$B = -3\left\{\left(S_{22}^{E} - \xi_{22}^{E(n)} + \Delta S_{22}^{E}\right)\left(\sigma_{22}^{E(n+1)} - \sigma_{22}^{E}\right) + \left(S_{33}^{E} - \xi_{33}^{E(n)} + \Delta S_{33}^{E}\right)\left(\sigma_{33}^{E(n+1)} - \sigma_{33}^{E}\right)\right.$$

$$\left. + 2\left(S_{23}^{E} - \xi_{23}^{E(n)} + \Delta S_{23}^{E}\right)\left(\sigma_{23}^{E(n+1)} - \sigma_{23}^{E}\right)\right\}, \text{ and}$$

$$C = 3\left\{\left(S_{22}^{E} - \xi_{22}^{E(n)}\right)\Delta\sigma_{22}^{E} + \left(S_{33}^{E} - \xi_{33}^{E(n)}\right)\Delta\sigma_{33}^{E} + 2\left(S_{23}^{E} - \xi_{23}^{E(n)}\right)\Delta\sigma_{23}^{E}\right\}$$

$$+ \Delta\sigma_{22}^{E\,2} + \Delta\sigma_{33}^{E\,2} - \Delta\sigma_{22}^{E}\Delta\sigma_{33}^{E} + 3\Delta\sigma_{23}^{E\,2}.$$

Note that $\Delta S_{ij} = \Delta\sigma_{ij} - \dfrac{\Delta\sigma_{kk}\delta_{ij}}{3}$ are the deviatoric components of the stress increment tensor $\Delta\sigma_{ij}$. The correct root of eqn.(5.48) will set $\Delta\mu$ as: $0 < \Delta\mu < 1$.

Equations (5.46-5.48) enable the increments in the back stress tensor of the active surface to be determined for an increment in the stress-strain state: $\Delta\sigma_{ij}^{E}$, $\Delta\varepsilon_{ij}^{E}$. The new state, $\sigma_{ij}^{E'}$, $\varepsilon_{ij}^{E'}$, can then be determined from

$$\sigma_{ij}^{E'} = \sigma_{ij}^{E} + \Delta\sigma_{ij}^{E}, \tag{5.49}$$

and

$$\varepsilon_{ij}^{E'} = \varepsilon_{ij}^{E} + \Delta\varepsilon_{ij}^{E}, \tag{5.50}$$

and lies on the active yield surface $F^{(n)}$ with central coordinates

$$\alpha_{ij}^{(n)E'} = \alpha_{ij}^{(n)E} + \Delta\alpha_{ij}^{(n)E}. \tag{5.51}$$

After the active surface $F^{(n)}$ has been translated, it is necessary to translate all surfaces interior to the active surface so that they are tangent to the active surface at the stress point. The center of the active surface $F^{(n-1)}$ for example can be found using eqn.(4.28) as

$$\alpha_{ij}^{E(n-1)} = \sigma_{ij}^{E'} - \frac{\sigma_o^{(n-1)}}{\sigma_o^{(n)}}\left(\sigma_{ij}^{E'} - \alpha_{ij}^{E(n)'}\right). \tag{5.52}$$

5.6.4 Incremental Neuber's Solution Set

Similar to the ESED solution set, the elastic-plastic stress strain response to an increment in the elastic stress history using the Neuber's method requires A) solving the equation set defined by the incremental constitutive relations (4.19) and the incremental Neuber's equations (3.8) simultaneously for the increments in elastic-plastic notch tip strains and stresses, and B) updating the yield surface configuration and the stress and strain tensor for subsequent elastic-plastic straining calculations.

A) Calculation of the Elastic-Plastic Strain and Stress Increments

Incremental Constitutive Equations

Expanded on the notch tip element, the constitutive relations given by eqns.(4.19) in Chapter Four are written for the Neuber's solution set as

$$\Delta\varepsilon_{11}^{N} = \left[-\frac{\nu}{E} + \frac{9\gamma^{(n)}}{4\sigma_o^{(n)2}}\,(S_{11}^{N} - \xi_{11}^{(n)N})(S_{22}^{E} - \xi_{22}^{(n)N})\right]\Delta\sigma_{22}^{N}$$

$$+\left[-\frac{\nu}{E} + \frac{9\gamma^{(n)}}{4\sigma_o^{(n)2}}\,(S_{11}^{N} - \xi_{11}^{(n)N})(S_{33}^{N} - \xi_{33}^{(n)N})\right]\Delta\sigma_{33}^{E} + \left[\frac{9\gamma^{(n)}}{2\sigma_o^{(n)2}}\left(S_{11}^{N} - \xi_{11}^{(n)N}\right)\left(S_{23}^{N} - \xi_{23}^{(n)N}\right)\right]\Delta\sigma_{23}^{E}, \tag{5.53}$$

$$\Delta\varepsilon_{22}^{N} = \left[\frac{1}{E}+\frac{9\gamma^{(n)}}{4\sigma_o^{(n)2}}\,(S_{22}^{N}-\xi_{22}^{(n)N})^2\right]\Delta\sigma_{22}^{N} + \left[-\frac{\nu}{E}+\frac{9\gamma^{(n)}}{4\sigma_o^{(n)2}}\,(S_{22}^{N}-\xi_{22}^{(n)N})(S_{33}^{N}-\xi_{33}^{(n)N})\right]\Delta\sigma_{33}^{N}$$

$$+\left[\frac{9\gamma^{(n)}}{2\sigma_o^{(n)2}}\,(S_{22}^{N}-\xi_{22}^{(n)N})(S_{23}^{N}-\xi_{23}^{(n)N})\right]\Delta\sigma_{23}^{N}, \qquad (5.54)$$

$$\Delta\varepsilon_{33}^{N} = \left[\frac{1}{E}+\frac{9\gamma^{(n)}}{4\sigma_o^{(n)2}}\,(S_{33}^{N}-\xi_{33}^{(n)N})(S_{22}^{N}-\xi_{22}^{(n)N})\right]\Delta\sigma_{22}^{N} + \left[-\frac{\nu}{E}+\frac{9\gamma^{(n)}}{4\sigma_o^{(n)2}}\,(S_{33}^{N}-\xi_{33}^{(n)N})^2\right]\Delta\sigma_{33}^{N}$$

$$+\left[\frac{9\gamma^{(n)}}{2\sigma_o^{(n)2}}\,(S_{33}^{N}-\xi_{33}^{(n)N})(S_{23}^{N}-\xi_{23}^{(n)N})\right]\Delta\sigma_{23}^{N}, \qquad (5.55)$$

and

$$\Delta\varepsilon_{23}^{N} = \left[\frac{9\gamma^{(n)}}{4\sigma_o^{(n)2}}\,(S_{23}^{N}-\xi_{23}^{(n)N})(S_{22}^{N}-\xi_{22}^{(n)N})\right]\Delta\sigma_{22}^{N} + \left[\frac{9\gamma^{(n)}}{4\sigma_o^{(n)2}}(S_{23}^{N}-\xi_{23}^{(n)N})(S_{33}^{N}-\xi_{33}^{(n)N})\right]\Delta\sigma_{33}^{N}$$

$$+\left[\frac{1+\nu}{E}+\frac{9\gamma^{(n)}}{2\sigma_o^{(n)2}}\,(S_{23}^{N}-\xi_{23}^{(n)N})^2\right]\Delta\sigma_{23}^{N}. \qquad (5.56)$$

where the only unknowns are the stress and strain increments $\Delta\sigma_{ij}^{N}$, $\Delta\varepsilon_{ij}^{N}$.

Incremental Neuber's Equations

The incremental Neuber's equations are given by eqn.(3.8) in Chapter Three. Expanded on the notch tip element and changing differentials to increments yields

$$(\sigma_{22}^{e}-\sigma_{22}^{eo})\Delta\varepsilon_{22}^{e} + (\varepsilon_{22}^{e}-\varepsilon_{22}^{eo})\Delta\sigma_{22}^{e} + \Delta\sigma_{22}^{e}\Delta\varepsilon_{22}^{e} = (\sigma_{22}^{N}-\sigma_{22}^{No})\Delta\varepsilon_{22}^{N} + (\varepsilon_{22}^{N}-\varepsilon_{22}^{No})\Delta\sigma_{22}^{N} + \Delta\sigma_{22}^{N}\Delta\varepsilon_{22}^{N}, \qquad (5.57)$$

$$(\sigma_{33}^{e}-\sigma_{33}^{eo})\Delta\varepsilon_{33}^{e} + (\varepsilon_{33}^{e}-\varepsilon_{33}^{eo})\Delta\sigma_{33}^{e} + \Delta\sigma_{33}^{e}\Delta\varepsilon_{33}^{e} = (\sigma_{33}^{N}-\sigma_{33}^{No})\Delta\varepsilon_{33}^{N} + (\varepsilon_{33}^{N}-\varepsilon_{33}^{No})\Delta\sigma_{33}^{N} + \Delta\sigma_{33}^{N}\Delta\varepsilon_{33}^{N}, \qquad (5.58)$$

$$\left(\sigma_{23}^{e}-\sigma_{23}^{e0}\right)\Delta\varepsilon_{23}^{e}+\left(\varepsilon_{23}^{e}-\varepsilon_{23}^{e0}\right)\Delta\sigma_{23}^{e}+\Delta\sigma_{23}^{e}\Delta\varepsilon_{23}^{e}=\left(\sigma_{23}^{N}-\sigma_{23}^{No}\right)\Delta\varepsilon_{23}^{N}+\left(\varepsilon_{23}^{N}-\varepsilon_{23}^{No}\right)\Delta\sigma_{23}^{N}+\Delta\sigma_{23}^{N}\Delta\varepsilon_{23}^{N}, \qquad (5.59)$$

where higher order terms have been added here for increased accuracy. It should be noted that the above equations represent energy increments on the local coordinate frame with the origin for the step i being at $O_i^e(\sigma_{ij}^{oe}.\varepsilon_{ij}^{oe})$ in the elastic body and $O_i^N(\sigma_{ij}^{oN}.\varepsilon_{ij}^{oN})$ in the elastic-plastic body.

The set of seven algebraic equations given by eqns (5.53-5.59) is sufficient to solve for the seven unknown stress and strain increments at the notch tip. It should be noted that the equation set is non-linear. As in the ESED method, it is proposed that equation sets first be evaluated ignoring the non-linear terms in Neuber's equations. That is, assuming that $\Delta\sigma_{\alpha\beta}\Delta\varepsilon_{\alpha\beta}=0$ in eqns.(5.57-5.59). For increased accuracy, a non-linear routine such as the Newton-Raphson method can be used to find the stress increments, with the initial guesses for the non-linear routine being the linear solution.

B) Translating the Yield Surface

Following the same method as the ESED solution for determining the active surface after the notch tip stresses have increased by $\Delta\sigma_{ij}^{N}$, the following equation is employed

$$\left[\left(S_{ij}^{N}+\kappa\Delta S_{ij}^{N}\right)-\xi_{ij}^{(n+1)N}\right].\left[\left(S_{ij}^{N}+\kappa\Delta S_{ij}^{N}\right)-\xi_{ij}^{(n+1)N}\right]=\frac{2}{3}\sigma_{o}^{(n+1)2}. \qquad (5.60)$$

Equation (5.60) results in the following quadratic in κ

$$\left[\left(\Delta S_{ij}^{N} \cdot \Delta S_{ij}^{N}\right)\right]\kappa^2 + \left[2\Delta S_{ij}^{N} \cdot \left(S_{ij}^{N} - \xi_{ij}^{(n+1)N}\right)\right]\kappa + \left[\left(S_{ij}^{N} - \xi_{ij}^{(n+1)N}\right) \cdot \left(S_{ij}^{N} - \xi_{ij}^{(n+1)N}\right) - \frac{2}{3}\sigma_{o}^{(n+1)2}\right] = 0, \tag{5.61}$$

where κ must be greater than zero. The value of κ determines the active yield surface as given in (5.42). If the value of κ is less than one, then the updated stress state $\sigma_{ij}^{N}+\kappa\Delta\sigma_{ij}^{N}$ lies on the yield surface $F^{(n-1)}$. As in the ESED solution set, the increment in the elastic total strain energy density that brought the stress state to the new yield surface must be divided into two increments. The first increment to bring the new elastic-plastic stress state to the new yield surface, and the next increment for subsequent straining.

To determine the portion of the elastic increment that brought the elastic-plastic strain and stress increment to the new surface, the energy equation given by eqn.(3.6) is used, or

$$\Delta\Omega^{N} = \Delta\Omega^{e}. \tag{5.62}$$

where again the absence of subscripts implies the equation of total strain energy densities, rather than total strain energy density axial contributions. In this part of the increment, the elastic-plastic quantities are known. That is, the stress increments are given by $\kappa\Delta\sigma_{ij}^{N}$ and the strain increments can be calculated from eqns.(5.56-5.53) on the active surface $F^{(n)}$. Thus, on the notch tip element

$$\Delta\Omega^{E} = \left(\sigma_{22}^{N} - \sigma_{22}^{No}\right)\Delta\varepsilon_{22}^{N} + \left(\varepsilon_{22}^{N} - \varepsilon_{22}^{No}\right)\Delta\sigma_{22}^{N} + \left(\sigma_{33}^{N} - \sigma_{33}^{No}\right)\Delta\varepsilon_{33}^{N} + \left(\varepsilon_{33}^{N} - \varepsilon_{33}^{No}\right)\Delta\sigma_{33}^{N} +$$

$$2\left(\sigma_{23}^{N}-\sigma_{23}^{No}\right)\Delta\varepsilon_{23}^{N}+2\left(\varepsilon_{23}^{N}-\varepsilon_{23}^{No}\right)\Delta\sigma_{23}^{N}+\tfrac{1}{2}\Delta\sigma_{22}^{N}\Delta\varepsilon_{22}^{N}+\tfrac{1}{2}\Delta\sigma_{33}^{N}\Delta\varepsilon_{33}^{N}+\Delta\sigma_{23}^{N}\Delta\varepsilon_{23}^{N}, \quad (5.63)$$

can be calculated from known quantities. The corresponding elastic energy increment, $\Delta\Omega^{e}$, can be determined by finding the elastic fraction ,κ^{e}, of the total elastic stress increment, $\Delta\sigma_{ij}^{e}$, that satisfies eqn.(5.62). For this purpose eqn.(5.45a,b,c) can again be applied with the constant C (5.45d) now being given by

$$C = -E\Delta\Omega^{N}. \quad (5.64)$$

Thus, the portion of the elastic increment, $\kappa^{e}\Delta\sigma_{ij}^{e}$, results in the elastic-plastic strain state lying just on the new active surface, $F^{(n+1)}$. The remainder of the increment, $(1-\kappa^{e})\Delta\sigma_{ij}^{e}$, results in an elastic-plastic state that moves with $F^{(n-1)}$. The equation set (5.53-5.59) must be recalculated for the remainder of the increment, with the surface $F^{(n-1)}$ being active.

The translation of the active yield surface can be found by using eqn.(4.20). Expanding eqn.(4.20) on the notch tip element, and changing differentials to finite increments gives the following equations for the translation of the active yield surface $F^{(n)}$:

$$\Delta\alpha_{22}^{N(n)} = \Delta\mu\,(\sigma_{22}^{N(n+1)}-\sigma_{22}^{N}),$$

$$\Delta\alpha_{33}^{N(n)} = \Delta\mu\,(\sigma_{33}^{N(n+1)}-\sigma_{33}^{N}), \quad (5.65a,b,c)$$

$$\Delta\alpha_{23}^{N(n)} = \Delta\mu\,(\sigma_{23}^{N(n+1)}-\sigma_{23}^{N}),$$

where

$$\sigma_{22}^{N(n+1)} = \alpha_{22}^{(n+1)} + \frac{\sigma_o^{(n+1)}}{\sigma_o^{(n)}}(\sigma_{22}^{N} - \alpha_{22}^{(n)}),$$

$$\sigma_{33}^{N(n+1)} = \alpha_{33}^{(n+1)} + \frac{\sigma_o^{(n+1)}}{\sigma_o^{(n)}}(\sigma_{33}^{N} - \alpha_{33}^{(n)}), \qquad (5.66a,b,c)$$

$$\sigma_{23}^{N(n+1)} = \alpha_{23}^{(n+1)} + \frac{\sigma_o^{(n+1)}}{\sigma_o^{(n)}}(\sigma_{23}^{N} - \alpha_{23}^{(n)}).$$

The parameter $\Delta\mu$ can be found by expanding the consistency condition (eqn.4.26) on the notch tip element, or

$$A\Delta\mu^2 + B\Delta\mu + C = 0, \qquad (5.67a,b,c,d)$$

where:

$$A = \left(\sigma_{22}^{N(n+1)} - \sigma_{22}^{N}\right)^2 + \left(\sigma_{33}^{N(n+1)} - \sigma_{33}^{N}\right)^2 - \left(\sigma_{22}^{N(n+1)} - \sigma_{22}^{N}\right)\left(\sigma_{33}^{N(n+1)} - \sigma_{33}^{N}\right) + 3\left(\sigma_{23}^{N(n+1)} - \sigma_{23}^{N}\right)^2,$$

$$B = -3\left\{\left(S_{22}^{N} - \xi_{22}^{N(n)} + \Delta S_{22}^{N}\right)\left(\sigma_{22}^{N(n+1)} - \sigma_{22}^{N}\right) + \left(S_{33}^{N} - \xi_{33}^{N(n)} + \Delta S_{33}^{N}\right)\left(\sigma_{33}^{N(n+1)} - \sigma_{33}^{N}\right)\right.$$

$$\left. + 2\left(S_{23}^{N} - \xi_{23}^{N(n)} + \Delta S_{23}^{N}\right)\left(\sigma_{23}^{N(n+1)} - \sigma_{23}^{N}\right)\right\},$$

$$C = 3\left[\left(S_{22}^{N} - \xi_{22}^{N(n)}\right)\Delta\sigma_{22}^{N} + \left(S_{33}^{N} - \xi_{33}^{N(n)}\right)\Delta\sigma_{33}^{N} + 2\left(S_{23}^{N} - \xi_{23}^{N(n)}\right)\Delta\sigma_{23}^{N}\right]$$

$$+ \Delta\sigma_{22}^{N2} + \Delta\sigma_{33}^{N2} - \Delta\sigma_{22}^{N}\Delta\sigma_{33}^{N} + 3\Delta\sigma_{23}^{N2},$$

where again the correct root yields a value of $\Delta\mu$ between zero and one.

Equations (5.65-5.67) enable the increments in the back stress tensor of the active surface to be determined for an increment in the stress-strain state, $\Delta\sigma_{ij}^{N}$, $\Delta\varepsilon_{ij}^{N}$. The new state, $\sigma_{ij}^{N'}$, $\varepsilon_{ij}^{N'}$, and the coordinates of the back stress tensor of the active yield surface $F^{(n)}$ can be found by summation.

Finally, it is necessary to translate all surfaces interior to that active so that they are tangent to the active surface at the stress point. As in the ESED solution, the center of the active surface $F^{(n-1)}$ for example can be found using eqn.(4.28) as

$$\alpha_{ij}^{N(n-1)} = \sigma_{ij}^{N'} - \frac{\sigma_o^{(n-1)}}{\sigma_o^{(n)}}\left(\sigma_{ij}^{N'} - \alpha_{ij}^{N(n)'}\right). \tag{5.68}$$

5.7 Computer Implementation

In order to implement the equations defined in this chapter for a notched body subjected to a history of cyclic loads, two computer programs were written in Fortran; the first, for the implementation of the incremental ESED equation set, and the second for the implementation of the incremental Neuber's equation set. The input to both programs is the descretized cyclic uniaxial curve and steps in the elastic notch tip history. The output is the history of elastic-plastic strains and stresses. The general algorithm for both programs is the same and the computer flow chart is shown in Figure 5.4.

Initially, all the strains are assumed to be elastic and thus the centers of the yield surfaces are concentric and centered at the origin (virgin loading). In this region, equations (5.13-5.16) apply. As soon as the material yields, it is necessary in subsequent steps to determine whether or not the stresses lie on the active surface. If they do, then the unloading criterion (5.19 or

5.20) can be used to determine whether elastic-plastic loading (5.22 or 5.23), or elastic unloading with the possibility of elastic-plastic loading (as governed by eqns.(5.29) or (5.30)) will take place during the step. If the stresses are not on the active surface, then they are elastic and again there is the possibility of elastic unloading or elastic unloading followed by elastic-plastic loading taking place during that step. It should also be mentioned that the origin and direction of the local coordinate system is determined for both the elastic and elastic-plastic solution at the beginning of each step. If the origin changes, then the coordinate system for the elastic and elastic-plastic solution is the known stress-strain state at the beginning of the step.

The heart of each program is the plasticity routine. The computer flow chart for the plasticity routine is shown in Figure 5.5. In each plasticity routine, the elastic step is divided into increments in accordance with eqns.(5.31) or (5.32). The elastic-plastic strain and stress increments are calculated using the linear terms in equation sets (5.33 - 5.39) or (5.53-5.59) and the solution to the set of seven linear equations is subsequently used as an initial guess in a non-linear solver. If it is found that the stresses exceed the outer surface, as governed by equations (5.41) or (5.61), then the stresses are updated only to the point where the new stress state lies on the new surface. The active surface is then translated in accordance with equations (5.46-5.48) or (5.65-5.67). The surfaces, if any, that lie within the active surface are then translated to be tangent to the active surface at the stress point (eqns.5.52 or 5.68). The active surface number is then updated. Finally the elastic-plastic stress-strain calculation is repeated for the portion of the elastic energy increment that is to travel with the surface $F^{(n+1)}$. If the stresses after the load increment has been applied remain on the current active yield surface,

then the surface is translated, stresses are updated, and if any surfaces are on the interior to the active surface, they are translated. As shown in Figure 5.5, the procedure is repeated until the last increment in the elastic step has been reached.

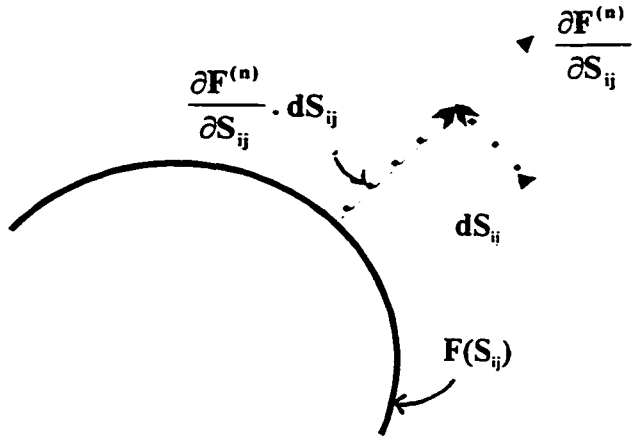


Figure 5.1: Unloading Criterion

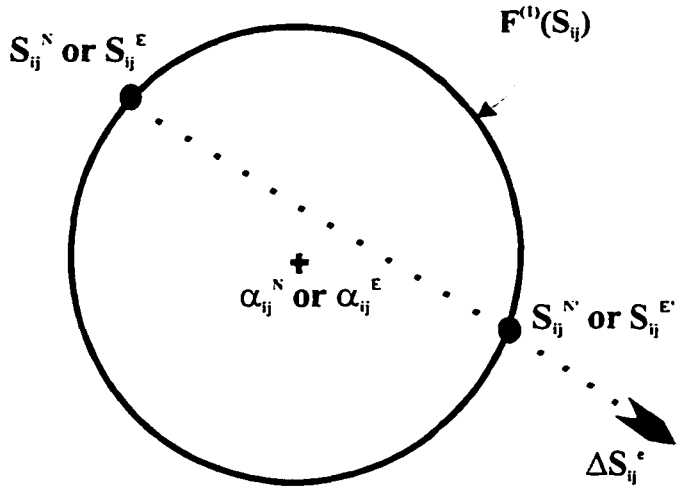


Figure 5.2: Elastic-Plastic Loading During Elastic Unloading Increment

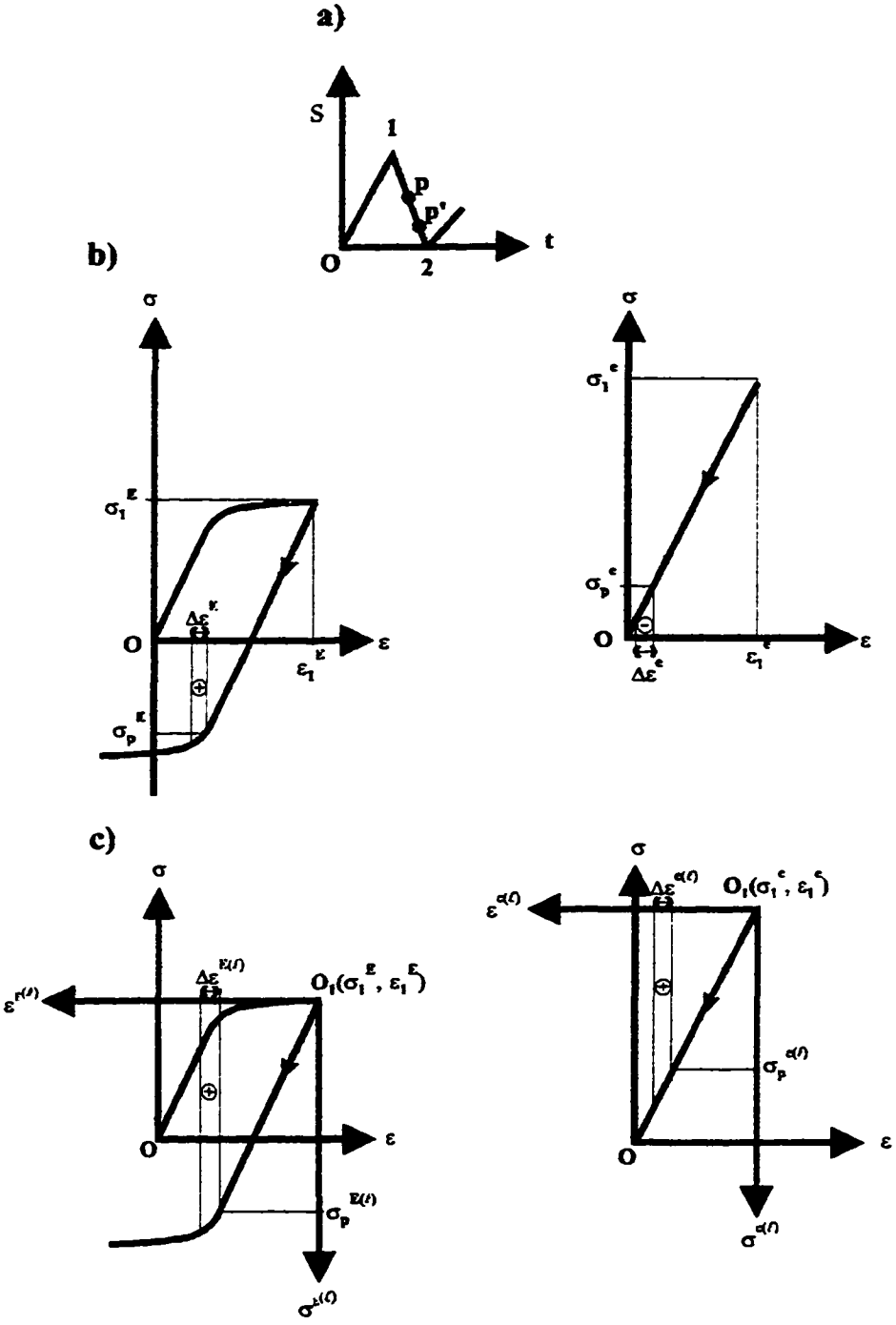


Figure 5.3: Comparison of Energy Densities in Body under Uniaxial Loading: a) Loading System, b) Fixed Coordinates, c) Local Coordinates

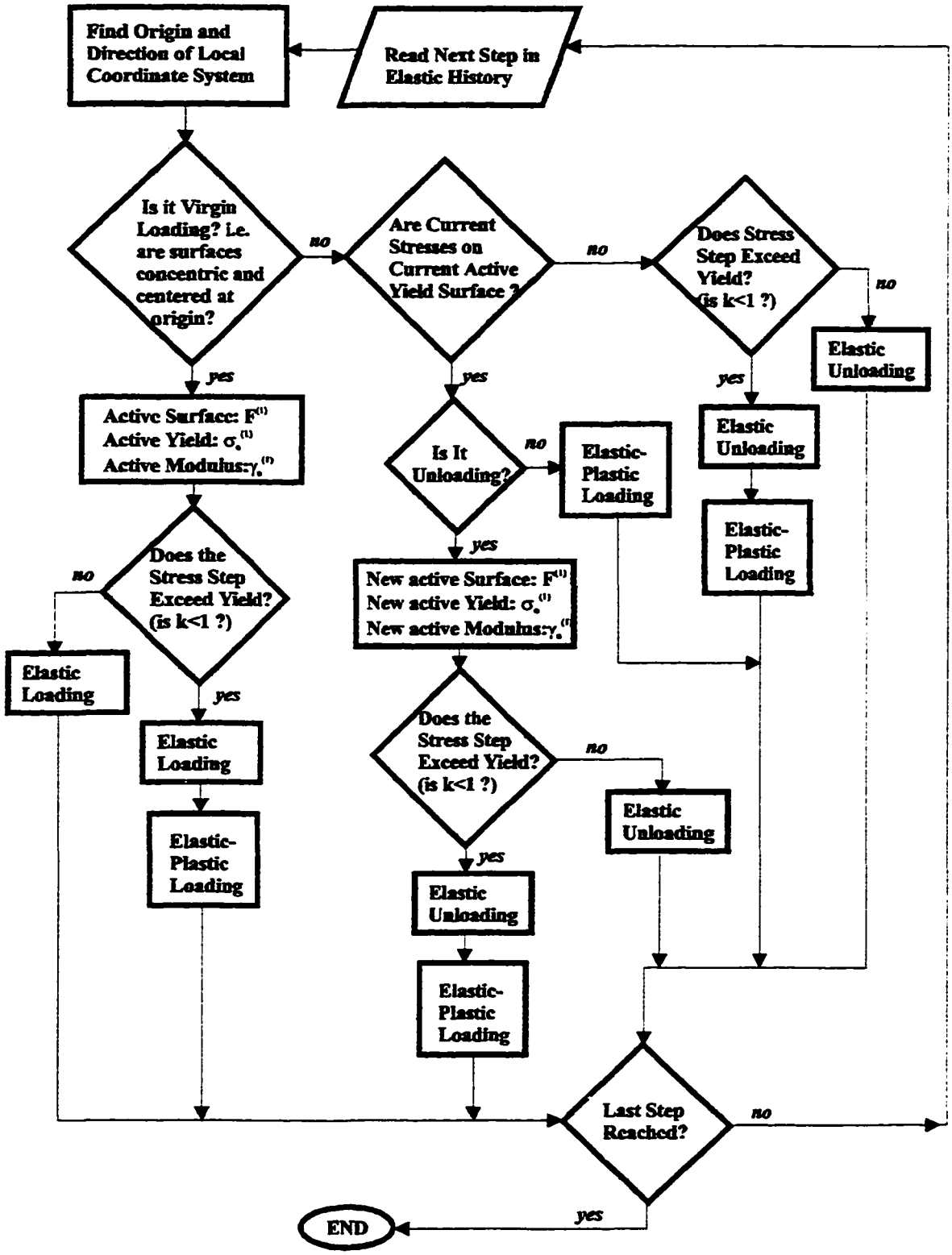


Figure 5.4: Computer Flow Chart for Notch Tip Cyclic Elastic-Plastic Stress-Strain Analysis

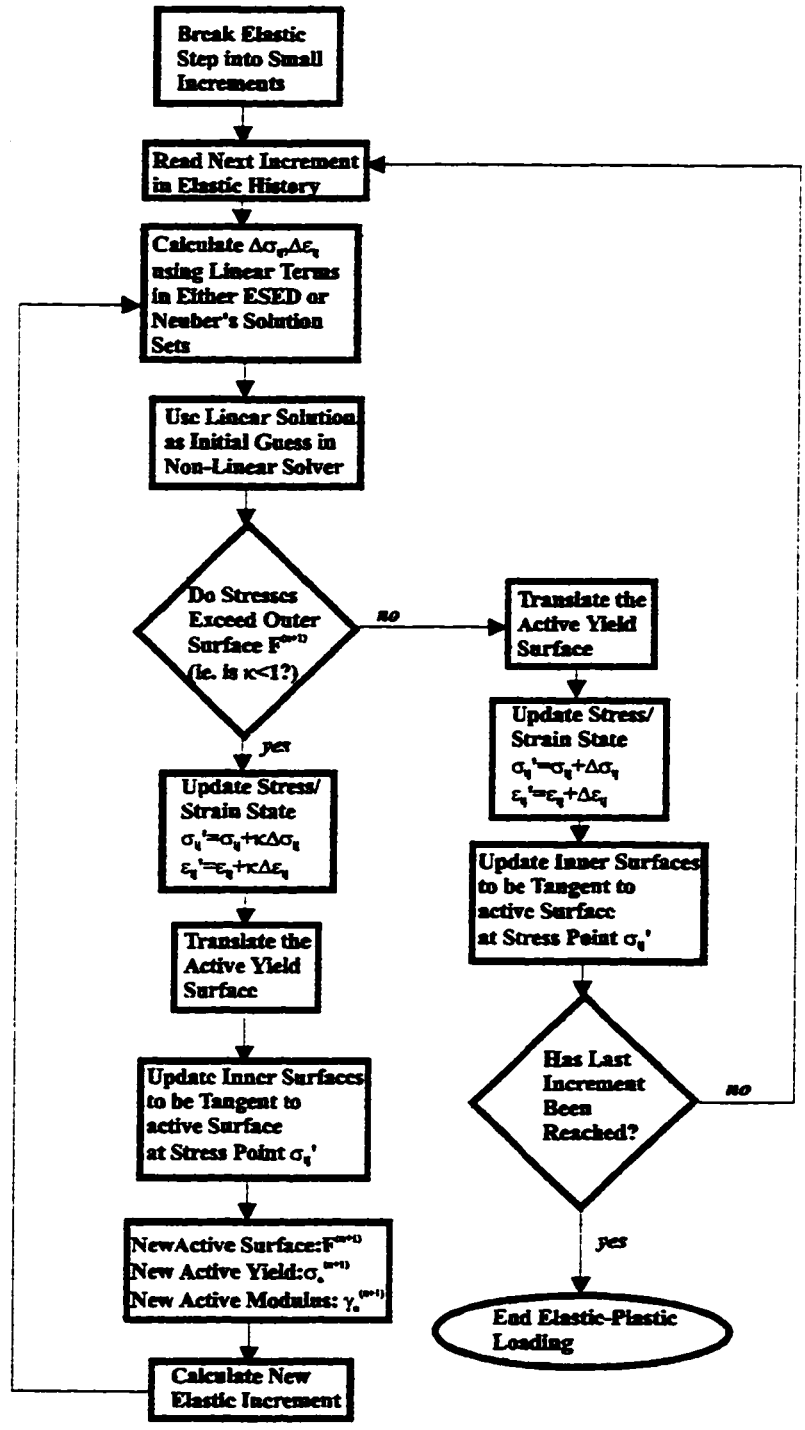


Figure 5.5: Computer Flow Chart for Plastic Straining

6. CHAPTER SIX:

COMPARISON OF SIMPLIFIED METHODOLIGIES TO EXPERIMENTAL AND FEM DATA

In this Chapter numerical results obtained on the basis of the incremental Equivalent Strain Energy Density and Neuber's solution sets, presented in Chapter Five, are compared with various sets of finite element and experimental data. These results are obtained for proportional and non-proportional monotonic loading, and for non-proportional cyclic loading.

6.1 Proportional Monotonic Loading

In [55], Hoffmann and Seeger examined the notch tip behavior in three types of notched steel bars. The bars contained a mild surface notch (Fig.6.1a), a deep surface notch (Fig.6.1b), and a sharp-deep surface notch (Fig. 6.1c). The stress concentration factors given for each notch are listed in the table below and reference the directions shown in Figure 2.2.

Type	$\sigma^e_{22}/\sigma_{n.s.}$	$\sigma^e_{33}/\sigma_{n.s.}$	$\sigma^e_{23}/\tau_{n.s.}$
mild	**1.40**	**0.25**	**1.22**
sharp	**3.32**	**0.89**	**2.19**
sharp-deep	**2.93**	**0.91**	**2.03**

Table 6.1: Stress Concentration Factors for Notched Bars in [55]

Each bar was subjected to a combined bending and torsional load applied in a proportional manner. That is, the ratio of the nominal torsional stress ($\tau_{n.s.}$) to the tensile stress ($\sigma_{n.s.}$) given by eqn.(3.9) was kept constant and equal to $\tau_{n.s}/\sigma_{n.s.} = 0.5$, during the application of the loads. This proportional load path is shown in Figure 6.2.

The material of all bars followed the power law given as

$$\sigma = \varepsilon E \qquad \text{for } \varepsilon \le 0.000335,$$

$$\sigma = \left(\frac{E\,\varepsilon}{\sigma_{o1}}\right)^{n_1} \qquad \text{for } 0.00035 < \varepsilon \le 0.006, \qquad (6.1)$$

$$\sigma = \left(\frac{E\,\varepsilon}{\sigma_{o2}}\right)^{n_2} \qquad \text{for } \varepsilon > 0.006,$$

where E = 209 GPa, ν= 0.29, σ_{o1} = 70 MPa, n_1 = 0.0463, σ_{o2} = 12.77 MPa, and n_2 = 0.4.

For the application of the incremental ESED and Neuber's solution sets, the material stress-strain curve given by eqn.(6.1) was descretized into piece-wise linear segments as shown in Figure 6.3. The elastic history was generated with the knowledge of the elastic stress concentration factors and the nominal stress ratio. The elastic-plastic approximations were subsequently obtained by applying the ESED and Neuber's equation sets from Chapter Five.

Plots of the principal surface strains ε_2 and ε_3 measured in [55], and estimated by the incremental ESED and Neuber's equations, are plotted against the equivalent net sectional stress ratio (eqn.3.11) in Figures 6.4, 6.5, and 6.6 for the mild, sharp, and sharp-deep notched bars, respectively. The results for all three notched bars indicate that the incremental Neuber's and ESED solution sets predict the general trend in the experimentally measured principal surface strains. It is further noted that well beyond general yielding of the net section, the solution sets form a band within which the measured notch tips strains fall. Specifically, strains predicted by the incremental Neuber's method are greater than, and those predicted by the ESED method are less than the experimentally determined values. The band width is generally small and thus each solution set gives a good prediction of the experimentally determined strains. The results for the mild notch are of particular interest since it offers little constraint to plastic flow relative to the sharper notches. As such, for the mild notch, the assumption of localized plasticity is easily violated. Regardless, both of the simplified solution sets give good predictions of the experimental data well beyond general yielding of the net section.

6.2 Non-Proportional Monotonic Loading

In this section, the elastic-plastic notch tip strains and stresses obtained from the FEM analysis conducted on the bar shown in Figure 3.3 are presented. The material of the bar had a stress-strain curve defined by eqn.(3.12) and was subjected to tensile and torsional stresses applied in a non-proportional manner. These FEM results are compared to results obtained from the incremental Neuber's and ESED methods for the three load paths described in Figures 3.12. In addition, a torsion-combined torsion-tension load path (Fig.6.10a) is analyzed.

The notch tip elastic stress histories for each load path were generated with the knowledge of the load path, the material elastic properties, and the elastic stress concentration factors. The elastic history was then used in the simplified solution sets to generate the approximate notch tip elastic-plastic strains and stresses.

The largest strain components ε_{22} and ε_{23} and the stress components σ_{22}, σ_{23} and σ_{33} found using the generalized ESED solution set, the generalized Neuber's solution set, and the elastic-plastic FEM model, are plotted together against the normalized equivalent net sectional stress ratio in Figures 6.7a-e - 6.10a-f. In all plots, both proposed models and the FEM results are identical in the elastic range. This is expected since in the elastic range, the final stress-strain state is load-path independent. Just after the final net sectional stresses insure notch tip plasticity, the

strain results predicted by each proposed model and the finite element results begin to diverge. The divergence becomes more pronounced as the final equivalent net section stress ratio (S_{eq}/σ_o) increases.

In almost all plots, both simplified solutions predict the general trend of the elastic-plastic finite element notch tip stress-strain histories. The exception to this is in Figures 6.7a and 6.8b since the generalized ESED solution set predicts a constant strain for the duration of the application of the second loading mode. This is attributed to the energy ratio equations used in the ESED formulation. For example, during the application of the torsional load (second loading mode) in load path 1, $\sigma_{22}^{e} = \sigma_{33}^{e}$ = constant, and therefore $\Delta\varepsilon_{22}^{e} = \Delta\varepsilon_{33}^{e} = 0$. Thus, according to eqn.(5.37), $\sigma_{22}^{E}\,\Delta\varepsilon_{22}^{E} = 0$. Since $\Delta\sigma_{22}^{E}$ cannot be zero, then it follows that ε_{22}^{E} = constant during the application of the torsional load (Fig. 6.7a). The same problem arises during the application of the tensile load (second loading mode) in load path 2, where the energy ratio equations predict that ε_{23}^{E} = constant (Fig. 6.8b). Closer examination of the energy equations shows that this inconsistency will only arise in the ESED approximated strain components in the direction in which the elastic stress components are constant throughout the loading duration.

In all strain plots it is noted that, as the load is increased, the generalized ESED solution set predicts the finite element strains better than does the Neuber solution set. Specifically, the

error in the ESED strain results at the end of the loading paths is in the range of 1% (Figs.6.9b, 6.10b) to 15% (Fig. 6.7a), whereas the error in the Neuber results at the end of the loading paths is in the range of 10% (Figs.6.7b, 6.8a, 6.10b) to 30% (Fig.6.8b). In both the ESED and the Neuber results, the errors are highest in those plots where the strain component is in the same direction as the first loading mode. It is also noted that the errors in the strains in the first loading mode direction are higher in load path 1 (Fig.6.7a) than in 3 (Fig.6.9a), and higher in load path 2 (Fig.6.8b) than in 4 (Fig.6.9c). This is as expected since load paths 1 and 2 represent a higher degree of non-proportionality than load paths 3 and 4. However, the errors in the strain predictions are quite low considering that they were calculated at the end of the loading paths, where the assumption of localized plasticity is violated. In all plots of the notch tip strain components, the generalized Neuber solution set predicts results to be higher than the generalized ESED solution set. Specifically in the cases of the strain components, Neuber's rule predicts an upper bound, and the generalized ESED method predicts a lower bound elastic approximation to the notch tip strains calculated in the elastic-plastic FEM analysis.

In the plots of the notch tip stress components, it is noted that the generalized Neuber solution set provides a better prediction of the FEM results than does the generalized ESED solution set. The Neuber and the ESED solution methods predict the upper and lower bound respectively on the stress components σ_{23}, and σ_{33} for all loading paths. For the largest stress component σ_{22}, both solutions tend to be nonconservative. However, it is noted that the

maximum percentage error in this case between the ESED solution and the finite element results is approximately 25%. As in both the ESED and the Neuber strain results, the errors are highest in those plots where the stress component is in the same direction as the first loading mode. The degree of non-proportionality also effects the stress components, where errors tend to be higher in the first two loading paths then they are in loading paths 3 and 4.

6.3 Non-Proportional Cyclic Loading

In [32], Barkey experimentally examined the notch tip behavior of an SAE 1070, circumferentially notched shaft subjected to cyclic tensile and torsional loads applied along various non-proportional loading paths. The experiments were conducted on Instron and MTS tension-torsion biaxial test frames under conditions of load control. Three-element rectangular rosette strain gauges were mounted to the notch root for strain measurement. Subsequent to the tests, the rosette strain gage data was corrected for rosette misalignment and transformed to specimen coordinates aligned in the axial direction of the shaft. The coordinates used here are those shown in Figure 2.2.

The experimental results were compared to the results of a finite element model by Köttgen [56], and the proposed simplified model discussed in Chapter Two. The finite element model was analyzed using ABAQUS. To model the non-proportional material behavior, an

ABAQUS user material implementation of the Mróz work-hardening plasticity model was used.

The stress concentration factors for the bars analyzed in this work are listed below with $\sigma_{n.s.}$ and $\tau_{n.s.}$ being defined in eqn.(3.9).

Type	$\sigma^{e}_{22}/\sigma_{n.s.}$	$\sigma^{e}_{33}/\sigma_{n.s.}$	$\sigma^{e}_{23}/\tau_{n.s.}$
Experimental	**1.42**	**0.30**	**1.15**
Converged FEA	**1.41**	**0.26**	**1.15**

Table 6.2: Stress Concentration Factors for Notched Bar in [32]

Comparing the above stress concentration factors to those in Table 6.1 of Hoffmann and Seeger [55] indicates that the notch is relatively mild.

The properties of SAE 1070 were given to follow the Ramberg-Osgood relationship (eqn.3.12) with parameters E = 210 GPa, $\nu = 0.3$, K' = 1736 MPa, and n' = 0.199. For implementation of the Mróz plasticity model, the curve was descretized into several linear segments in the FEM model and a yield limit of 250 MPa was used. The descretization of the material curve as used in the FEM model and the ESED and Neuber's simplified equation sets is shown in Figure 6.11.

The incremental ESED and Neuber's notch tip data was obtained following the methodology detailed in Chapter Five with the knowledge of the elastic stress concentration factors, the loading paths, and the material properties. From the elastic notch tip stress history, the constant increments in the strain energy and total strain energy density were calculated using equation (5.31). The number of increments (N) were initially chosen to reflect the relative magnitude of the stress amplitude between steps in the history. The programs written for each of the simplified methods were run and the results were plotted. The step size was then reduced and the above procedure was repeated until there was no observable difference in the stress and strain results between subsequent runs.

6.3.1 Comparison of Results

In this section, the results obtained using the incremental ESED and Neuber methods are compared to the experimental and finite element results presented in [32] for various cyclic tension-torsional loading paths. Only notch tip strain results were obtained in the experiments and thus stress results are not presented here.

Box Path

The box-shaped path analyzed is shown in nominal tension-torsion stress space in Figure 6.12 a. At the corners of the box, the equivalent net sectional stress ratio is: $S_{eq}/\sigma_o = 1.56$, indicating that the net section has yielded. The box path indicates a high degree of non-proportionality and was designed to highlight regions where the axial and shear response is uncoupled (elastic regions) and where they are coupled (elastic-plastic regions). Specifically, it is expected that elastic unloading will occur at the corners of the box, and if loads are high enough, elastic-plastic loading will follow to the next corner of the box.

The notch tip axial strain versus shear strain history obtained using the incremental ESED and Neuber's method are compared to experimental results in Figure 6.12b and to finite element results in Figure 6.12c. The results are plotted for 10 cycles of loading. Both the incremental Neuber's and ESED methods predict elastic unloading at each corner of the box, followed by elastic-plastic loading to the next corner. This is most prevalent in the incremental Neuber's response where the axial and shear strain are uncoupled (indicated by straight lines parallel to the coordinate axes) at the corners of the box, and become coupled (indicated by curved lines) to the next corner. The ESED solution, as shown in load paths 1 and 2 for the analyzed monotonic non-proportional loading paths, predicts a constant strain in the direction in which the elastic stress components remain constant. Although it may appear that the ESED method

is generating an elastic solution, it is in fact giving an elastic-plastic response, as would be apparent if the strains or stresses were plotted against the applied load.

As can be seen from both Figure 6.12b and 6.12c, the incremental ESED method predicts lower strains than does the Neuber's method up until point 4 shown in Figure 6.12a, where for the last step in the cycle, the ESED method yields higher strains. This is expected for non-proportional cyclic loading. Specifically, when unloading from a higher stress level on a constant radii yield surface, the material may start to deform plastically before it would if unloading were to start at a lower stress level. Thus, if strains are initially predicted higher using the Neuber's equations than predicted by the ESED equations, they may be predicted lower upon reverse elastic-plastic loading.

Figure 6.12 shows that both the simplified methodologies give a fair prediction of the experimental strain history. It should be noted, as indicated in [32], that the values of the applied loads used in the experiments were slightly different than shown in the idealized load path (Fig. 6.12a). This is because the sharp corners of the load path were not always obtained in the experiment. The rounded corners in the loads applied to the bars are reflected in the experimental strain response as rounded corners of the box in Figure 6.12b.

In Figure 6.12c, it can be seen that the simplified methods give a much better prediction of the FEM results than of the experimental results. This is clearly seen in the incremental Neuber's

results where there is virtually no difference between the calculated values and the FEM results.

Figure 6.13a shows the same box path as in Figure 6.12a, but with higher applied load levels at the corners of the box where $S_{eq}/\sigma_o = 1.79$. Both of the simplified methods show the same trend as in the previous case. The numerical values of the shear and axial strains calculated using the simplified methods give a fair prediction of the experimental results (Fig 6.13a). Again, the Neuber's solution set predicts the finite element results very well (Fig. 6.13b).

Unequal Frequencies of Applied Load

In [32], several experiments were conducted on the bar in which unequal frequencies in the torsional to tensile load were applied to the bar. Here, three of those paths were analyzed. In the first (Fig 6.14a), two cycles of the tensile load were applied in the same time period as one period of the torsional load. In the second (Fig. 6.15a), two cycles of torsional load were applied for one cycle of tensile load, and in the third (Fig.6.16a), five cycles of the torsional load for one cycle of tensile load. In all paths, the final applied loads correspond to the second box shaped path in which $S_{eq}/\sigma_o = 1.79$.

Plots of the shear versus axial strain history obtained by both simplified methods and the experiments are plotted in Figures 6.14b, 6.15b and 6.16b for the tensile to torsional frequency ratios of 2:1, 1:2, and 1:5 respectively. It should be noted that finite element data for these paths were not presented in [32].

In all plots, it is noted that both methods predict the general trend in, and closely predict the numerical values of the strain histories obtained in the experiments.

Non-Zero Mean Stress

To evaluate the effect of a non-zero mean load, the loading path shown in Figure 6.17a with a maximum value of the equivalent net sectional stress ratio of $S_{eq}/\sigma_o = 1.79$, was analyzed. Cycling about a non-zero mean load induces ratchetting, or the increasing in strain results even though the nominal loading path stays at the same mean load value. Experimental results for the load path were not given in [32].

The axial versus shear strain histories are calculated using the incremental ESED, Neuber's and finite element method for 50 cycles in Figures 6.17b, 6.17c and 6.17d, respectively. The plots here were not superimposed for clarity in analyzing the results, but the scales on all three plots are identical.

It is noted that both the incremental ESED and Neuber's method predict the general trend in the notch tip strains calculated using the finite element method. At the outset, the strains progressively get larger after each cycle and then tend towards a limiting value. This indicates that the stress relaxes and this results in a decreased rate of strain accumulation. The Mróz model, when used under non-proportional load or stress controlled conditions, generally yields a constant rate of ratchetting. However, in the simplified models, the input is increments of strain energy density and thus limiting values of strains are attainable. In the case of the incremental Neuber's rule, the strain predictions are numerically almost the same as the FEM results.

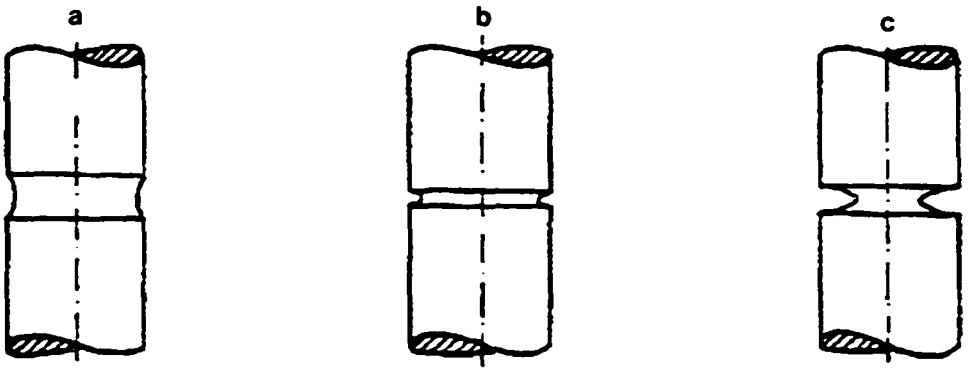


Figure 6.1: Notched Bars in [55]: a) Mild Notch, b) Sharp Notch, c) Sharp-Deep Notch.

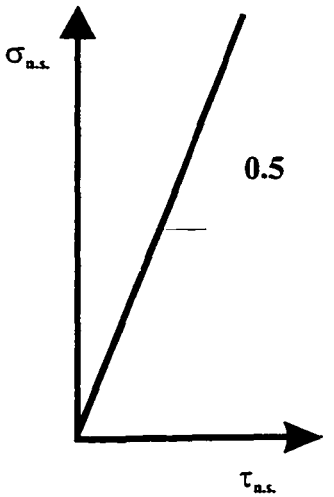


Figure 6.2: Proportional Loading Path in [55]

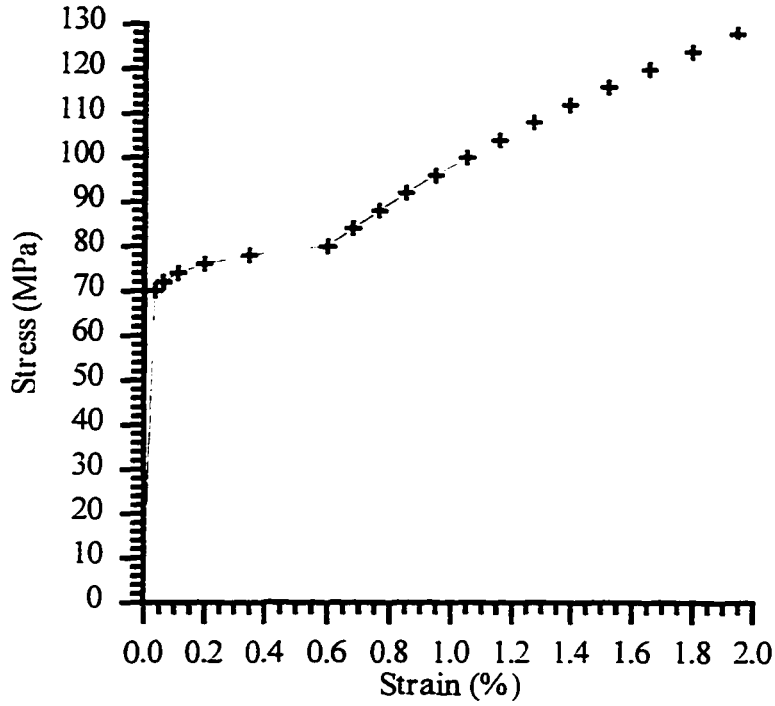


Figure 6.3: Descretization of the Material Stress-Strain Curve in [55]

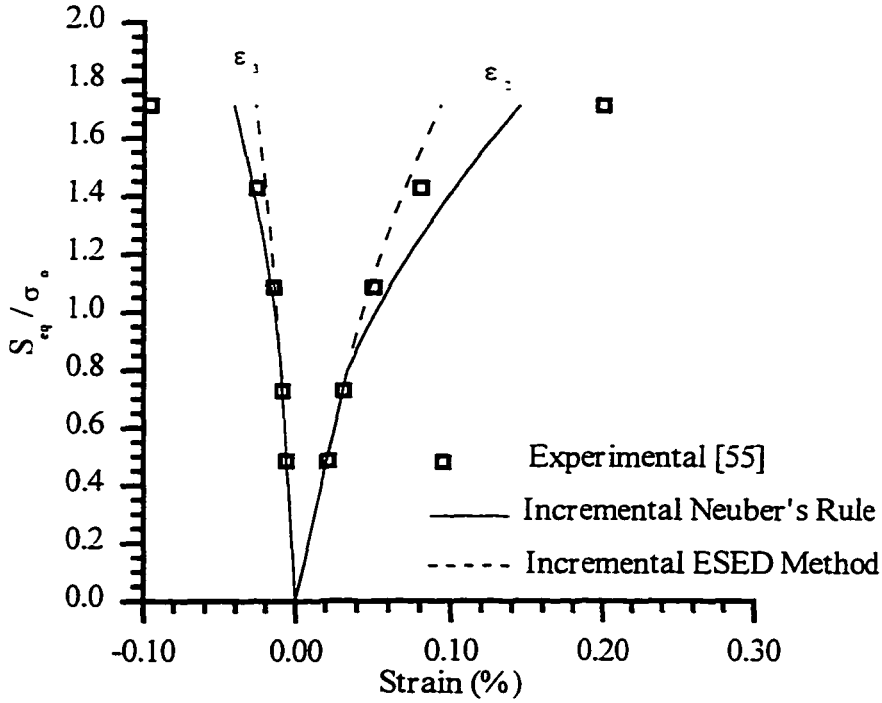


Figure 6.4: Principal Surface Strain Components For Mild Notch

NOTE TO USERS

Page(s) not included in the original manuscript are unavailable from the author or university. The manuscript was microfilmed as received.

UMI

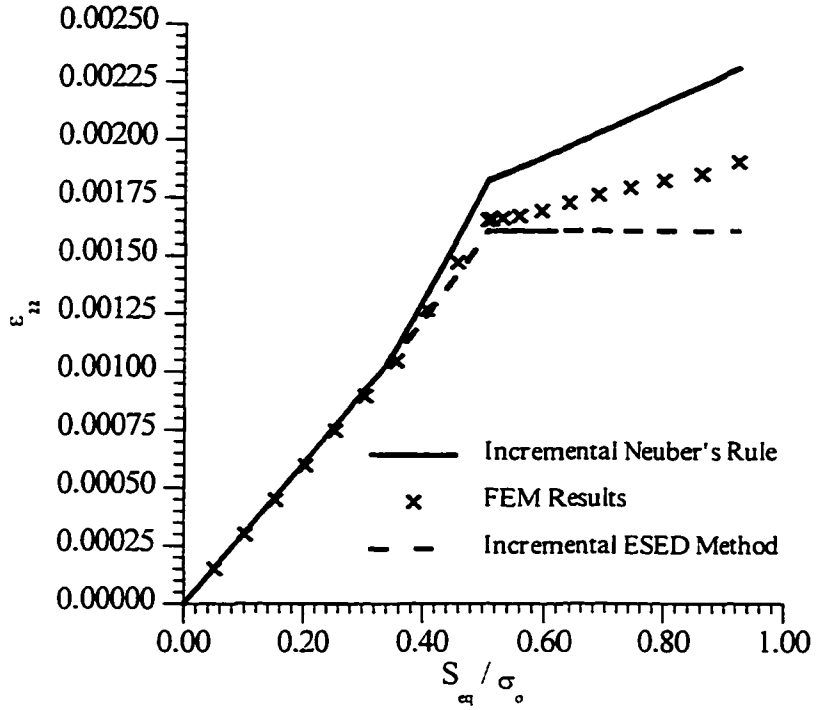


Figure 6.7a: Axial Strain History for Tension-Torsion (Path 1).

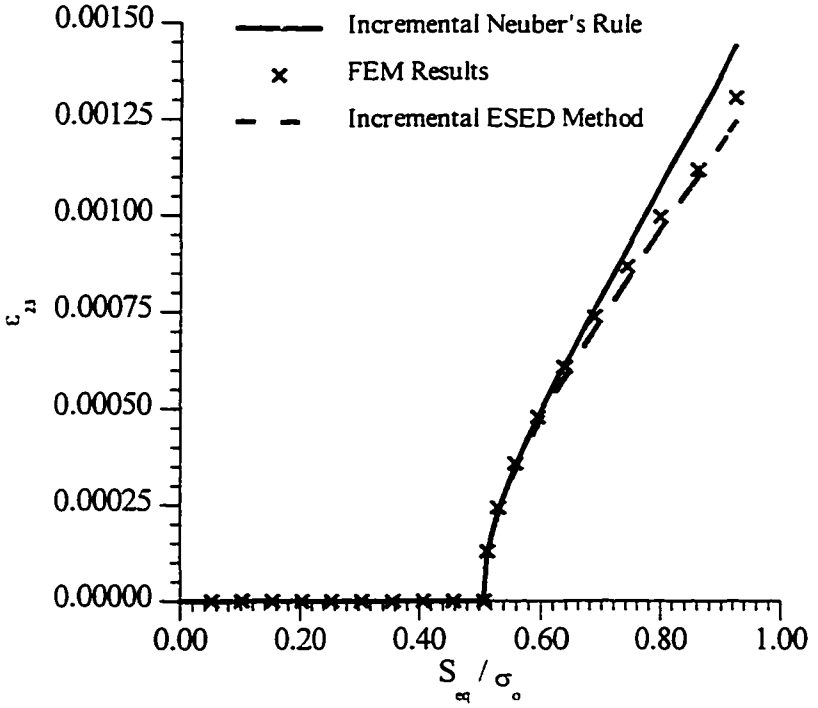


Figure 6.7b: Shear Strain History for Tension-Torsion (Path 1).

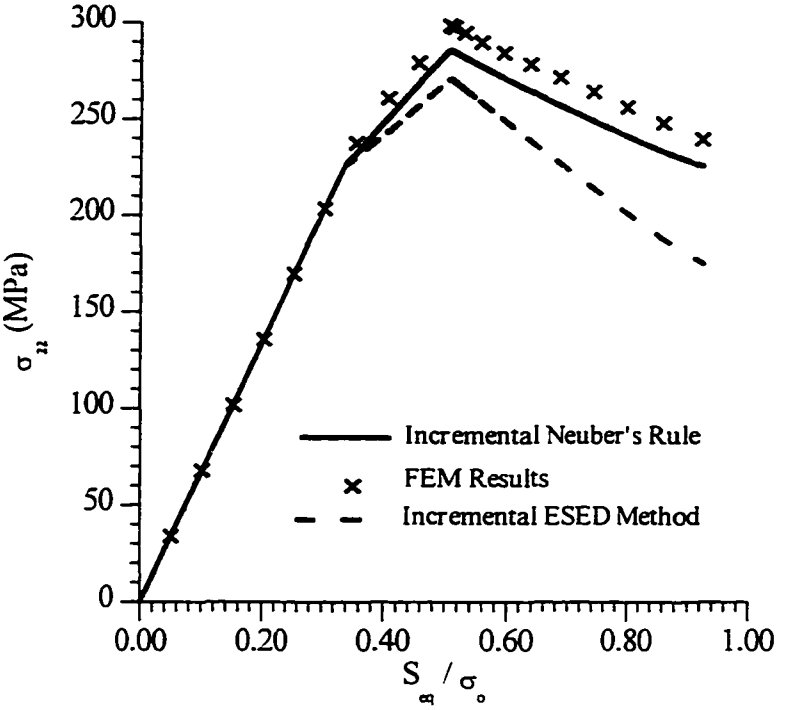


Figure 6.7c: Normal Stress History for Tension-Torsion (Path 1).

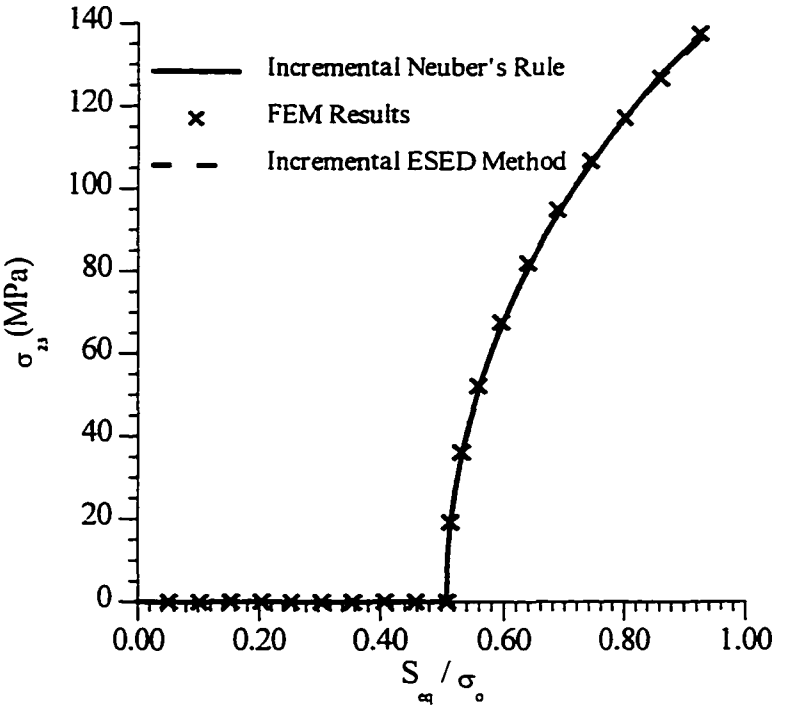


Figure 6.7d: Shear Stress History for Tension-Torsion (Path 1).

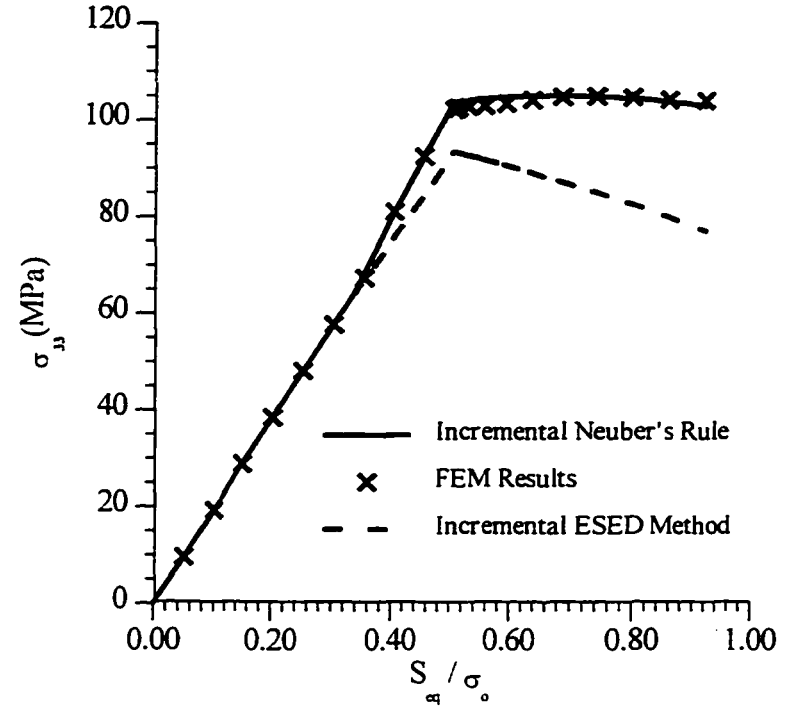


Figure 6.7e: Transverse Stress History for Tension-Torsion (Path 1).

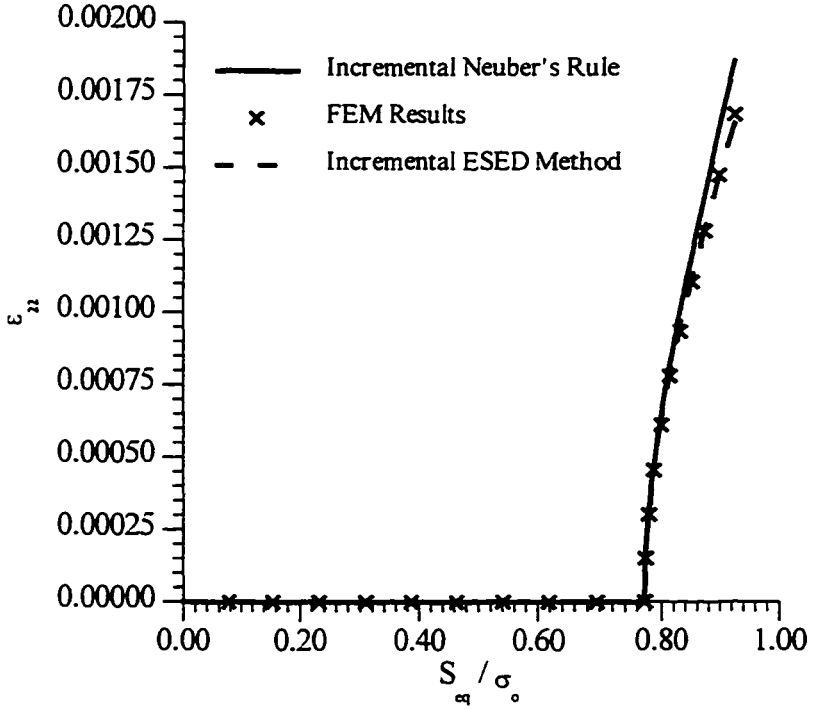


Figure 6.8a: Axial Strain History for Torsion-Tension (Path 2).

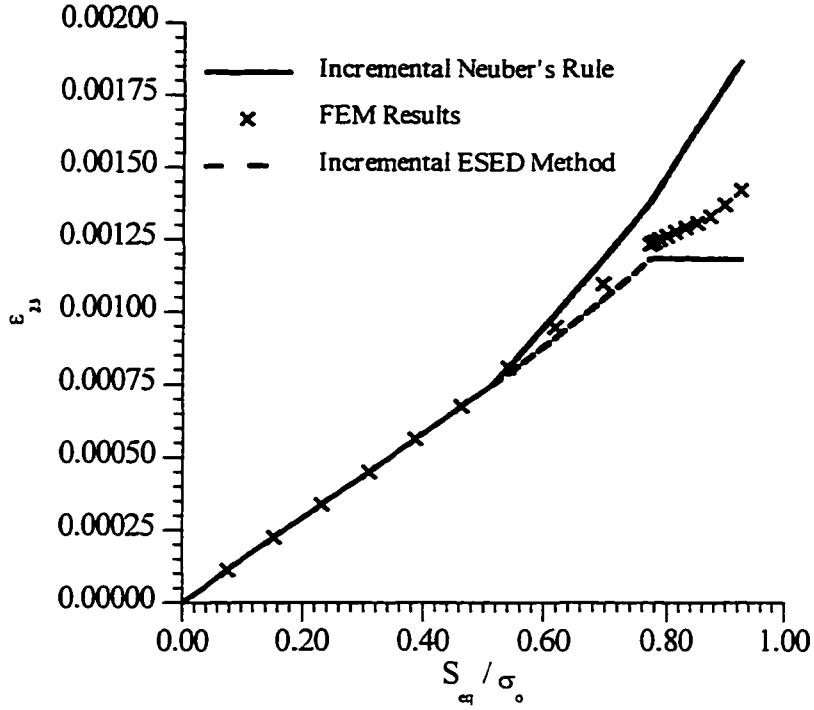


Figure 6.8b: Shear Strain History for Torsion-Tension (Path 2).

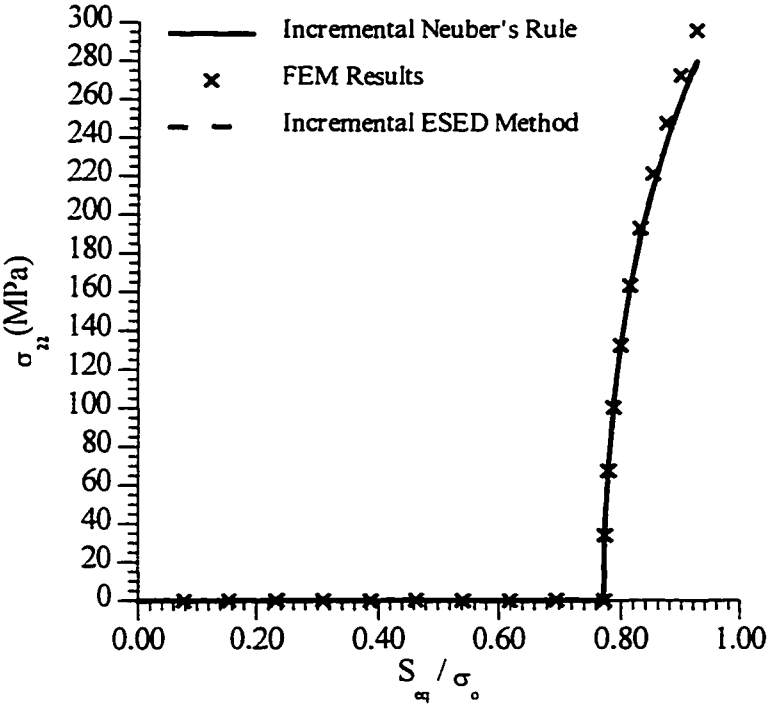


Figure 6.8c: Normal Stress History for Torsion-Tension (Path 2).

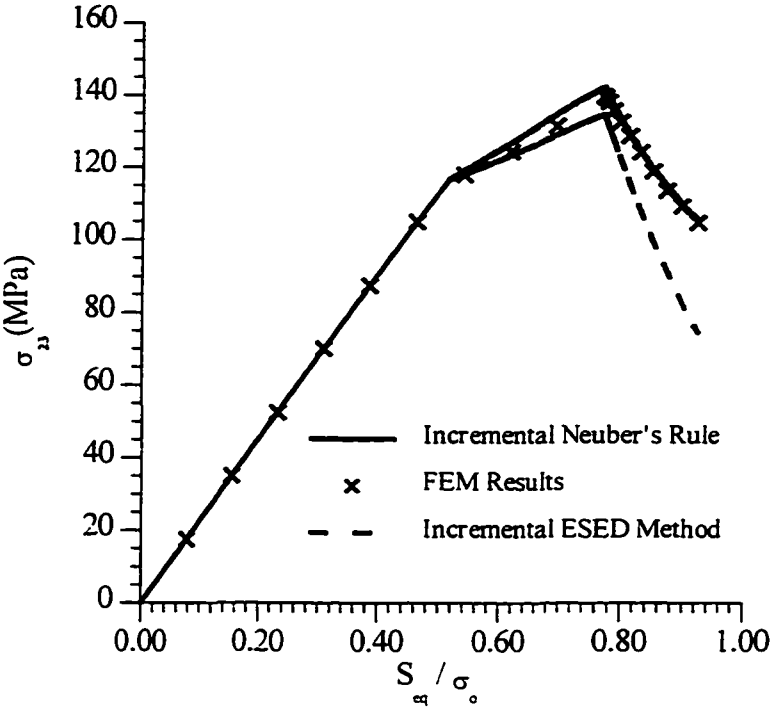


Figure 6.8d: Shear Stress History for Torsion-Tension (Path 2).

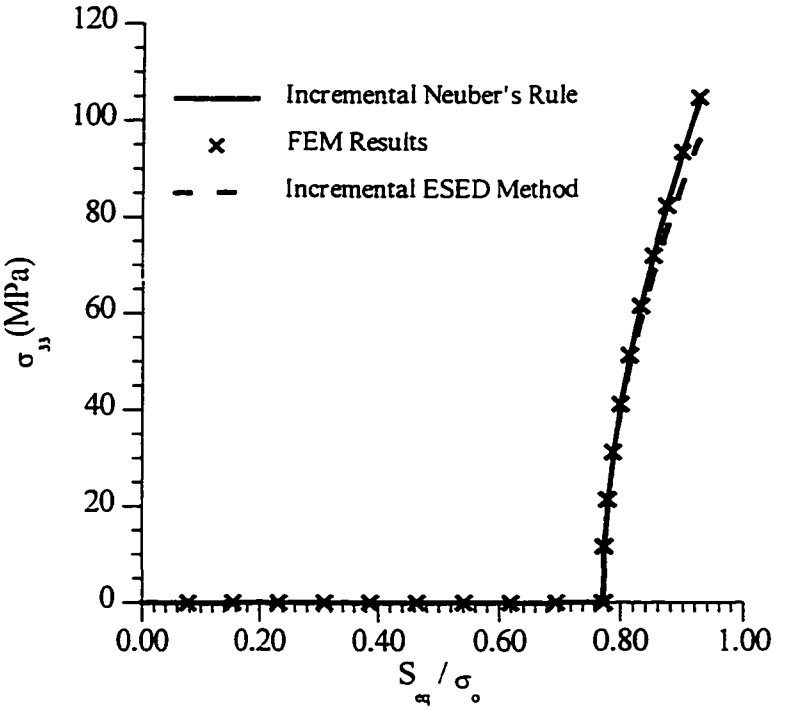


Figure 6.8e: Transverse Stress History for Torsion-Tension (Path 2).

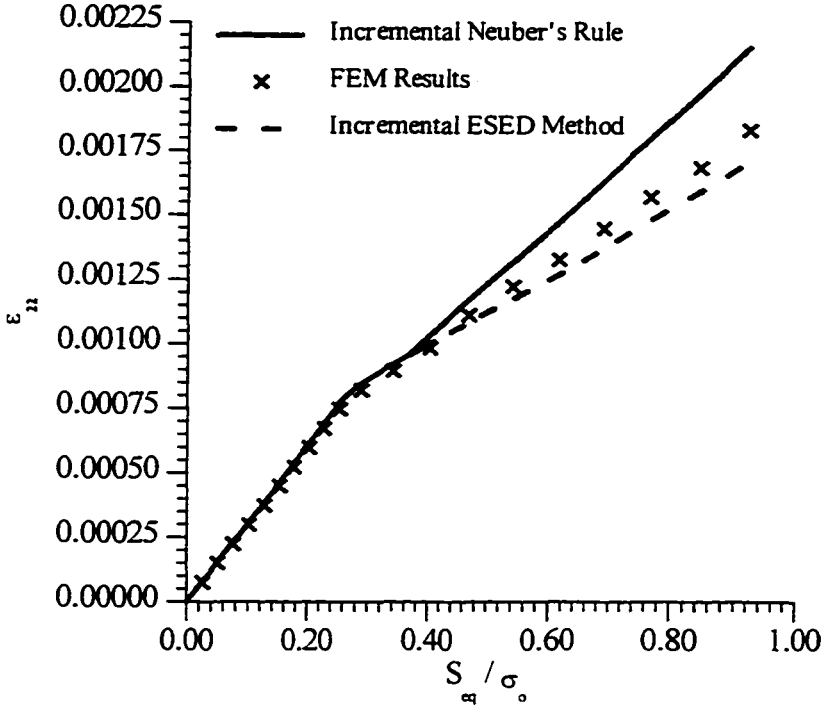


Figure 6.9a: Axial Strain History for Tension-Combined Torsion-Tension (Path 3).

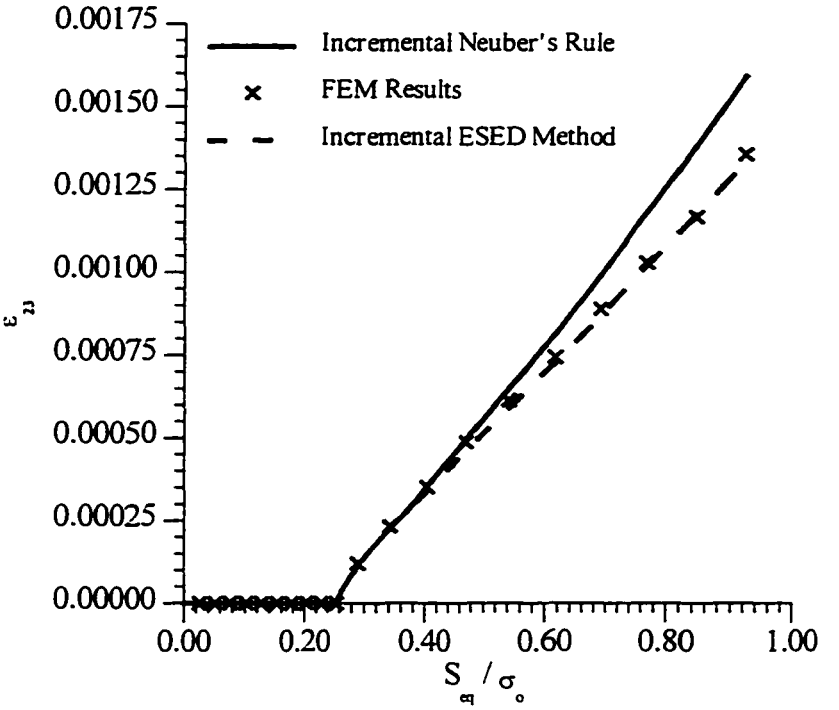


Figure 6.9b: Shear Strain History for Tension-Combined Torsion-Tension (Path 3).

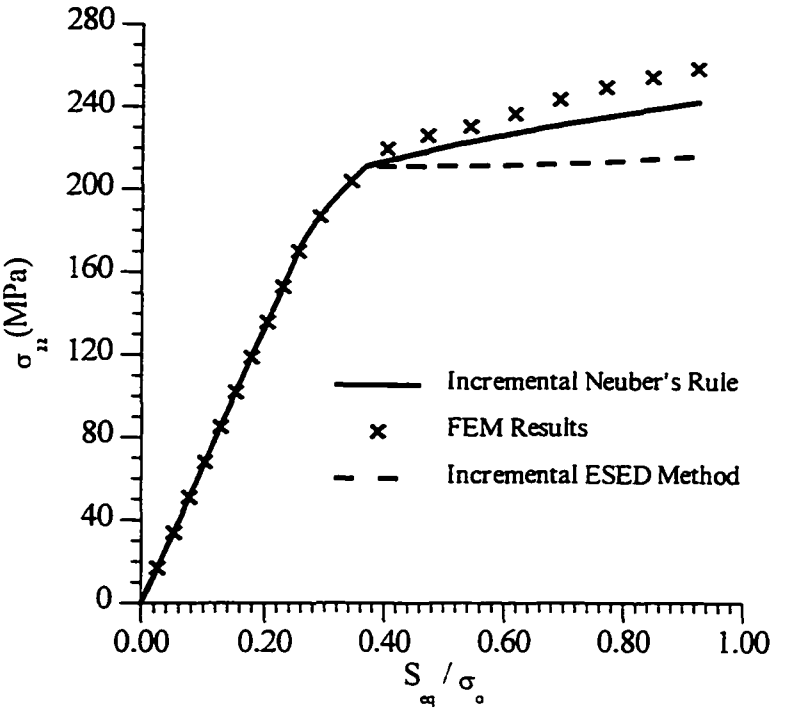


Figure 6.9c: Normal Stress History for Tension-Combined Torsion-Tension (Path 3).

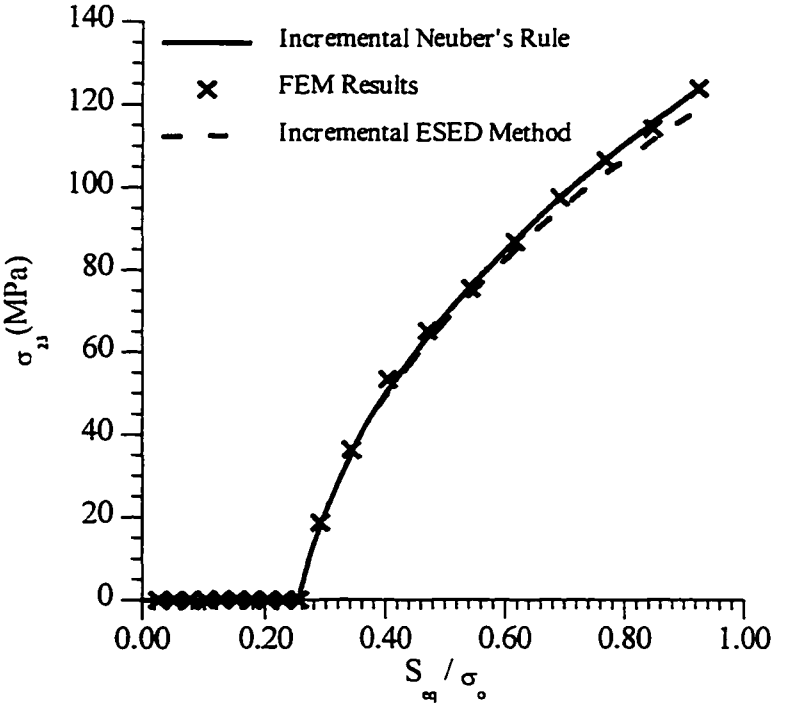


Figure 6.9d: Shear Stress History for Tension-Combined Torsion-Tension (Path 3).

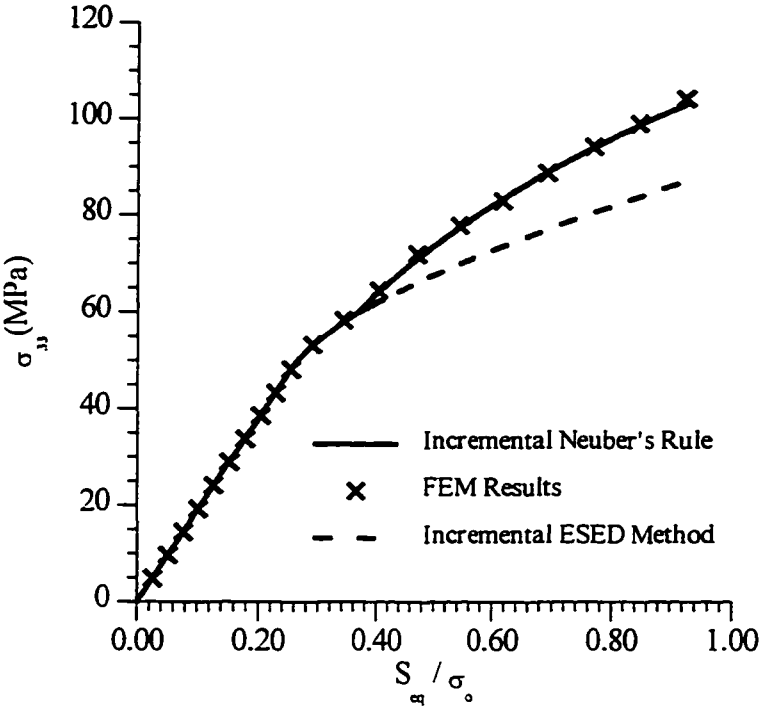


Figure 6.9e: Transverse Stress History for Tension-Combined Torsion-Tension (Path 3).

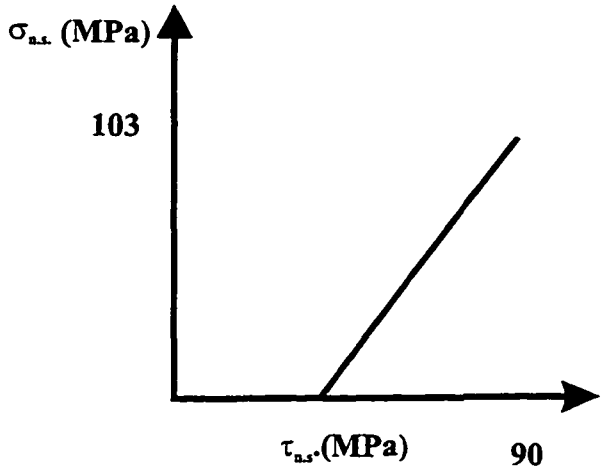


Figure 6.10a: Load Path 4 - Torsion Combined Tension-Torsion
($\sigma^{f}_{n.s.}$ = 103MPa, $\tau^{f}_{n.s.}$ = 90MPa).

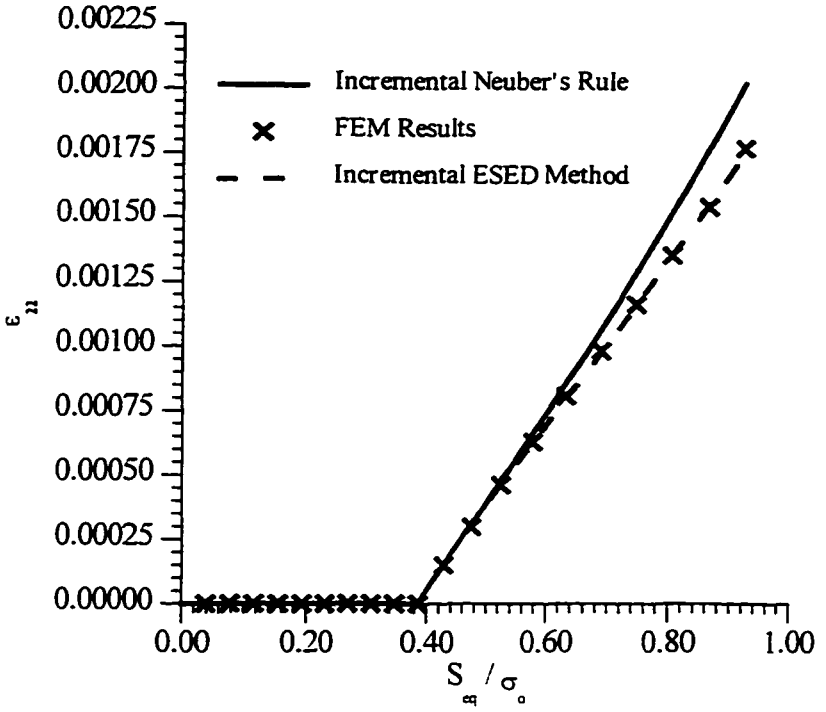


Figure 6.10b: Axial Strain History for Torsion Combined Tension-Torsion (Path 4).

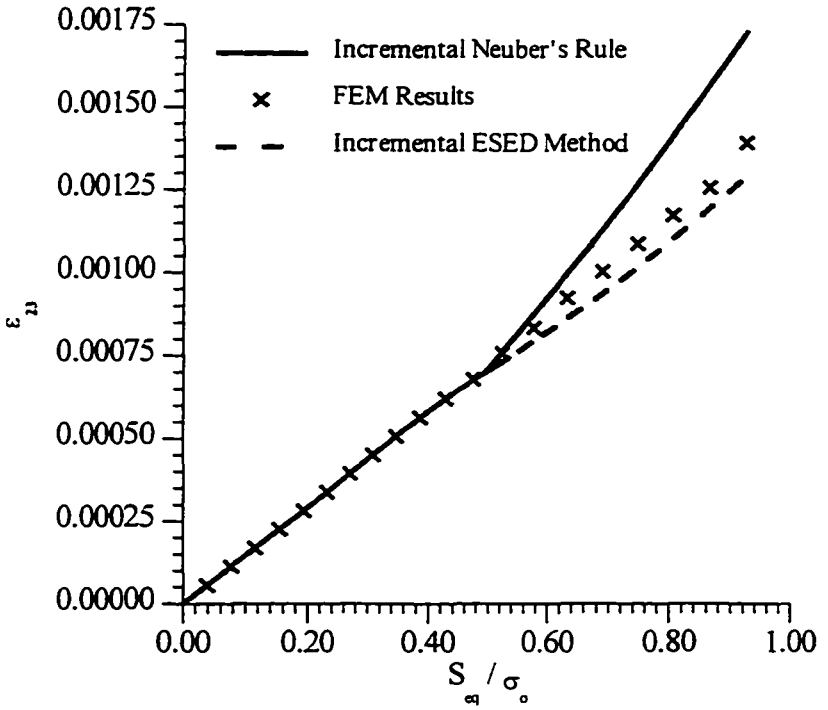


Figure 6.10c: Shear Strain History for Torsion Combined Tension-Torsion (Path 4).

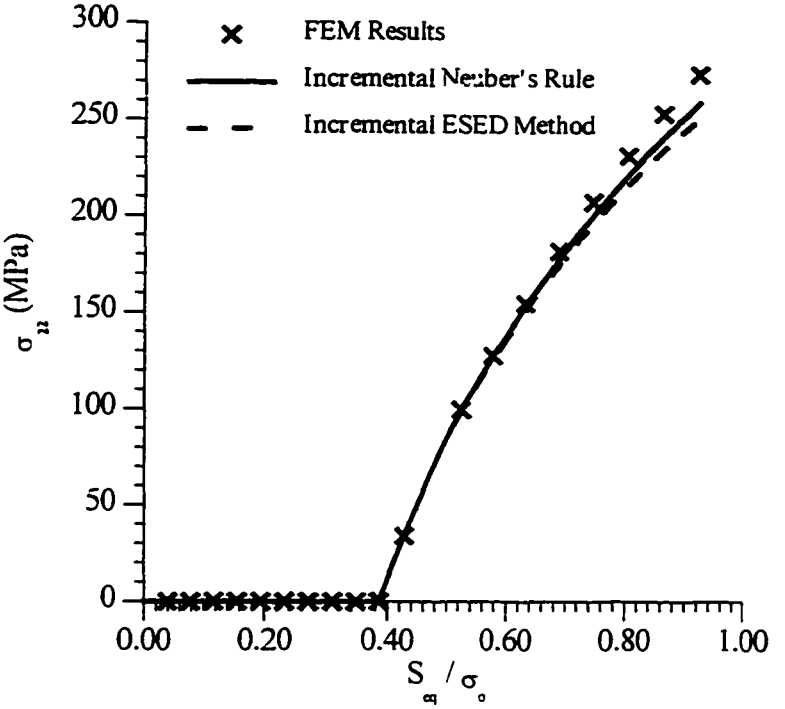


Figure 6.10d: Normal Stress History for Torsion Combined Tension-Torsion (Path 4).

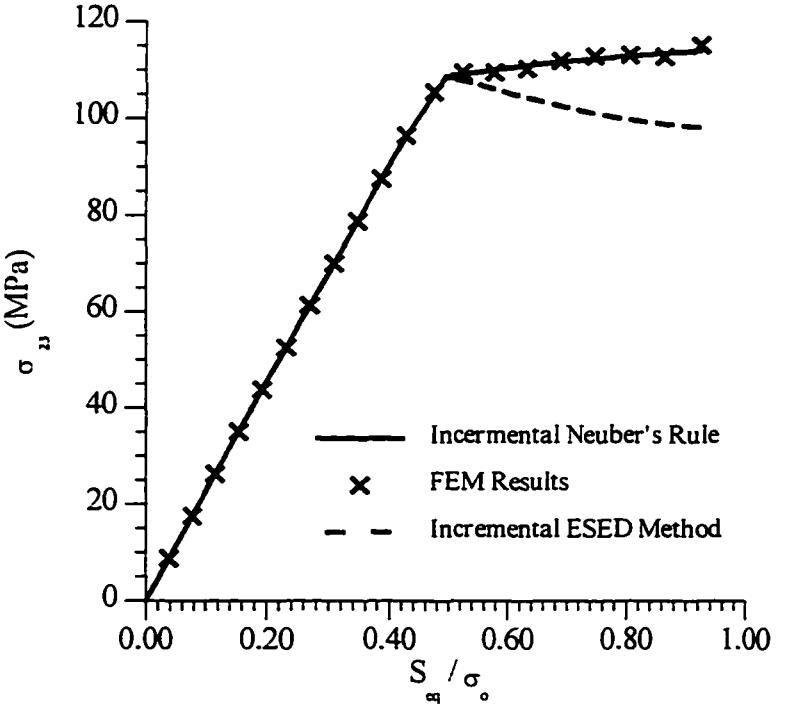


Figure 6.10e: Shear Stress History for Torsion Combined Tension-Torsion (Path 4).

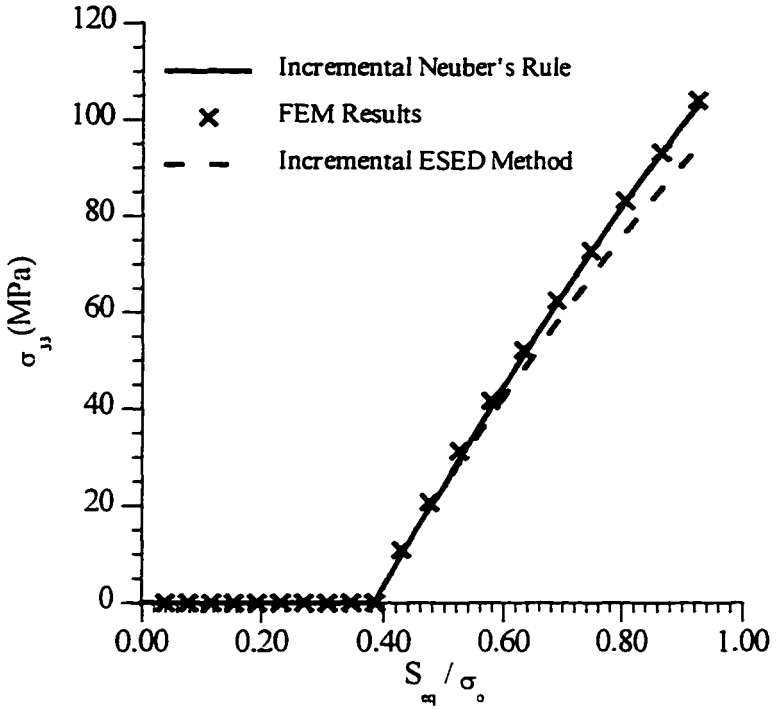


Figure 6.10f: Transverse Stress History for Torsion Combined Tension-Torsion (Path 4).

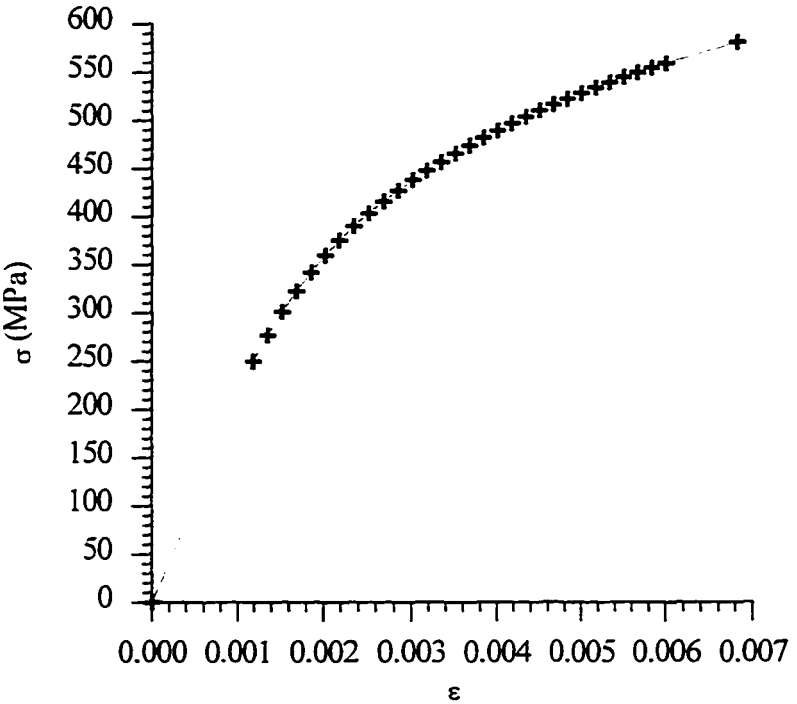


Figure 6.11: Descretization of the Stabilized Cyclic Stress-Strain Curve in [32]

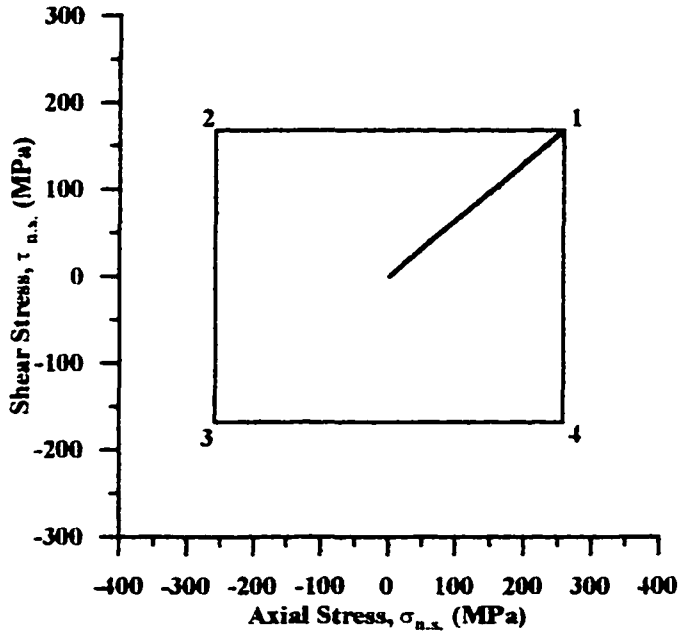


Figure 6.12a: Box Path A) Analyzed in [32] ($\sigma_{n.s.}$ = 258 MPa $\tau_{n.s.}$ = 168 MPa).

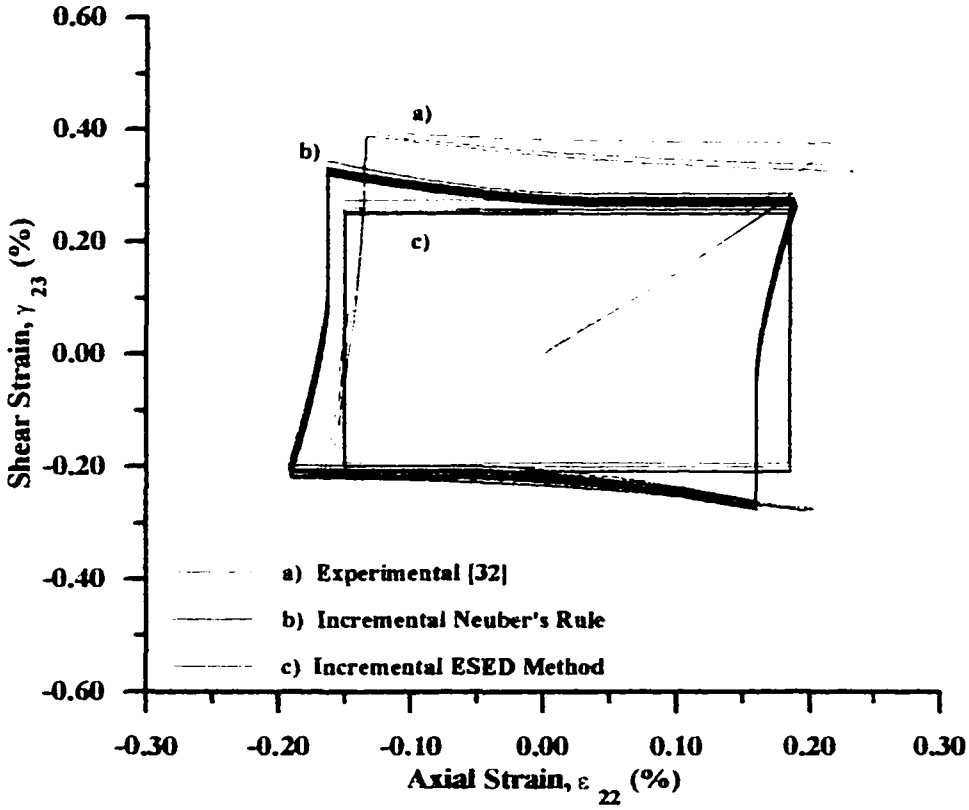


Figure 6.12b: Comparison of Simplified Models to Experimental Results for Box Path A).

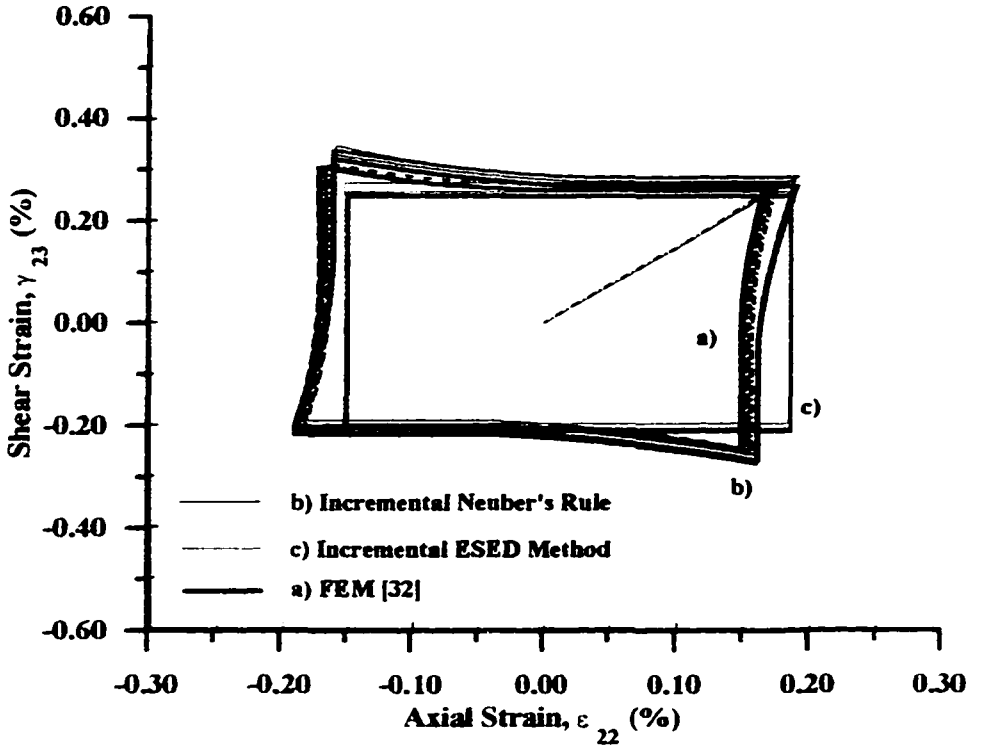


Figure 6.12c: Comparison of Models to Finite Element Results for Box Path A).

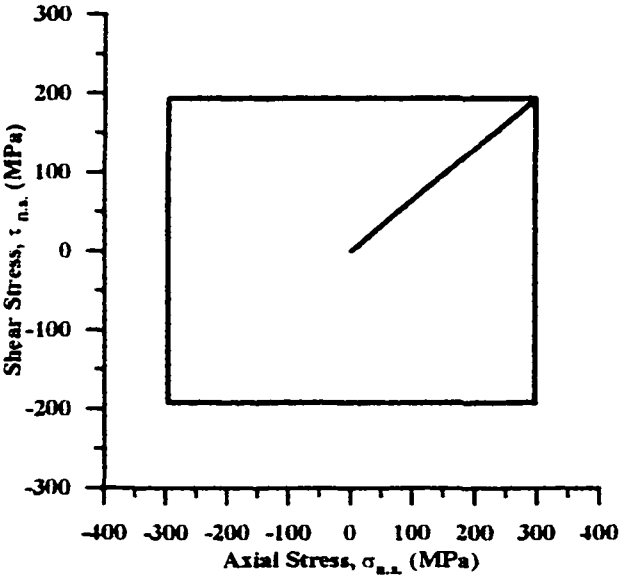


Figure 6.13a: Box Path B) Analyzed in [32] ($\sigma_{n.s.}$ = 296 MPa $\tau_{n.s.}$ = 193 MPa).

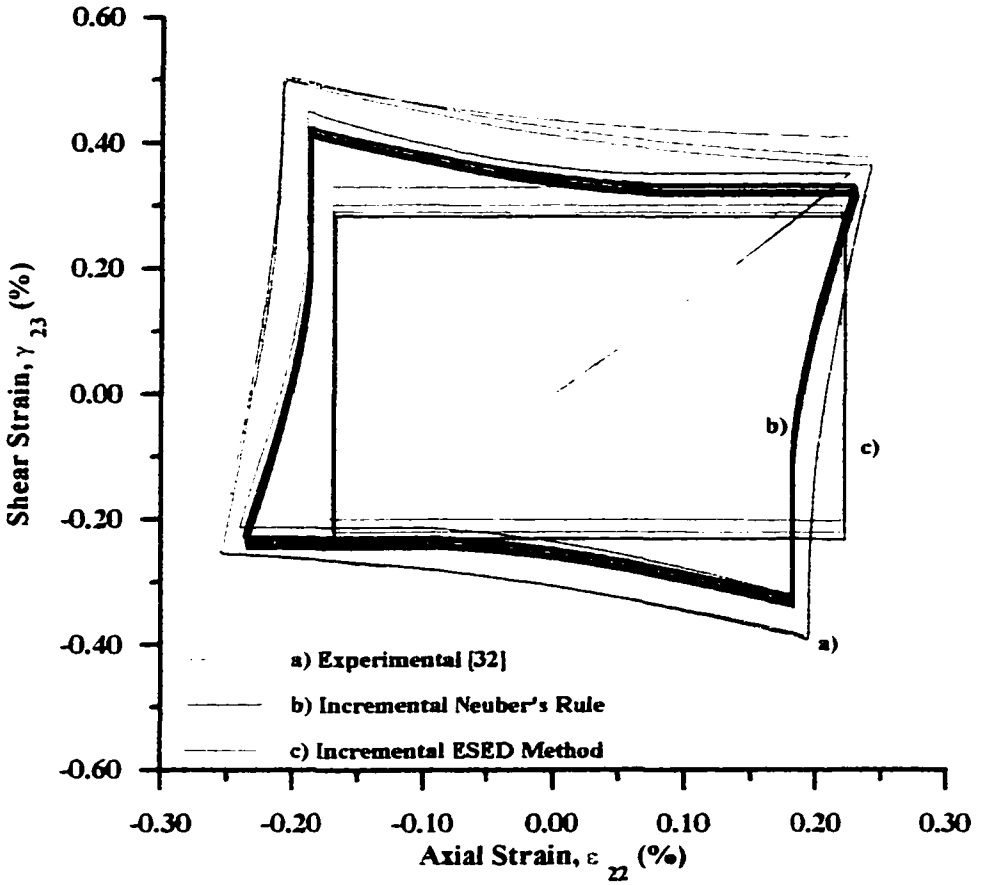


Figure 6.13b: Comparison of Simplified to Experimental Results for Box Path B).

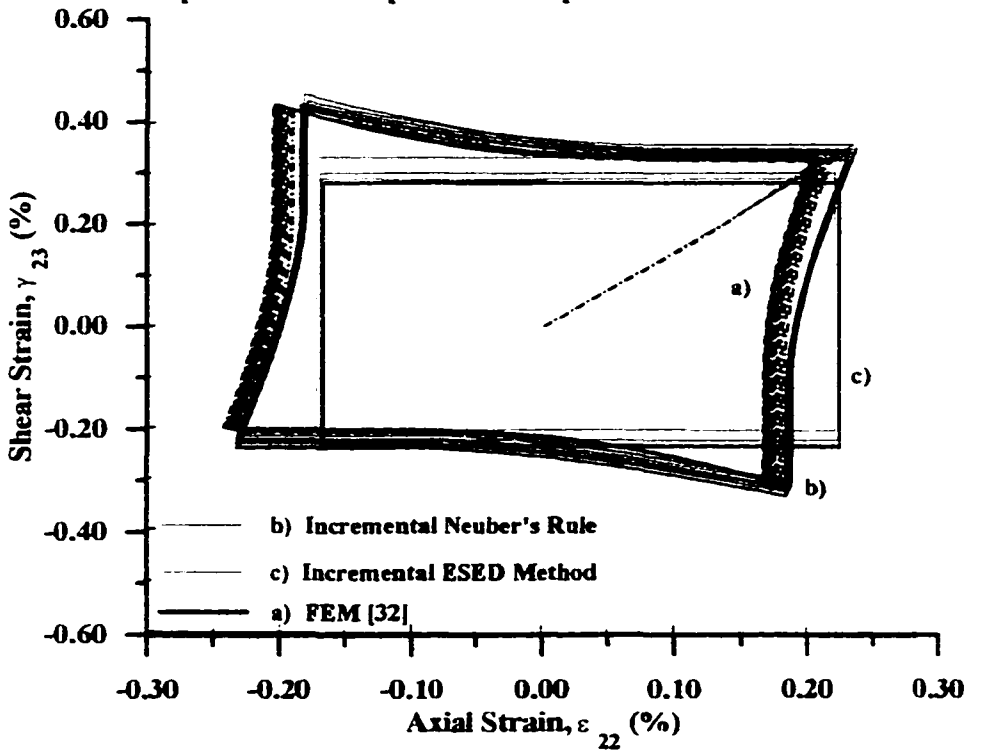


Figure 6.13c: Comparison of Models to Finite Element Results for Box Path B).

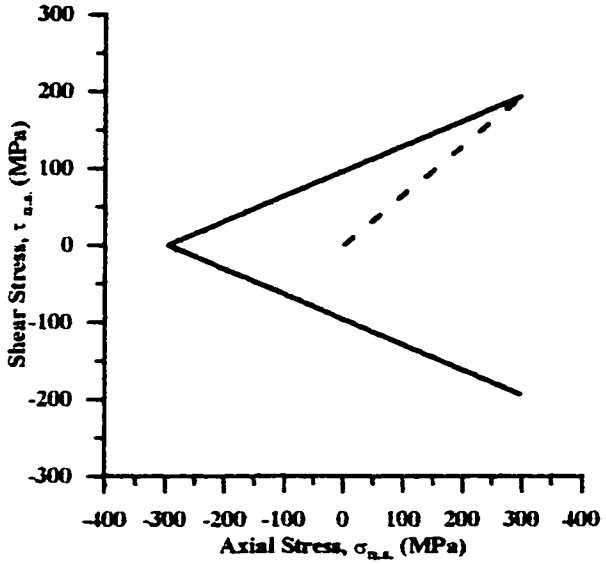


Figure 6.14a: Stress Path in [32] With 2:1 Ratio of Applied Tensile to Torsional Cycles.

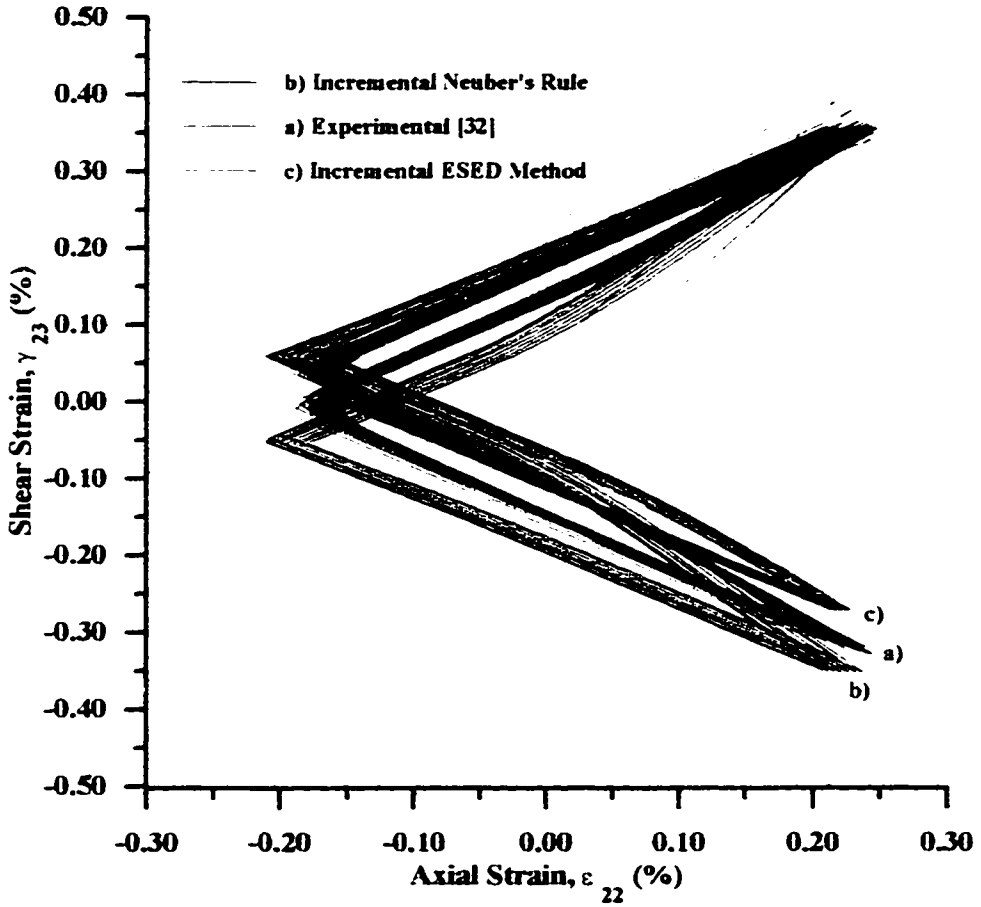


Figure 6.14b: Comparison of Simplified Models to Experimental Results for 2:1 Ratio.

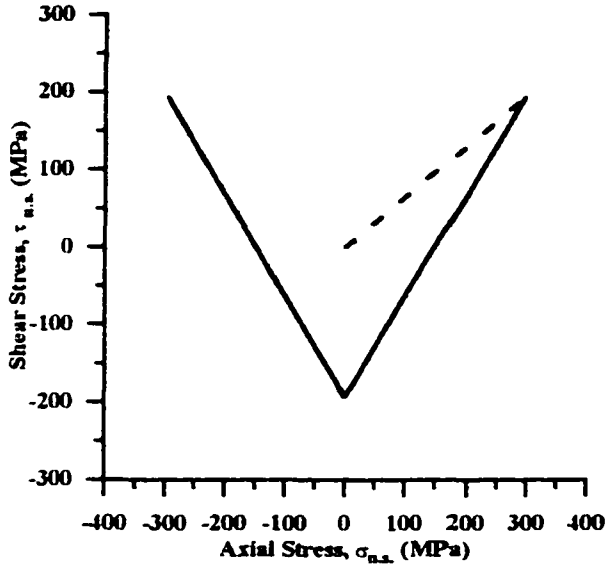


Figure 6.15a: Stress Path in [32] With 1:2 Ratio of Applied Tensile to Torsional Cycles.

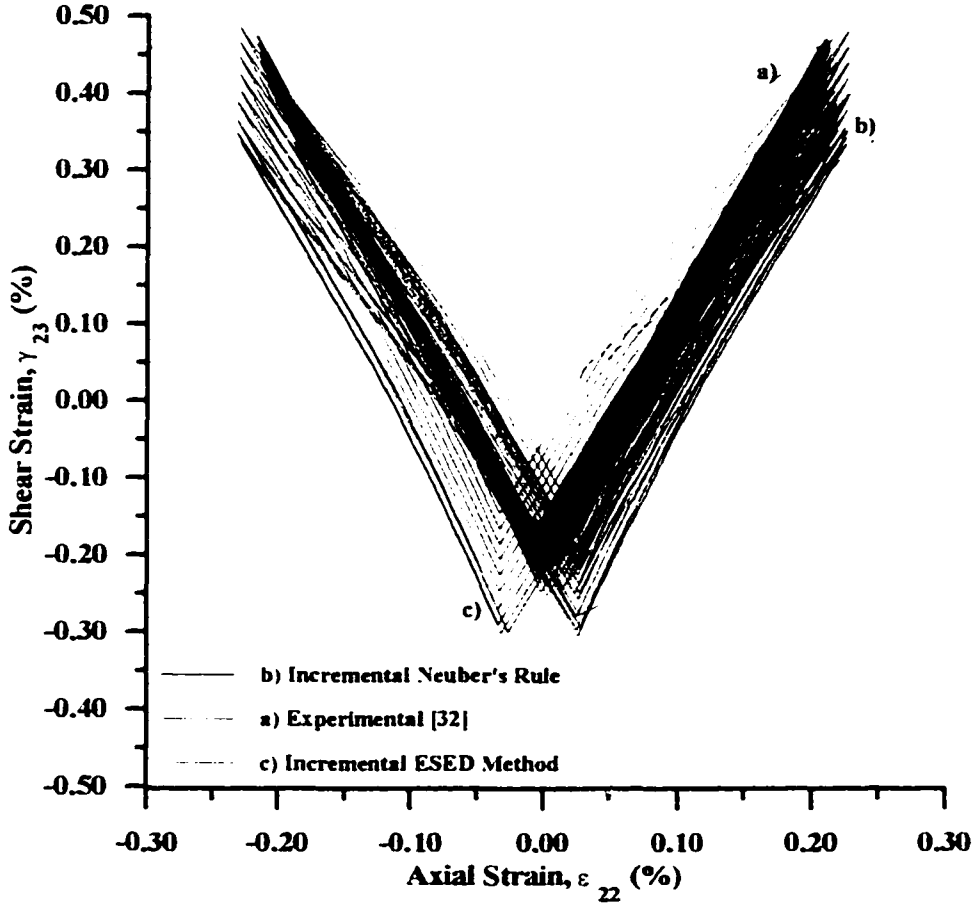


Figure 6.15b: Comparison of Simplified Models to Experimental Results for 1:2 Ratio.

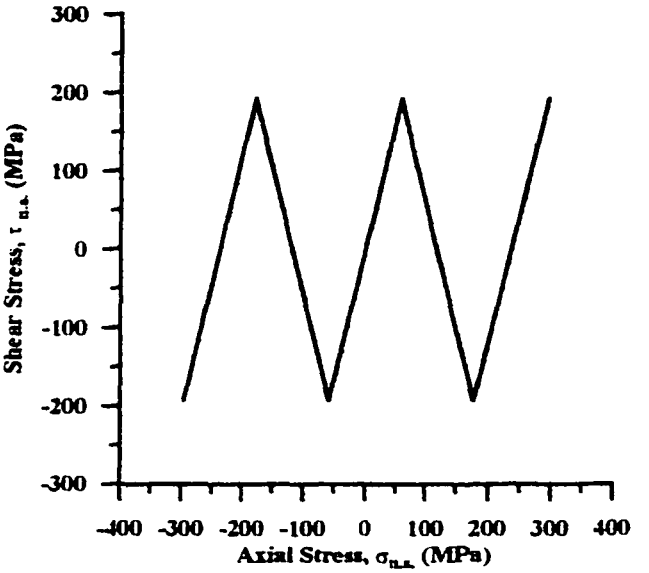


Figure 6.16a: Stress Path in [32] With 1:5 Ratio of Applied Tensile to Torsional Cycles.

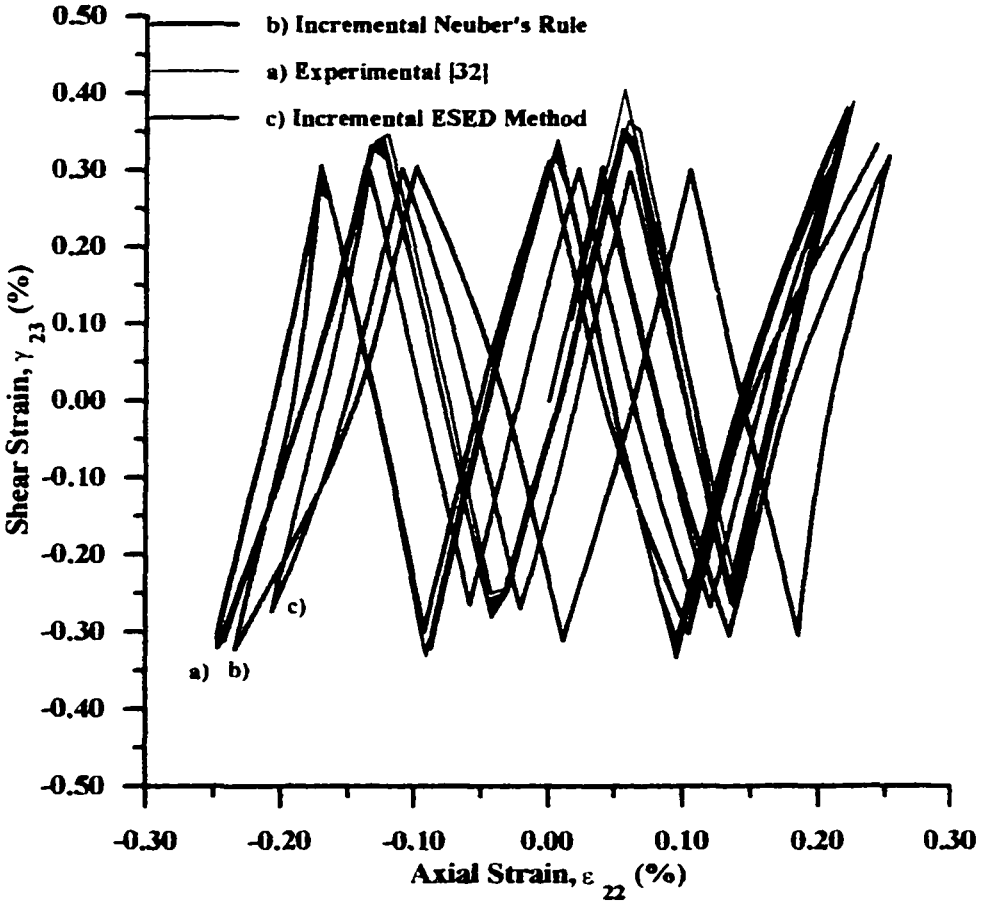


Figure 6.16b: Comparison of Simplified Models to Experimental Results for 1:5 Ratio.

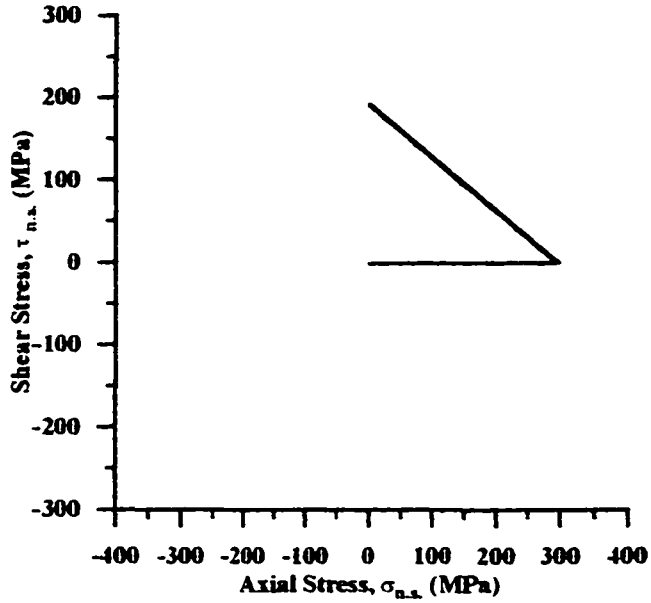


Figure 6.17a: Stress Path in [32] With Non-Zero Mean Stress.

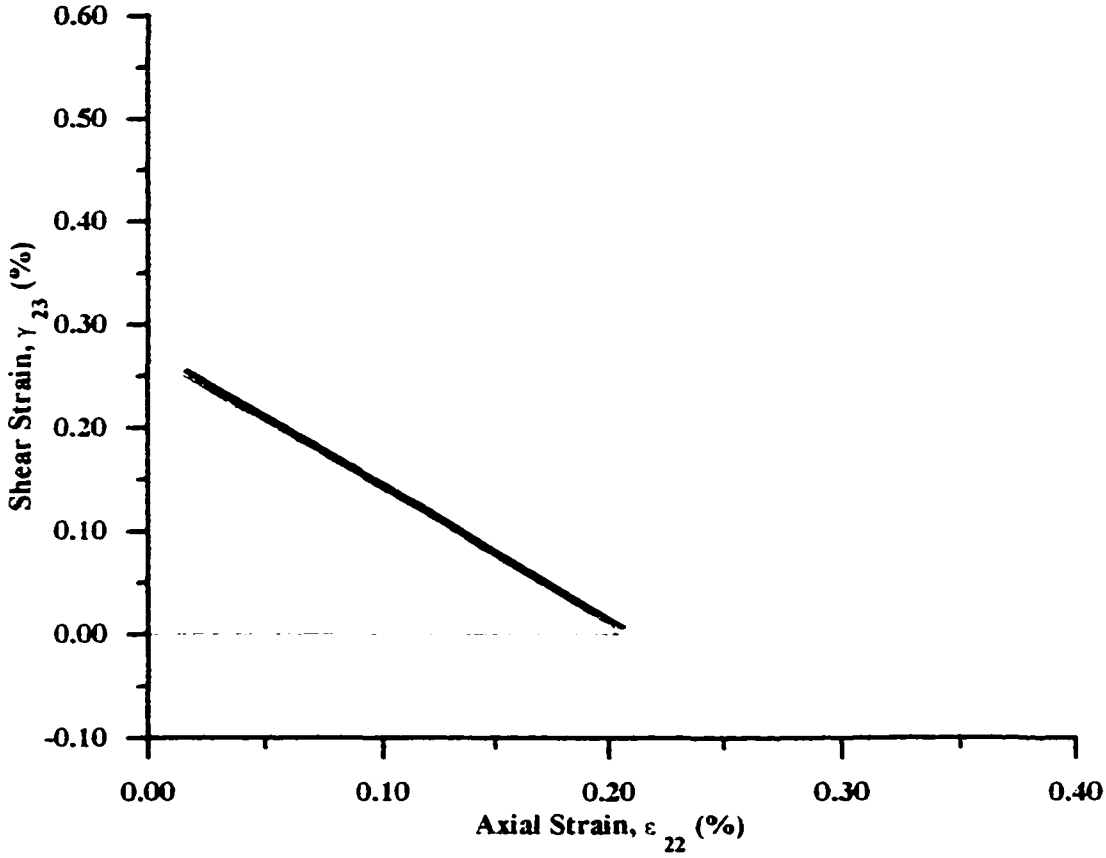


Figure 6.17b: Incremental ESED Results for Non-Zero Mean Stress.

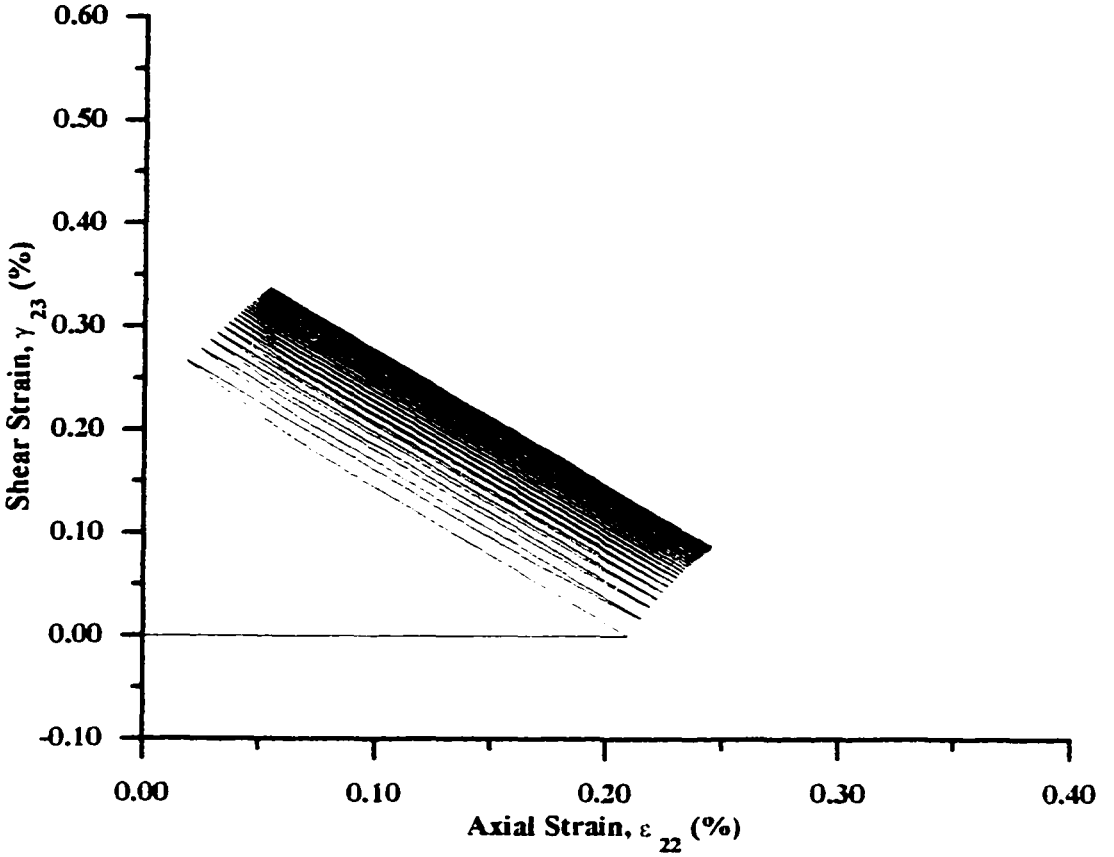


Figure 6.17c: Incremental Neuber's Results for Non-Zero Mean Stress.

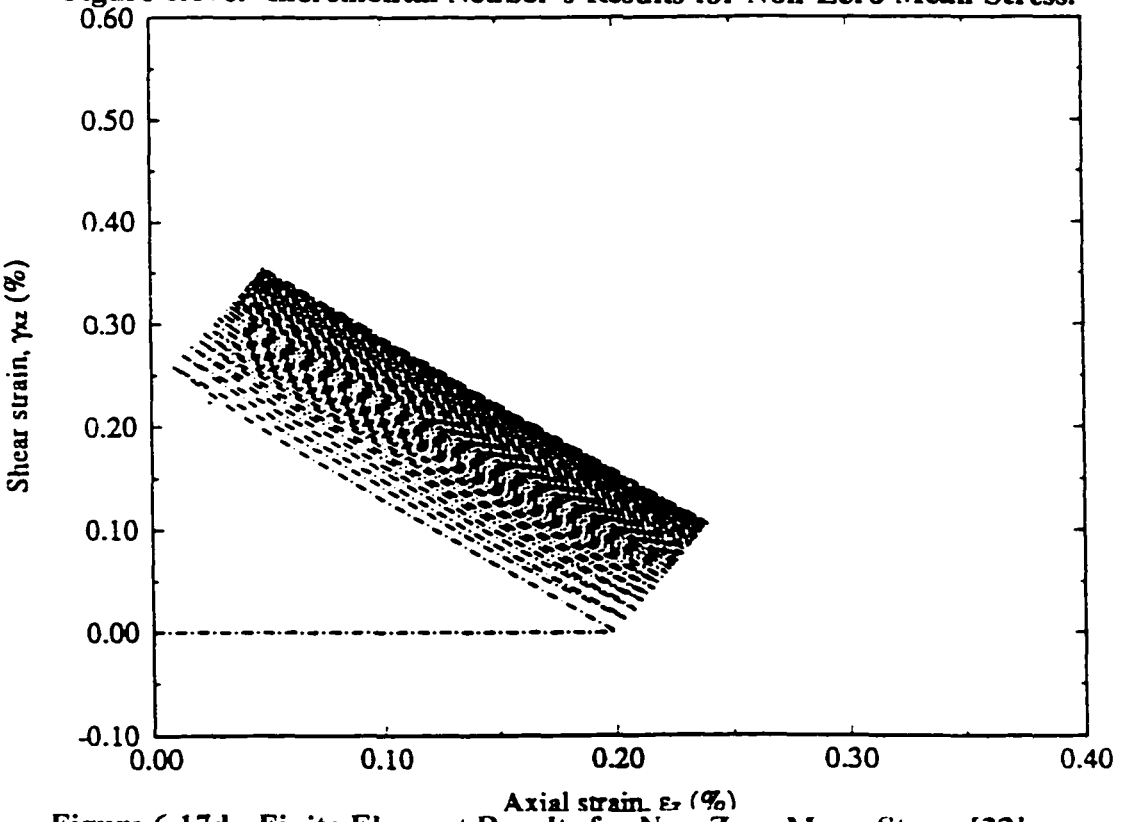


Figure 6.17d: Finite Element Results for Non-Zero Mean Stress [32].

7. CHAPTER SEVEN:

CONCLUSIONS / RECOMMENDATIONS

Two simplified methods have been proposed that enable the estimation of notch root stress and strain histories in bodies subjected to cyclic non-proportional loads. The first method, the incremental Equivalent Strain Energy Density (ESED) method, is based on the assumption that an increment in strain energy density at the notch tip in an elastic-plastic body can be approximated by that increment obtained if the body were to only deform elastically. The second method, the incremental Neuber's method, is based on the assumption that an increment in the **total** strain energy density at the notch tip in an elastic-plastic body can be approximated by that obtained if the body were to only deform elastically. It was shown that, in an elastic-plastic body, if the plastic zone is localized, both the strain energy density and the total strain energy density are somewhat insensitive to the loading path. Utilizing elastic approximations to these quantities is therefore reasonable.

To form complete sets of relations that enable the notch tip stress and strain tensors to be determined, each simplified method was used in conjunction with material constitutive relations. For this purpose, a background in plasticity was presented with specific emphasis on modeling cyclic deformations. Although any constitutive model that incorporates path dependent material behavior can be used in conjunction with the proposed simplified methods,

the Mróz multi-surface work hardening model was chosen for the purpose of this work. If more transient effects such as mean stress relaxation or ratchetting are to be better modeled, future research may focus on using an alternate translation rule such as that presented in [51].

A detailed description of the use of the incremental ESED and Neuber's methods for notch tip stress-strain estimation during a loading cycle was presented. This encompassed a description of the regions of elastic loading, elastic-plastic loading, and elastic unloading. Methods that delineate each region of loading were also presented. For the purposes of computer implementation, a flow chart was given. The required input into the developed program is the elastic notch tip stress history and the material stabilized uniaxial cyclic stress-strain curve.

In comparing the results of each method to experimental and finite element data for monotonic loading, it was found that both methods predict the trend of the elastic-plastic FEM and experimental results. However, it was found that the additional energy ratio equation used in conjunction with the ESED method will restrict this solution set to predict a constant strain in the direction where the elastic stresses are constant during the loading step. Furthermore it was shown that as the degree of non-proportionality is reduced, so is the error in the solutions. However, for all the loading paths analyzed, the differences in both the generalized Neuber's solution set and the ESED solution set from the FEM results was found to be small well beyond general yielding in the net section, when the localized plasticity assumption is violated. Finally, it was shown for all loading paths that the ESED simplified solution set predicts a

lower bound, and that Neuber's solution set predicts an upper bound to the notch tip strains predicted in the elastic-plastic finite element analysis.

The results of the incremental ESED and Neuber's method were also compared to limited finite element and experimental data for the case when cyclic external loads are applied in a non-proportional manner. It should be mentioned that the experimental data presented [32] and used in this thesis for the simplified model assessment, is virtually the only reliable experimental data set published for notched bodies subjected to non-proportional cyclic loading histories. Although good results were obtained using the proposed methods for the most severe non-proportional loading case (the box path), and the material stress-strain curve used was relatively flat, it is felt that experiments on different notched geometries subjected to alternate loading histories would provide further confidence in the proposed methods.

In all of the non-proportional cyclic load paths examined, both methods predicted the general trend in the elastic-plastic stress-strain results. In non-proportional cyclic loading, the statement that the Neuber's rule forms the upper bound approximation, and the ESED method forms the lower bound approximation to the actual notch-tip strains cannot be made. Instead, each method independently gives a good prediction of the notch tip strain and stress histories. In cases where the elastic notch tip stress tensor remains constant, the incremental Neuber's solution set be used. It is recommended that future research may focus on a procedure for averaging the cyclic strains obtained by each method (since one method generally overpredicts

when the other method is underpredicting the notch strains), and subsequently using a cyclic plasticity model to determine the stresses. This procedure may yield results closer to the actual vales than those results predicted independently by either the ESED or Neuber's method.

Although the methods presented are, in general, applicable to any notched body subjected to any arbitrary loading condition, there are a few exceptions for which the solution procedure, as presented, needs refinement. The first exception is the case of the presence of a residual stress at a notch tip before a loading history is applied. In such a case, the yield surface configuration that resulted from the loads applied causing the residual stresses must be known before applying the proposed simplified methods. For this purpose, it is recommended that a fictitious stress history be applied to the notched member and the resulting strains and yield surface configuration be calculated using a cyclic plasticity model. This would continue until the stress state at the notch tip matched the given residual stresses. The mode of loading, if not known, would depend on which components of residual stresses were present at the notch tip. Once the yield surface configuration, and the notch tip strains and stresses are known, the proposed methods, as presented, can be used to approximate the notch tip elastic-plastic strain and stress history for subsequent loading histories. An alternative, and perhaps simpler, method to account for residual stresses is to compute an elastic equivalent state of the known elastic-plastic residual strain and stress state using either the incremental ESED or Neuber's energy density equations. The programs for each method could then be used with no

modifications, with the first step starting from zero to the calculated elastic equivalent of the residual stress distribution.

The second exception to the general applicability of the proposed methods is the case of a pipe with an internal notch that has an internal pressure, and is further subjected to external non-proportional loading histories. In such a case, the notch tip is no longer traction free and thus the notch tip stress state is no longer biaxial. The expansion of Neuber's method and the ESED method on the notch tip element would thus have an added known internal pressure term.

The final exception occurs in some variable amplitude loading paths. Specifically, in some cases, even the accepted uniaxial forms of Neuber's method and the ESED method induce strain accumulation that does not occur in reality. This induced ratchetting occurs primarily in variable amplitude loading where there is a small unloading and reloading cycle during a relatively large cycle. This arises because of the method of choosing the origin of the local coordinate frame. Specifically, when reloading in the smaller cycle, with the coordinate frame being at the reversal point, the very small elastic region followed by a relatively flat portion of the uniaxial tensile curve will result in large strain increments when comparing elastic-plastic energy density increments to the to those calculated using the relatively steep elastic stress-strain curve. In the case of uniaxial and multiaxial proportional loading, these large predicted strain results are generally overcome by using rainflow counting, where by each cycle is

analyzed separately. In effect, the rainflow counting procedure results in the stress path starting at zero on the uniaxial stress-strain curve for each loading cycle. To overcome this strain accumulation induced in the case of non-proportional loading, it is recommended that a similar philosophy be incorporated into the incremental solution methods. One approach would be to translate the origin of the local coordinate frame to the origin of the active surface for such small loading cycles.

In conclusion, non-proportional loading is the most general form of cyclic loading and has traditionally been analyzed using lengthy experimental or costly non-linear finite element analysis. The simplified ESED and Neuber's solution methods provide a practical alternative to such analyses since only a linear elastic analysis is required. The methods can be used to determine elastic-plastic cyclic non-proportional behavior at any geometrical discontinuity in bodies subjected to any arbitrary loading cycles. There are a few exceptions to the general applicability of the methods which can be overcome by small adjustments to the methods presented.

REFERENCES:

[1] Peterson, R.E. , Stress Concentration Design Factors, John Wiley and Sons, New York, Fifth Printing, 1966.

[2] Griffith, G.E., "Experimental Investigation of the Effects of Plastic Flow in a Tension Panel with a Circular Hole," NACA TN 1075, Washington, 1948.

[3] Hardrath, H.F., and Ohman, L., "A Study of Elastic and Plastic Stress Concentration Factors due to Notches and Fillets in Flat Plates," NACA TN 2566, Washington, 1951.

[4] Stowell, E.Z., "Stress and Strain Concentration at a Circular Hole in an Infinite Plate," NACA TN 2073, Washington, 198.

[5] Neuber, H., "Theory of Stress Concentration for Shear-Strained Prismatical Bodies with Arbitrary Nonlinear Stress-Strain Law," *Journal of Applied Mechanics*, American Society of Mechanical Engineers, Vol. **26**, No. **4**, 1961, pp. 544-550.

[6] Moftakhar, A., "Calculation of Time-Independent and Time Dependent Strains and Stresses in Notches," Ph.D. Thesis, The University of Waterloo, Waterloo, Ontario, 1994.

[7] Papirno, R., "Plastic Stress-Strain History at Notch Roots in Tensile Strips under Monotonic Loading," *Experimental Mechanics*, Vol. **11**, 1971, pp. 446-453.

[8] Topper, T.H., Wetzel. R.M., and Morrow, J., "Neuber's Rule Applied to Fatigue of Notched Specimens," *Journal of Materials*, Vol. **4**, No. **1**, 1969, pp. 200-209.

[9] Lies, B.N., Gowda, C.V.B., and Topper, T.H., "Some Studies of the Influence of Localized and Gross Plasticity on the Monotonic and Cyclic Concentration Factors," *Journal of Testing and Evaluation*, Vol. **1**, No. **4**, 1973, pp. 341-348.

[10] Conle, A., and Nowack, H., "Verification of a Neuber based Notch Analysis by the Companion-Specimen Method," *Experimental Mechanics*, Vol. **17**, 1977, pp. 57-63.

[11] Guillot, M.W., and Sharpe, W.N. Jr., "A Technique for Cyclic-Plastic Notch-Strain Measurement," *Experimental Mechanics*, Vol. **23**, 1951, pp. 354-360.

[12] Hutchinson, J.W., "Singular Behavior at the End of a Tensile Crack in a Hardening Material, " *Journal of the Mechanics an Physics of Solids*, Vol. **16**, 1968, pp. 13-31.

[13] Molski, K., and Glinka, G., "A Method of Elastic-Plastic Stress and Strain Calculation at a Notch Root," *Material Science and Engineering*, Vol. **50**, 1981, pp. 93-100.

[14] Glinka, G., "Energy Density Approach to Calculation of Inelastic Strain-Stress Near Notches and Cracks," *Engineering Fracture Mechanics*, Vol. **22**, No. **3**, 1985, pp. 485-508.

[15] Glinka, G., "Calculation of Inelastic Notch-tip Strain-Stress Histories Under Cyclic Loading," *Engineering Fracture Mechanics*, Vol. **22**, No. **5**, 1985, pp. 839-854.

[16] Walker, K., " Multiaxial Stress-Strain Approximations for Notch Fatigue Behaviors." *Journal of Testing and Evaluation*, Vol. **5**, No. **2**, 1977, pp. 106-113.

[17] Dowling, N., Brose, W.R., and Wilson, W.K., "Notched Member Fatigue Life Predictions by the Local Strain Approach," *Fatigue under Complex Loading: Analyses and Experiments, Advances in Engineering*, Vol. 6, edited by R.M. Wetzel, Society of Automotive Engineers, Warrendale, Pa., 1977, pp. 55-84.

[18] Gemma, A.E., "An Approximate Elasto-Plastic Analysis of the Effect of Plain Strain at the Surface of a Notch," *Engineering Fracture Mechanics*, Vol. **22**, No. **3**, 1985, pp. 495-501.

[19] Fuchs, H.O., and Stephens, R.I., *Metal Fatigue in Engineering*, Wiley, New York, 1980, p. 139.

[20] Sharpe, W.N.Jr. and Wang, K.C., "Evaluation of a Modified Monotonic Neuber Relation," *Journal of Engineering Materials and Technology*, Vol. 113, 1991, pp. 350-353.

[21] Glinka, G., Ott., W., and Nowack, H., "Elastoplastic Plane Strain Analysis of Stresses and Strains at the Notch Root," *Journal of Engineering Materials and Technology*, Vol. **110**., 1988, pp. 195-204.

[22] Sharpe, W.N.Jr., Yang, C.H., and Tregoning, R.L., "An Evaluation of Neuber and Glinka Relations for Monotonic Loading," *Journal of Applied Mechanics*, Vol. **59**, No. **2**, 1992, pp.S50-S56.

[23] Tipton, S.M., "A Review of the Development and Use of Neuber's Rule for Fatigue Analysis," *Society of Automotive Engineers* technical paper 910165, Warrendale, PA, 1991.

[24] Hoffman, M., and Seeger, T., "A Generalized Method for Estimating Elastic-Plastic Notch Stresses and Strains, Part 1: Theory," *Journal of Engineering Materials and Technology*, Vol. **107**, 1985, pp. 250-254.

[25] Hoffmann, M., and Seeger, T., "A Generalized Method for Estimating Multiaxial Elastic-Plastic Notch Stresses and Strains, Part 2: Applications," *Journal of Engineering Materials and Technology*, Vol. **107**, 1985, pp. 255-260.

[26] Lemaitre, L., and Chaboche, J.L., *Mechanics of Solid Materials*, Cambridge University Press, Cambridge, U.K., 1990.

[27] Moftakhar, A., and Glinka, G., "Elastic-Plastic Stress-Strain Analysis Methods for Notched Bodies," *Theoretical Concepts and Numerical Analysis of Fatigue*, Proceedings of the International Conference on Fatigue, Birmingham, U.K., May, 1992.

[28] Moftakhar, A., Buczynski, A., and Glinka, G., "Calculation of Elasto-Plastic Strains and Stresses in Notched Bodies Under Multiaxial Cyclic Loading," *Fatigue '93*, Vol. **1**, 1993, pp. 441-452.

[29] Sørbø, S., and Härkegård, G., "Evaluation of Approximate Methods for Elastic-Plastic Analysis of Notched Bodies," *Localized Damage '94*, Udine, Italy, 1994.

[30] Hoffmann, M., Amstutz, H., and Seeger, T., "Local Strain Approach in Non-Proportional Loading," *Fatigue under Biaxial and Multiaxial Loading* ESIS10, Edited by K. Kussmaul, D. McDiarmid, and D. Socie, Mechanical Engineering Publications, London, 1991, pp. 357-376.

[31] Barkey, M.E., Socie, D.F., and Hsai, K.J., "A Yield Surface Approach to the Estimation of Notch Strains for Proportional and Nonproportional Cyclic Loading," Journal of Engineering Materials and Technology, Vol. **116**, 1994, pp. 173-179.

[32] Barkey, M.E., "Calculation of Notch Strains Under Multiaxial Nominal Loading", Ph.D. Thesis, Univerisity of Illinois, Urabana, Illinois, 1993.

[33] Köttgen, V.B., Barkey, M.E., and Socie, D.F., "$^{e}\sigma$ and $^{e}\varepsilon$ Based Approaches to Multiaxial Notch Analysis," *Theoretical and Applied Mechanics Report #169*, University of Illinois, Urbana, Illinois, 1995.

[34] Lee, Y, Chiang, Y., and Wong, H., "A Constitutive Model for Estimating Multiaxial Notch Strains," *Journal of Engineering Materials and Technology*, Vol. **117**, 1995, pp. 33-40.

[35] Gu. R.J., and Lee, Y., "A New Method for Estimating Nonproportional Notch-Root Stresses and Strains," *Journal of Engineering Materials and Technology*, Vol, **119**, 1997, pp. 40-45.

[36] Singh, M.N.K., Glinka, G., and Dubey, R.N., "Elastic-Plastic Stress-Strain Calculation in Notched Bodies Subjected to Non-Proportional Loading," *International Journal of Fracture*, Vol. 76, 1996, pp. 39-60.

[37] Singh, M.N.K., Glinka, G., and Dubey, R.N., "Notch Tip Stresses and Strains under Non-Proportional Loading," *Multiaxial Fatigue and Deformation Testing Techniques, ASTM STP 1280*, Eds. S. Kalluri and P. Bonacuse, 1997, pp. 131-155.

[38] Chu, C.C., and Conle, F.A., "Multiaxial Neuber-Type of Elastic-Plastic Stress-Strain Correction," presented at the *Fourth International Conference on Biaxial/Multiaxial Fatigue*, Paris, France, June, 1994.

[39] Hibbitt, Karlsson & and Sorensen, Inc., *ABAQUS Theory Manual*, Version 5.3, 1993.

[40] Hill, R., *The Mathematical Theory of Plasticity*. Oxford University Press, 1950.

[41] Jain, S.K., *Introduction to the Theories of Plasticity Part 1: Stress-Strain Relations*, Engineering Publications, Virginia, 1990.

[42] Mendelson, A., *Plasticity: Theory and Applications*, The Macmillan Company, New York, 1968.

[43] Prager, W., "A New Method of Analyzing Stresses and Strains in Work Hardening Plastic Solids," *Journal of Applied Mechanics*, Vol. **23**, 1957, pp. 493-496.

[44] Ziegler, H., "A Modification of Prager's Hardening Rule," *Quarterly of Applied Mathematics*, Vol. **17**, No. **1**., 1959, pp. 55-65.

[45] Lamba, H., and Sidebottom, D., "Cyclic Plasticity For Nonproportional Paths: Part 1-Cyclic Hardening, Erasure of Memory, and Subsequent Strain Hardening Experiments," *Journal of Engineering Materials and Technology*, Vol. **100**, 1978, pp. 96-103.

[46] Lamba, H., and Sidebottom, D., "Cyclic Plasticity For Nonproportional Paths: Part 2-Comparison with Predictions of Three Incremental Plasticity Models," *Journal of Engineering Materials and Technology*, Vol. **100**, 1978, pp. 104-111.

[47] Mróz, Z., "On the Description of Anisotropic Work Hardening," *Journal of the Mechanics and Physics of Solids*, Vol. **15**, 1967, pp. 163-175.

[48] Garud, Y., "A New Approach to the Evaluation of Gatigue Under Multiaxial Loading," *Journal of Engineering Materials an Technology*, Vol. **103**, 1981, pp. 118-125.

[49] Jiang, Y., Sehitoglu, H., "Comments on the Mróz Multiple Surface Type Plasticity Models," *International Journal of Solids and Structures*, Vol. **33**, 1996, pp. 1053-1068.

[50] Chu, C.C., "A Three-Dimensional Model of Anisotropic Hardening in Metals and its Application to the Analysis of Sheet Metal Forming," *Journal of the Mechanics and Physics of Solids*, Vol. **32**, 1984, pp. 197-212.

[51] Jiang, Y., and Kurath, P., "Characteristics of the Armstrong-Frederick Type Plasticity Models," *Journal of the Mechanics and Physics of Solids*, 1997.

[52] Dafalias, Y., and Popov, E., "A Model of Nonlinearly Hardening Materials for Complex Loading," *Acta Mechanica*, Vol. 23, 1975, pp. 173-192.

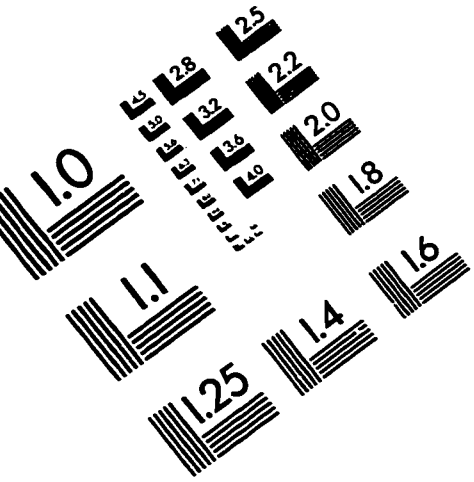
[53] Masing, G., "Eigenspannungen und Verfestigung bei Messing," *Proceedings of the Second International congress for Applied Mechanics*, Zurich, 1926.

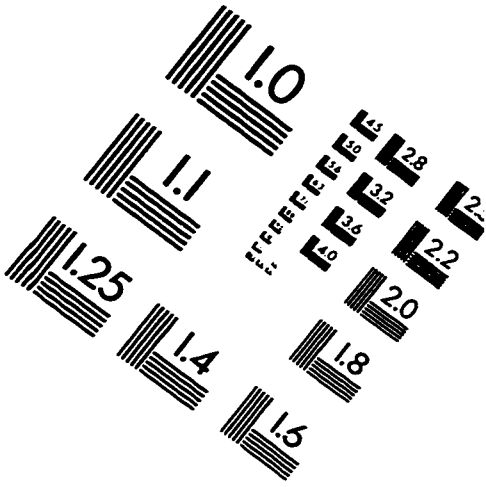
[54] Langlais, T., *Computer Methods for Multiaxial Cyclic Plasticity*, Master's Thesis, the University of Minnesota, 1994.

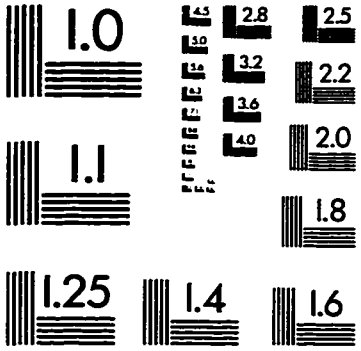
[55] Hoffmann, M., and Seeger, T., "Kerbbeansprunchungen I. Ermittlng und Beschreibung Mehrachsiger Kerbbeanspruchungen im nichtlinearen Bereich," Abschlubericht zum FKM-Vorhaben Nr. 71. Forschungshefte Forschungskuratorium Maschinenbau e.v. Heft 115, 1985 (in German).

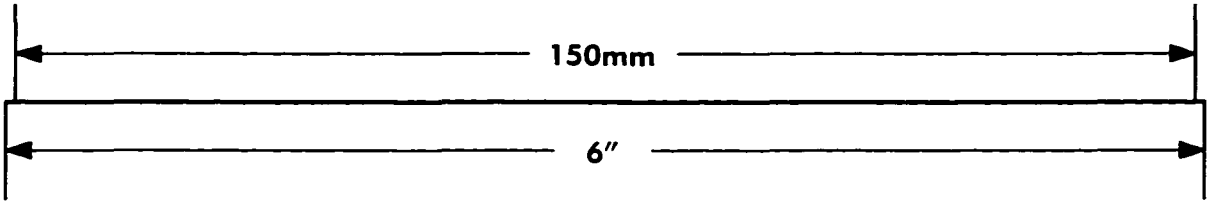
[56] Köttgen, V.B., and Seeger, T., "Finite Element Analyses of a Notched Bar Under Multiaxial Nonproortional Loading Using the Mróz Model," Bericht FF-7. Fachgebiet Werkstoffmechanik, Technische Hochschule Darmstadt, 1993.

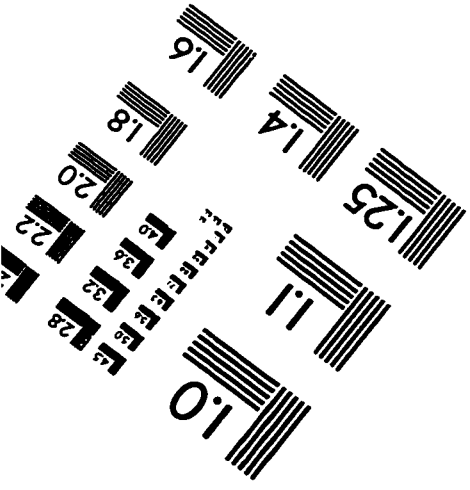
IMAGE EVALUATION TEST TARGET (QA-3)

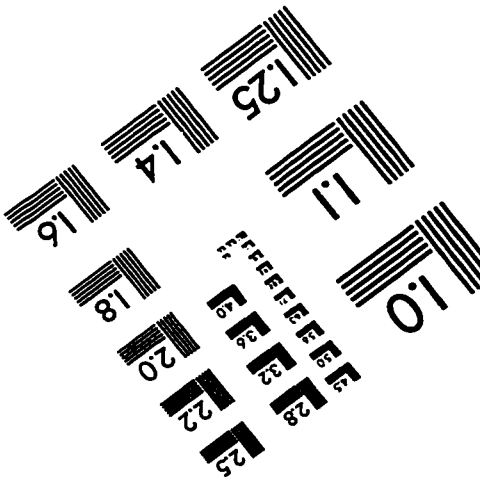












APPLIED IMAGE, Inc
1653 East Main Street
Rochester, NY 14609 USA
Phone: 716/482-0300
Fax: 716/288-5989

© 1993, Applied Image, Inc., All Rights Reserved